11-2019

THE STABILITY ANALYSIS FOR WIND TURBINES WITH DOUBLY FED INDUCTION GENERATORS

Baohua Dong
University of Nebraska-Lincoln, baohua.dong@gmail.com

THE STABILITY ANALYSIS FOR WIND TURBINES WITH DOUBLY FED INDUCTION GENERATORS

by

Baohua Dong

A DISSERTATION

Presented to the Faculty of

The Graduate College at the University of Nebraska

In Partial Fulfillment of Requirements

For the Degree of Doctor of Philosophy

Major: Engineering

(Electrical Engineering)

Under the Supervision of Professors Sohrab Asgarpoor and Wei Qiao

Lincoln, Nebraska

November, 2019

THE STABILITY ANALYSIS FOR WIND TURBINES WITH DOUBLY FED INDUCTION GENERATORS

Baohua Dong, Ph.D.

University of Nebraska-Lincoln, 2019

Advisors: Sohrab Asgarpoor and Wei Qiao

The quickly increasing, widespread use of wind generation around the world reduces carbon emissions, decreases the effects of global warming, and lowers dependence on fossil fuels. However, the growing penetration of wind power requires more effort to maintain power systems stability.

This dissertation focuses on developing a novel algorithm which dynamically optimizes the proportional-integral (PI) controllers of a doubly fed induction generator (DFIG) driven by a wind turbine to increase the transient performance based on small signal stability analysis.

Firstly, the impact of wind generation is introduced. The stability of power systems with wind generation is described, including the different wind generator technologies, and the challenges in high wind penetration conditions.

Secondly, the small signal stability analysis model of wind turbines with DFIG is developed, including detailed rotor/grid side converter models, and the interface with the power grid.

Thirdly, Particle swarm optimization (PSO) is selected to off-line calculate the optimal parameters of DFIG PI gains to maximize the damping ratios of system

eigenvalues in different wind speeds. Based on the historical data, the artificial neural networks (ANNs) are designed, trained, and have the ability to quickly forecast the optimal parameters. The ANN controllers are designed to dynamically adjust PI gains online.

Finally, system studies have been provided for a single machine connected to an infinite bus system (SMIB), a single machine connected to a weak grid (SMWG), and a multi machine system (MMS), respectively. A detailed analysis for MMS with different wind penetration levels has been shown according to grid code. Moreover, voltage stability improvement and grid loss reduction in IEEE 34-bus distribution system, including WT-DFIG under unbalanced heavy loading conditions, are investigated.

The simulation results show the algorithm can greatly reduce low frequency oscillations and improve transient performance of DFIGs system. It realizes off-line optimization of MMS, online forecasts the optimal PI gains, and adaptively adjusts PI gains. The results also provide some useful conclusions and explorations for wind generation design, operations, and connection to the power grid.

ACKNOWLEDGEMENTS

I would like to express my gratitude and sincere thanks to my advisor, Dr. Sohrab Asgarpoor, for his continuous guidance and support of my research, through which I developed the independent thinking skills that are essential for a researcher. His comprehensive knowledge, enthusiasm, and commitment to high-quality research have been inspirational to me. He supported me and encouraged me to join more conferences, which enabled me to gain valuable experience and to broaden my horizons. In addition, his efforts in helping me to revise my papers and dissertation are truly appreciated.

I also have to thank Dr. Wei Qiao, who has given a great help in my research and made many contributions to my dissertation. I am also grateful to Dr. Jerry Hudgins and Dr. David Jones, who served on my Dissertation Committee, for their constructive advice, valuable suggestions, and encouragement in completing this dissertation.

In addition, I would like to thank my parents, Shuili Dong and Yuexiang Hu, for their continuous encouragement throughout my Ph.D. studies. In particular, I would like to thank my wife, Lingling Wang, for her patience and tremendous support and for her great effort in holding our family together in the U.S. Finally, I would like to express my thanks to my friends in Lincoln. Their kindness, sincerity, and generosity have made life most enjoyable.

I will always be proud to be a graduate of the University of Nebraska-Lincoln and will think of this place as my hometown in the U.S. This research was supported by an assistantship offered by Dr. Asgarpoor through the Nebraska Center for Energy Sciences Research. I am also grateful to the Electrical Engineering Department at the University of Nebraska-Lincoln for providing me with additional financial support.

TABLE OF CONTENTS

LIST OF FIGURES

LIST OF TABLES

CHAPTER 1
INTRODUCTION

1.1 Wind Energy Development

Wind energy is a clean, renewable, green, indigenous energy resource. Human beings have been harnessing wind energy for thousands of years, e.g., windmills and sailboats. In the early stages, the mechanical energy of wind has been directly used for pumping water, grinding grain, or moving a boat.

The oil crises of the 1970s led to development and demonstration work on renewable energy sources, especially wind energy. Today, the windmill's modern evolution, the wind turbine with a generator, can use wind energy to generate electricity. Wind turbines (WTs) are mounted on a tower (30~100 meters above ground) to capture the mechanical energy of wind with their propeller-like blades. Usually, two or three blades are mounted on a shaft to form a rotor. A generator is attached to the rotor to convert the mechanical power into electrical power. A basic WT with a generator model is shown in Figure 1.1. Wind power plants (WPPs) can be used as stand-alone applications, connected to a power grid, or even combined with an energy storage system (ESS), such as flywheels, batteries, or pumped hydro storage, etc. Usually, a large number of WTs are built close together to form a wind farm connected to the electric power transmission system, or the grid.

With the quick development of WPPs over the last 30 years, their capacity has increased significantly, from 10KW to 5 MW; and the total capacity of one wind farm, including hundreds of WTs, amounts to 100~1000MW. It is one of the fastest growing forms of electricity generation in the world. Worldwide, wind power capacity has

increased about 20% annually over the last ten years because it is a relatively low MWh cost renewable energy [1]. According to 2018 U.S. Wind Industry Market Reports [2], U.S. wind power capacity increased 8% in 2018, to 96,433 MW of cumulative installed wind capacity, more than double the capacity the U.S. had in 2010. Wind energy now reliably delivers more than 20% of the electricity produced Kansas, Iowa, Oklahoma, North Dakota, South Dakota and Maine. In 2018, wind turbines generated 6.5% of all the electricity delivered to U.S. consumers. The U.S. Department of Energy (DOE) and the wind industry evaluate possible costs, benefits, challenges and hope to meet the goal of supplying 20% of the nation's electricity using wind power. The penetration of wind power may increase significantly from 2% in 2012 to 20% in 2030 [3].

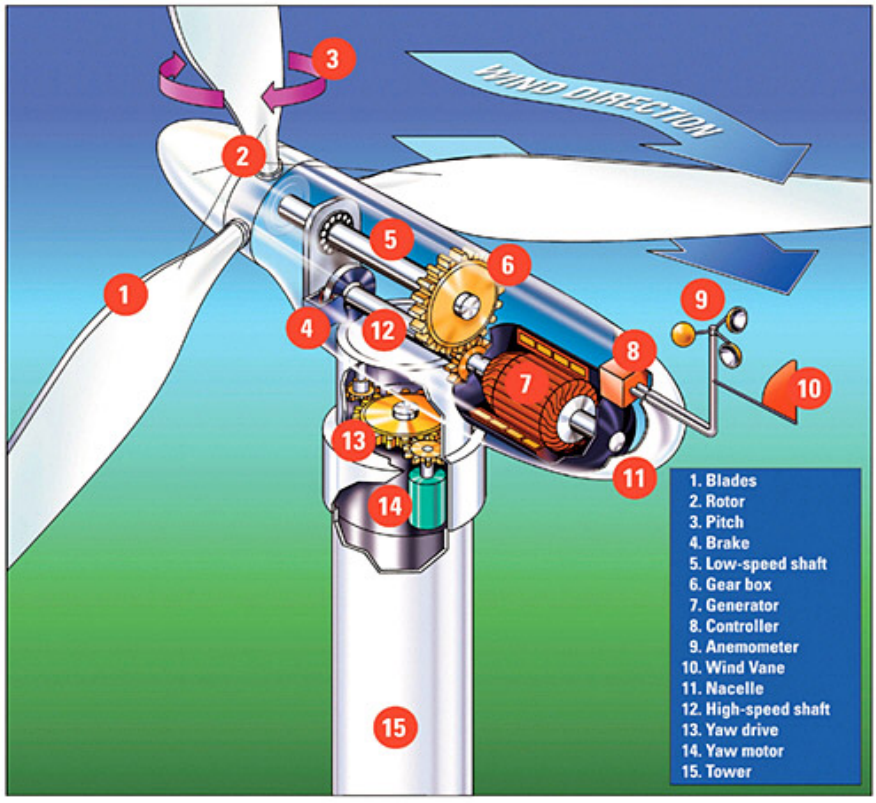

Figure 1.1. Wind turbine with generator model.

1.2 Benefits of Wind Energy

Generally, the benefits of Wind-generated electricity (WGE) fall into three distinct areas: environmental, economic/social, and technical (power systems). The biggest benefit is that it reduces the combustion of fossil fuels and the consequent emissions. There are no emissions of carbon dioxide (CO_2), sulfur dioxide (SO_2), or nitrous oxides (NO_x) with WGE production. WGE is a clean, secure, renewable power-generating technology.

The introduction of WGE can also produce significant economic/social benefits. Some of these benefits are national, such as reducing the risk of dependence on imported fuels and the creation of jobs in the manufacturing sector. Others are local, such as providing jobs to maintain and operate a wind farm and reducing the electric bills of homeowners, farmers, and ranchers in windy areas. WGE has become more economical to produce in the past ten years, dropping from as much as 30 cents per KWh to 4 to 6 cents, making it more competitive with other energy sources [4]. With tax credits and technology developments, WGE can become a major player in the future energy market.

Distributed WGE is usually comprised of a variety of small, modular power-generating technologies that can be combined to improve the operation of the distribution system. Some of the often-quoted benefits include [5-11]:

- Emergency backup during sustained utility outages.
- Voltage support and improved power quality, in some cases.
- Loss reduction.
- Improved utility system reliability (if proper supporting equipment is in place).

- Transmission and distribution capacity release.
- Potential deferral of expanding utility capacity.

1.3 Power Systems Challenges

The quickly increasing, widespread use of WGE is decreasing carbon emissions, reducing the effects of global warming, and decreasing dependence on fossil fuels. However, wind energy is an intermittent, non-dispatched power generation resource; and it is known to exhibit high variability in space and time due to the influence of other climatic factors. In addition, the probability distribution of fluctuations is very difficult to predict due to various uncertainties. Moreover, a number of wind resources in the U.S. are in the Midwest while load centers are mostly on the East and West coasts. It is also a tremendous challenge as to how to deliver so much electric power safely and economically from the Midwest to the East/West coasts via a transmission system.

Similar to large conventional synchronous power plants (coal, oil, and nuclear), WGE needs to provide adequate power to ensure the stability and reliability of power systems and to satisfy customers connected to the same grid. When WGE began to develop 30 years ago, their capacities and penetration were very small. Thus, the impact on the grid was very small; and any disturbances within or created by the plants were considered to be in the acceptable noise level. In the past 30 years, however, the size of WT has significantly increased; and the total capacity of wind farms can achieve the GW level. Moreover, the penetration of wind power has significantly increased, especially in some European countries. This rapid increase in penetration has triggered many challenges in the electric power industry [12-17]:

- Power systems stability and reliability: The intermittent, non-dispatched, energy-limited characteristics of wind power plants (WPPs) continue to have a big impact on system stability. How to balance the sudden reduction of WPPs while keeping power system stability and reliability in check is the most difficult issue for system operators.
- Transmission system planning and operation: WPPs are often located in remote areas with an undersized transmission grid. How to deliver the power to customers is also a big challenge for transmission system planning and operation.
- Reactive power compensation: WPPs usually cannot produce enough reactive power, as do conventional synchronous generators; and they need more reactive power compensation.
- Voltage regulation and frequency control: The intermittency of WPPs may disturb the connection point voltage, and power systems have additional requirements for maintaining frequency control.
- Protection: Distributed WPPs can change the initial power flow, and the fault current of the distribution feeder cannot accurately attain the initial "pick-up" value when a fault occurs.
- Power quality/harmonics: WPPs intermittency and "cut-in and cut-out" operation create various power quality/harmonics problems.
- Dynamic power flow: WPPs intermittency and non-dispatched characteristics require increased power flow tracking and dynamic scheduling.

- Power markets and economic dispatch: How to optimally dispatch power systems to maximize the utilization of WPPs, while maintaining system security and reliability following specific market mechanisms, is a challenging problem for system operators.
- Costs: Additional operating reserve and ancillary service costs increase.

In general, most of these challenges relate to the variability, intermittency, and non-dispatched characteristics of WPPs. Moreover, power system stability and reliability are the most important issues.

1.4 Significance of This Research

Usually, power systems contain thousands of dynamic elements with different response times and many static elements. The whole dynamic system must be kept balanced throughout. The ability of power systems to return to the initial steady state or to go to a new acceptable steady state after small or large disturbances is defined as power system stability. As the penetration of WPPs continues to increase, they will play a more important role in power systems stability; and the improvement of their transient performance is becoming more significant. Essentially, the conflict between WPPs variability, intermittency, and non-dispatched characteristics, and load variability creates the main problem: the stability of power systems with WPPs.

There are several important factors which influence stability, including different wind turbine generator technologies, wind power forecasting, energy storage systems, reactive power compensation, and various system operating conditions. These will be discussed briefly in Chapter 2.

This dissertation focuses mainly on the stability of wind turbines with doubly fed induction generators (DFIGs) because of their superior characteristics, wide applications, and rapid development.

In the past 15 years, many researchers have attempted to improve the stability and the transient performance of DFIGs by developing different algorithms. These important algorithms in [18-34] mainly include crowbar switching, series dynamic braking resistor (SDBR), novel converter designs, application of flexible AC transmission systems (FACTS) devices, adding power system stabilizers (PSS), evaluating wind farm transient stability using a probabilistic approach, adding energy storage systems, developing novel converter control strategies, and optimizing Proportional-Integral (PI) gain parameters for advanced control.

- Crowbar switching: In [18], the authors used a crowbar to short circuit the rotor-side converter to protect the DFIG from overcurrent during a severe grid fault. It is one of the simplest, low-cost techniques to improve DFIG transient performance.
- Series dynamic braking resistor: The authors in [19] used SDBR to dissipate active power and boost generator voltage of fixed-speed wind turbine generators. They also showed that a small resistance, inserted for less than one second, can displace a substantial capacity of dynamic reactive power compensation. Yet, a lot of thermal loading on the resistor in a short time will create a very high requirement for the actual product; and it is not easy to satisfy that requirement in manufacturing. With the quick developments of power electronics, the

algorithms of crowbar protection and series dynamic braking resistor are now outdated.

- Novel converter control strategies and converter designs: By using an uninterrupted operation scheme and the fast control of the DFIG converters in [20], DFIGs can successfully ride through grid faults and have no problem with angular stability associated with the conventional synchronous generators and can do so without crowbar switching. The new techniques are developed based on the open-loop and close-loop dynamic response of the DFIG in [21]. In [22], the frequency variation of a DFIG based wind farm terminal bus was used to modulate the torque reference and the output power of the DFIG in the post-disturbance condition. This in turn modifies the electrical power of the nearby alternators and causes improvement of stability. In [23], a 9-MW DFIG based wind farm integrated with one superconducting fault current limiter (SFCL)-based passive voltage compensator and one transient voltage control (TVC)-based active voltage compensator are investigated to achieve a higher stator voltage level and higher output reactive power for efficient grid connection. An energy capacitor system with a fuzzy-logic-controlled reference signal adjuster under the control of a DC-DC Buck-Boost converter to smooth the fluctuation of variable speed wind generation output was presented in [24]. The fuzzy-logic-controlled adjuster can reduce the

cost of an energy capacitor system and enhance the control ability of the overall system.

- Energy storage systems: There are many papers published which discuss the applications for battery, flywheel, air pump, water pump, and hydrogen energy storage systems to balance wind power output [25]. Reference [26] focused on the application of a large capacity superconducting magnetic energy storage (SMES) unit to significantly improve wind farm transient performance by controlling the charging and discharging of the SMES. Rapidly battery energy storage systems (BESS) evolving innovations, increasing interest by utilities and consumers, coupled with more competition in this space are key drivers that are making storage more and more attractive to utilities and related companies. On the positive side, prices are projected to continue a downward trend and storage is now being seriously looked at for several different applications on the grid. The downside is that costs are still fairly high and, without regulatory requirements or subsidies, BESS's still may not be cost-effective in many regions. Most ESSs are very expensive; or they have some special geographical limits.
- PI gain parameter optimization and advanced control: The algorithms improve the transient performance of wind generators through PI gain parameter optimization of converters [27, 28, 29, and 30].

- Flexible AC transmission systems devices: In [31], the static reactive compensator (STATCOM) based on a voltage source converter (VSC) pulsed width modulation (PWM) technique is used to improve transient and dynamic stability of WPPs. However, FACTS is very expensive.
- Probabilistic approach to evaluating wind farm transient stability: In [32], the authors presented a probabilistic approach to evaluating wind farm transient stability; and the resulting indices provide the ability to quantitatively assess the likelihood of system instability due to the occurrence of transmission line faults. This was useful to system planners involved in assessing the need to reinforce critical transmission lines in order to improve the transient stability of the overall system. However, this algorithm requires the support of a large amount of historical data about wind farm faults; and this is not practical now.
- Power system stabilizer: The authors in [33] proved that adding a power system stabilizer (PSS) by a DFIG-based wind farm for reduced order 16-machine 5-area dynamic equivalent model of the New England-New York power system with replacement of one existing synchronous generator could significantly influence network damping and achieve good voltage control capacity. However, how to add PSS to hundreds of wind turbine generators is a big problem. In practical situations, hundreds of wind turbine generators cannot be integrated

into one large wind turbine generator. This paper [34] presented a novel center of inertia (COT) approach to understand how integrated DFIGs affect the transient dynamics of a power system.

This dissertation cannot detail all of the applications listed above and focus on the PI parameter optimization algorithm. Others have developed a particle swarm optimization (PSO) algorithm to design the optimal PI controllers for rotor-side converters to improve transient performance [27]. The authors in [28] developed PSO to design the optimal PI controllers for the rotor-side and grid-side converters of a DFIG for a particular wind speed. More recently, the authors in [29] presented the Bacteria Foraging technique to separately optimize the parameters of a DFIG and the damping controller to increase the damping of low frequency angular oscillations of a DFIG in three different wind speeds. An application of an adaptive PI-fuzzy controller is applied in the back-to-back converter of variable speed permanent magnet wind generators to enhance transient stability in various operating conditions [30].

However, all of the approaches described so far only optimize the controller parameters at one special operating point (fix-optimal model); and the parameters are constant. The controllers do not have the ability to dynamically adjust PI gain values according to wind speed changes. These approaches are based on a single machine connected to the infinite bus system (SMIB), and the impacts of transmission lines and multi-machine systems are simply neglected.

The proposed artificial neural network (ANN) based adaptive PI control DFIG model is designed to improve DFIG transient performance and stability. PSO is used to optimize PI parameters of DFIG rotor-side and grid-side converters at different operating

points (different wind speeds) in order to maximize the damping ratios of the system eigenvalues in small signal stability analysis. Based on the calculated optimal values and the given wind speed data set, a two-layer, feed-forward ANN is designed and trained. The calculations for optimization and training are relatively slow and are done off line. After that, the ANN has the ability to quickly forecast the optimal values at each wind speed. The calculations for prediction are relatively fast and are done on line. A sensor captures the wind speed, which is the ANN's input, and the ANN forecasts the optimal values and outputs them into the smart PI controllers. The controllers dynamically change values according to the different wind speeds to increase the DFIG transient performance in a global operating range.

The contributions of this dissertation are as follows:

- Adaptive controllers: In the new algorithm, the ANN controllers smartly adjust the PI parameters to the optimal state and improve the transient performance of the DFIG in a wide range of wind speeds.
- Off-line optimization and online forecast: The ANN is trained by off-line optimized data and then used online to forecast the optimal values of the PI controllers' parameters. It is almost equal to real-time optimization for DFIGs at the different operating points.
- Fast and accurate prediction: ANN controllers can predict the optimal values quickly and accurately because a suitable, efficient structure is selected in the novel algorithm.

- Improved performance and stability: The transient performance and stability of the ANN optimal DFIG model is significantly improved, especially during wind speed step change.
- Greatly reduced low frequency oscillations.
- Increased voltage stability.
- Enhancements to the safety of the gearbox, rotor winding, and converter.
- Reduced variability of DFIG output.

According to the simulation results of SMIB, SMWG, and MMS test system, the ANN optimal DFIG model holds an obvious advantage when wind speeds change rapidly and often. This is particularly important since this disturbance may occur hundreds of times in one day; therefore, improving the transient performance and stability subject to speed changes is crucial. This is the most important contribution of the dissertation. Afterward, the algorithm is applied to SMWG and MMS to optimize the controllers of multi-DFIGs simultaneously. The results also indicate the deep mutual interaction between the DFIG, the weak grid, the synchronous generator (SG), the grid code low voltage ride through requirements and the different penetrations. The optimal DFIG can partially weaken the negative influence of the weak grid; but the weak grid obviously has a stronger impact on this system. With the penetration increase from 30% to 60%, the stability and DFIG transient performance may be slightly degraded, but not obviously. If the penetration continuously increases to 90%, the system has a better performance in the wind speed change disturbance than low/medium penetration systems, but it bears some worse low frequency oscillations in the fault disturbance.

The effects of a DFIG on voltage stability and grid loss in distribution systems under unbalanced load conditions have been investigated based on the simulation results of a DFIG in the IEEE 34-bus distribution test system. A new index (system unbalanced voltage variance), which is more reasonable and more accurate than using system average voltage, is proposed to evaluate system unbalanced voltage. A new multi-objective optimization function is provided to calculate the optimal location while simultaneously considering the voltage profile and grid loss. A comparison between a single large DFIG system and a multiple machine small DFIG system may find that the latter could provide higher system voltage advancement and almost the same grid loss reduction as the former. Moreover, the latter has a less dynamic impact and needs less time to return to its initial state. Therefore, the multiple machine small DFIG system has better stability.

1.5 Overview of Dissertation

The organization of this dissertation is as follows:

- Chapter 2: Includes an introduction to the stability of power systems with wind turbine generators as well as a discussion on power systems stability (small signal stability, transient stability, rotor angle stability, frequency stability, voltage stability) and system stability indicators. Various factors which influence stability, including different wind turbine generator technologies, wind power forecast, energy storage systems, reactive power compensation, and some of the system operations for addressing the challenges inherent to high penetration conditions are described. The interconnection requirements and grid code of wind generation are also briefly discussed. Afterward, a small

signal stability analysis model and a reduction of the damping ratio are introduced.

- Chapter 3: Provides a complete description of a wind turbine with a DFIG, including models for a wind turbine, induction generator, rotor-side converter, grid-side converter, and interface to a power grid. The impact of crowbar activation on wind generation is also briefly discussed.
- Chapter 4: Covers the optimization of wind turbine generators, including the optimization of wind turbine generators and the objective function (maximize the damping ratios of system eigenvalues). The advantages and disadvantage of different mathematical optimization techniques are analyzed. The basic PSO algorithm is introduced and PSO is improved based on small signal stability analysis.
- Chapter 5: Provides approaches for predicting the optimal parameters of PI gains according to historical data via the PSO. Predictions are defined, and an ANN algorithm is introduced. Then, the ANN construct based on a single machine connected to an infinite bus system is provided. An ANN adaptive controller is introduced.
- Chapter 6: Provides a flowchart of the optimal ANN DFIG model design and system studies for SMIB, SMWG, and MMS connected to the grid, respectively. Moreover, the issues of voltage stability improvement and grid loss reduction of distribution systems (IEEE 34-bus test system), including DFIG under unbalanced heavy loading

conditions, are investigated and some transient responses of disturbances are carried out in a single large DFIG system and a multiple small DFIGs system.

- Chapter 7: Conclusions and future research are provided.

CHAPTER 2
STABILITY OF POWER SYSTEMS WITH WIND TURBINE GENERATORS

Modern power systems usually contain tens of thousands of dynamic/static components and other control equipment in Figure 2.1, such as generators, loads, transmission lines, breakers, flexible AC transmission systems devices, unified power flow controllers (UPFC), energy storage systems, etc.

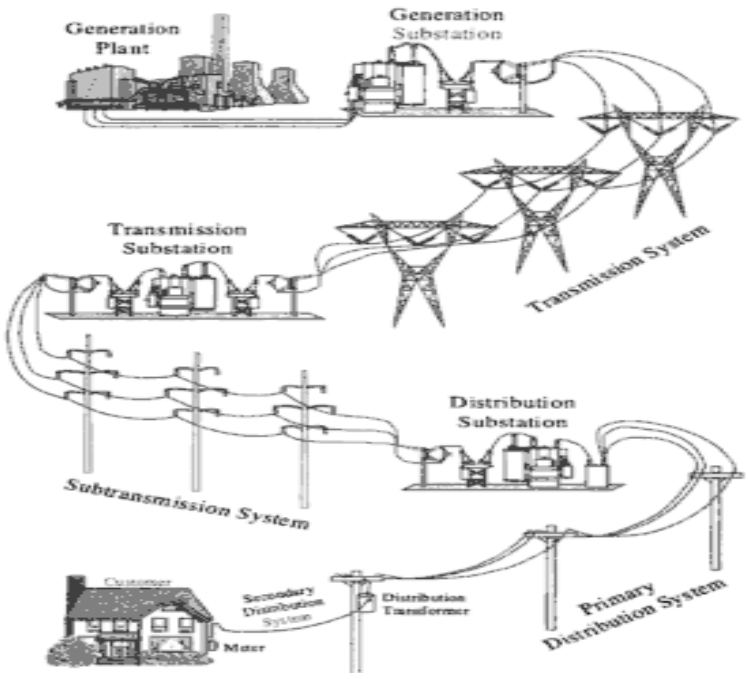

Figure 2.1. Typical structures of electric power systems in [35].

In fact, modern power systems are large-scale, nonlinear, dynamic systems that must balance electricity supply and demand and grid loss at any time, while taking disturbances into consideration. The dynamics of modern power systems can be characterized by extensive system interconnections and increasing dependence on control equipment and proper system planning and secure operations.

2.1 Classification of Power Systems Stability

There is a wide variety of disturbances in power systems at any time, even under normal operating conditions. The disturbances usually include sudden changes in load/generator active and reactive power output, changes in topology of the grid, malfunctioning or failing equipment, control/storage elements in switching operations, etc. The ability of a power system to remain in a state of operating equilibrium under normal operating conditions and to regain an acceptable state of equilibrium after being subjected to disturbances is defined as **power systems stability** [35-36].

In power systems, tens of thousands of dynamic/static components, control equipment, and the topology of the grid can be represented by a set of differential and algebraic equations, such as:

$$\begin{cases} \dot{\mathbf{x}} = \mathbf{f}(\mathbf{x}, \mathbf{y}) \\ \mathbf{0} = \mathbf{g}(\mathbf{x}, \mathbf{y}) \end{cases} \tag{2.1}$$

Where $\mathbf{x}, \mathbf{y}$ are the vectors of state and algebraic variables, respectively. Power system stability is essential to solving Equation (2.1) under a set of restraints. If all physical quantities which describe the operating condition, such as the magnitude/phase angle of each bus voltage, are constant at any time, the system is in **steady state**. Depending on the origin of disturbances and their magnitude, disturbances can be divided into two categories: small disturbances or large disturbances [37]. After a small disturbance, the system can go back to a steady state operating condition, which is identical to, or close to, the pre-disturbance operating condition. It is called steady state stable or **small signal stable**. The small disturbances are usually small variations in load and generation. The

small signal stability can be analyzed by using linearized system equations (2.1) **(small signal analysis).** This will be discussed in detail later in this chapter.

If the disturbance is large, the system will go to a newly acceptable steady state operating condition which is different from the initial steady state operating condition. It is called **transiently stable**. Generally, disturbances, such as transmission system faults, significant load changes, substantial loss of generation, and line switching, are examples of large disturbances. In these cases, small signal analysis is obviously no longer valid to solve the system dynamics.

Small signal stability is a function of the operating condition of the system, whereas transient stability is a function of both the operating condition and the disturbances, including different disturbance clearing time and location. Therefore, the analysis of transient stability is considerably complex. System linearization cannot be directly used, and repeated analysis is required for different disturbances at different locations with different clearing times. There are mainly two methods for analyzing power system transient stability. The first is the time domain numerical integration method (the step-by-step time domain solution). The second is the Lyapunov function method (constructing Lyapunov functions to directly prove the stability of the dynamic system) [38]. The latter is not commonly used because it is very difficult to construct an appropriate Lyapunov function. The time domain numerical integration method is commonly used. Therefore, the solution for power system transient stability requires solving equations (2.1) which describe the system under different disturbances and some restrictions to determine if the criterion is satisfied. This criterion requires that the difference between any two synchronous machines' rotor angle is smaller than 180

degrees as long as power systems can rely on synchronous machines for the generation of electrical power [35]. There are several methods for solving the equations (2.1): Euler, Advanced Euler, Runge-Kutta, and Buteher [39], etc. The fourth-order Runge-Kutta method is widely used in the industry mainly because of its higher accuracy and relatively less computation time [39].

Small signal stability of the dynamic system is necessary at all times. However, the system can operate even if it is transiently unstable under these operating conditions [37]. In general, stability closely depends on the system loading conditions, and an increase in loading can bring about instability. In fact, although small signal stability and transient stability are not directly related, transient stability can be enhanced correspondingly when small signal stability is improved. This dissertation focuses mainly on transient performance improvement of DFIG-based power systems achieved by increasing small signal stability of DFIG.

The parameters which are most affected by disturbances include rotor angle, voltage, and frequency. These parameters influence three types of instability mechanisms classified as: rotor angle stability, voltage stability, and frequency stability. Furthermore, power systems stability can be further distinguished based on the typical range of response times, i.e., short term (seconds) or long term (minutes). The various types of power systems stability are identified in the diagram in Figure 2.2 [35].

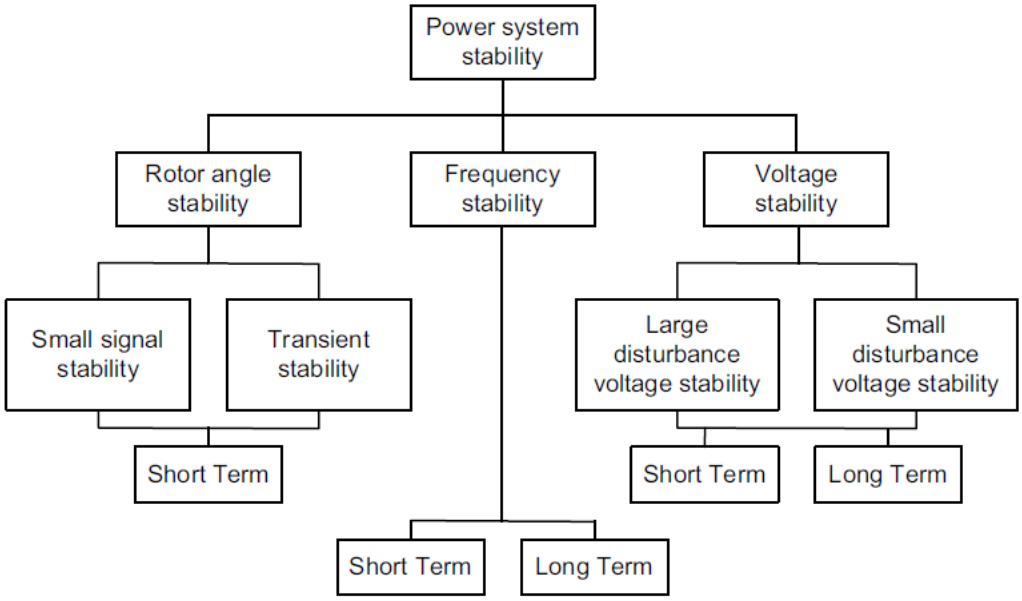

Figure 2.2. Classification of power systems stability.

Rotor angle stability is the ability of interconnected synchronous machines in power systems to remain in synchronism under normal operating conditions and after disturbances. Rotor angle instability may result in an increase in angular swings of some generators and a loss of synchronism [35]. The loss of synchronism may make the system split into islands or cause the removal of some generators for a period of time. This may lead to more serious damage, and many customers could lose electricity. The traditional small signal stability analysis and transient stability analysis are mainly based on rotor angle stability and are well developed. Although the rotor angle stability of a wind turbine generator system (WTGS) does not use strict angle synchronous stability, because most WTGS decouple with other synchronous machines via power electronic converters, it could be analyzed by the similar small signal stability method.

Voltage stability is classified as the ability of a power system to maintain all system bus voltages at an acceptable level under both normal operating conditions and

following disturbances. The nominal voltage level is usually 0.9~1.05pu. Voltage instability may occur in the form of a progressive or uncontrollable voltage drop [34]. This has become an increasingly important issue in modern power systems since 1990, as it can affect large areas and cause serious damage and possible injury. In general, voltage stability has a close relationship with reactive power. In most cases, reactive power compensation can solve the problem of voltage instability. However, reactive power compensation does not work in the cases of large load fluctuations or large transmission line loss [40]. Voltage stability is quite complex, and it is not the focus of this dissertation. Voltage stability of a DFIG in a distribution system is discussed in Chapter 6, Section 6.5.

Frequency stability is the ability of power systems to keep the frequency within an acceptable range following a system disturbance resulting in a significant unbalance between generation and load [35]. The nominal frequency range is usually 59.5~60.5 Hz in the U.S. From tens of cycles to several seconds, frequency control is normally provided by fast autonomous control of individual turbine generators (e.g., governor control). Over a slightly longer time frame, centralized automatic generation control (AGC) directs selected generators (hydro and steam plants) to adjust their output in order to satisfy both frequency and power flow objectives. In a still longer time frame, load following, unit dispatch, and switching off of some loads occurs to satisfy these requirements. Frequency instability may result when some generators/loads/transmission lines are switched off, some transmission lines are overloaded, and the whole system is split into subsystems. It is important to note that frequency stability cannot be classified as small signal stability and transient stability because it can affect any disturbance. Therefore, frequency stability is determined by the overall response of the whole system

(or each island if the system is split into islands) not only the relative generators or disturbances [35], [41]. Analyzing frequency stability is not within the scope of this dissertation.

2.2 System Stability Indicators

Assessing power systems stability performance is accomplished using several indicators. Based on the application of the swing equation and equal area criterion in simple power systems [35], critical clearing angle (CCA) and critical clearing time (CCT) indicate the borderline of a power system being subjected to a disturbance or a fault to regain steady state. The system can go to steady state as long as the synchronous machine rotor angle displacement of the rotor from the synchronously rotating reference axis is less than CCA or the fault clearing time is shorter than CCT [35]. Otherwise, the rotor angle of generators will increase without limits; and the system will lose synchronism when both CCA and CCT are surpassed. Therefore, CCA and CCT are often used as power system stability indicators. When a fault occurs in power systems, the difference between CCA and the actual clearing angle, or between CCT and the actual clearing time, is defined as the "stability margin" of the system (if there is a positive margin). However, when simulations or analysis are done in large power systems, CCA and CCT cannot be easily determined without considerable time-domain numerical integration calculation or time domain simulation runs [42]. In this case, additional practical indicators are used, namely, maximal rotor speed deviation and oscillation duration [43].

The maximum rotor speed deviation is classified as the maximum centralized synchronous generator rotor speed value attained during the transient phenomenon [43]. This indicator suggests that by increasing the rotor speed deviation from the rated value

after a disturbance, the system becomes increasingly unstable. The oscillation duration is defined as the time interval between the start of the disturbance and the instant after which the rotor speed stays within a bandwidth of 0.0001pu during a time interval longer than 2.5s [43].

This indicator implies that the longer the rotor speed oscillates from the rated value after a disturbance, the more unstable the system becomes. In other words, the smaller deviation of the rotor speed oscillates from the rated value after a disturbance, the more stable the system is. In the absence of damping, the rotor speed continuously oscillates and cannot reach convergence. It indicates that the system is unstable, and the generators lose synchronism.

Therefore, it is more efficient in terms of computation time to use these indicators rather than CCT/CCA. The indicators of maximum rotor speed deviation and the oscillation duration [43] are shown in Figure 2.3, and Equations (2.2) and (2.3) are used to quantify the indicators:

$$\text{maximum rotor speed deviation}=\left|\omega_{r,\max}-\omega_{r,nom}\Big/\omega_{r,nom}\right| \tag{2.2}$$

where $\omega_{r,\max}$ *and* $\omega_{r,nom}$ are the maximum and the rated rotor speed of a generator, respectively.

$$\text{oscillation duration}=t_{osc}-t_f \tag{2.3}$$

where t_f is the time when the fault happens, and t_{osc} is defined in Equation (2.4):

$$t_{osc}=\min\left\{t:\left|\omega_r(t+n\cdot\Delta t)-\omega_r(t)\right|\le 10^{-4};\ n=1,\mathrm{L}\ ,\frac{2.5}{\Delta t}\right\} \tag{2.4}$$

where $\omega_r(t)$ the rotor is speed at time t and Δt is the simulation step.

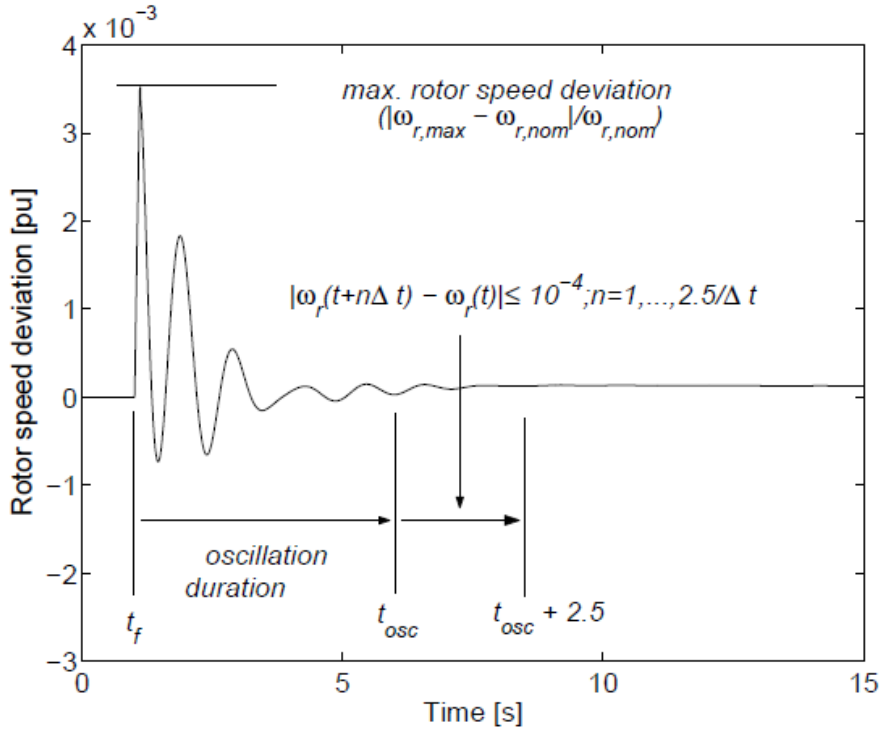

Figure 2.3. Transient stability indicators: maximum rotor speed deviation and oscillation duration.

2.3 Key Factors Influencing Wind Power Plant Systems Stability

Pollution free, virtually limitless and relatively low cost make WPP a viable option in the power generation mix. However, the variability and intermittency of WPP can create a tremendous challenge to power systems stability. With the rapidly increasing penetration of WPPs into the grid, it is vital to analyze wind power plant system stability. When considering the impact of WPPs on power system stability, it is necessary to be acquainted with system properties, location of wind resources, generator technologies, ESS, reactive power compensation, wind power forecast, etc. An important principle is that the problem has to be analyzed individually case by case. Several key factors will be discussed as follows.

2.3.1 Wind Turbine Generator Technologies

There are mainly three wind turbine generator technologies that have been installed to date:

- Type a. Fixed speed induction generator (FSIG).
- Type b. Doubly fed induction generator (DFIG).
- Type c. Direct drive synchronous generator (DRSG).

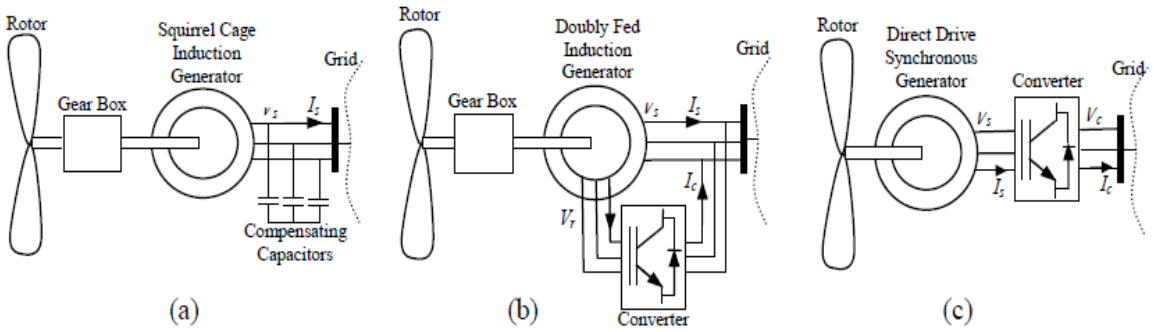

Figure 2.4. Three wind turbine generator models connected to the grid.

The diagram in Figure 2.4 shows all three kinds of wind turbine generator technologies. FSIG is simple and inexpensive; however, it has several disadvantages, as reported in [44]:

1. Lack of control of both active and reactive power output is possible.
2. Large fluctuations in output power.
3. Easy gearbox breakdown due to large fluctuations in output power.

With the recent developments in power electronics, DFIGs have become very popular, and the worldwide market share of DFIGs has reached more than 30% [45]. The rotor windings of DFIGs are connected to the grid through four-quadrant ac-dc-ac converters based on insulated gate bipolar transistors (IGBTs). Above synchronous speed, the converters operate as generators of active power delivering power to the grid parallel

to the stator windings of DFIGs. Below synchronous speed, they deliver active power from the grid into the rotor circuit. The converters, composed of two Pulse width modulation converters (PWM), are connected back to back by a DC link. The rotor-side converter (RSC) injects an AC voltage at slip frequency to the rotor circuit. The grid-side converter (GSC) works as a controlled voltage source by generating AC voltage at power frequency and keeping the DC link voltage constant. The main advantages of DFIGs are that they can operate in a wider wind speed range and produce or consume reactive power through controlling the grid-side converter. DFIGs also offer other advantages [45]:

1. Reduced converter cost, and converter rating is typically 30% of total power.
2. Easy power factor control and reactive power compensation at lower cost.
3. Reduced inverter filters cost.
4. Improved WT efficiency.

The large rotor inertia of a DFIG can smooth the variation of wind speed; and, as a result, it has fewer fluctuations in output power. The most important advantage is that a DFIG has uninterruptable operation and can successfully ride through grid faults with the selection of good converter control or other advanced control applications. Immediate disconnection of wind farms from power systems at the time of a fault, particularly with the high penetration condition, may create a significant problem in transient stability. Uninterruptable operation can be achieved by properly arranging the operation and quick control of converters to maximize power system transient stability [20].

A comparison between an FSIG and a conventional synchronous generator connected to an infinite bus is depicted in [46], and an FSIG has a strong characteristic against power system oscillation. The authors in [47] studied the different impacts of constant and variable speed wind turbines on New England power systems and point out that an improvement in transient behavior can be observed when an FSIG is replaced by a DFIG.

Direct-drive synchronous generators usually are one of two types: a synchronous generator with electrical excitation or a synchronous generator with permanent magnet excitation. The former appears to be the heaviest and most expensive when compared to other types, while Enercon (a wind turbine manufacturer) claims that it can improve reliability, including immunity to problems from voltage disturbances due to grid faults, as a result of the use of a fully rated converter [48]. However, the latter seems much more attractive because permanent magnet excitation eliminates the excitation losses with the highest energy yield [49-52].

In principle, a direct-drive permanent magnet synchronous generator (PMSG) could be the best solution in the future because it doesn't need brushes and a gear box; and it has the advantages of a fully rated converter, if cost is not a major factor. However, compared to an FSIG and a DFIG, the PMSG is more expensive and has greater volume because of its greater and more expensive permanent magnet excitation. Yet, further improvements of PMSG may be expected because the cost of the permanent magnets and the power electronics is decreasing; and further optimization and integration methods are possible [51-52].

Stability analysis of FSIGs and DFIGs has been discussed in many research projects while stability analysis of PMSG has not been thoroughly analyzed. The papers [53-54] present a detailed study of the transient stability of PMSG with a proposed control system considering various different types of symmetrical and nonsymmetrical faults. Simulation results show that the transient stability can be enhanced when a single line-to-ground fault occurs close to a PMSG, and the terminal voltage can return back to its prefault level. In [55-56], the two-mass drive train model is applied to evaluate the dynamic performance of the PMSG while the simulation results indicate that the output power of the PMSG is oscillating; and the system is prone to instability if no external damping is provided. In [57], the torque compensation strategy contains a feed-forward compensator in the torque control loop, which is formulated based on the DC current injected into the DC link capacitor of the converters. With such compensation, the oscillatory mode is effectively suppressed; and the stability of the PMSG is improved.

Unfortunately, there is a gap in the research when comparing the different impacts of stability of a DFIG and a PMSG. In [58], the authors use a power system analysis software package (PSASP) user-defined model to compare the operational difference between a DFIG and a PMSG. The results show that voltage fluctuation curves and system frequency response curves between two wind generators are almost the same when wind speed changes; however, the voltage stability and frequency stability of a DFIG is better than PSMG when considering faulted power systems. However, the conclusion is not solid and reliable.

Generally, the following conclusions can be drawn from all of those studies:

1. FSIGs, DFIGs, and PMSGs are, respectively, the old popular, now popular, and future popular wind turbine generator technologies.
2. An FSIG can improve power system transient stability; but in comparison with a DFIG, it is poor. A DFIG has a good ability to ride through faults. It can work as a power reactive compensator during faults. Therefore, a majority of wind farms are equipped with DFIGs.
3. Comparison of the different impacts on the stability of DFIGs and PMSGs is not sufficient, and there is no generally accepted conclusion to date.
4. Power system transient stability is noticeably degraded at high penetration levels due to the high reactive power demand of wind generators under some disturbances. Therefore, high penetration wind levels not only stop improving power system stability in comparison to low penetration levels, but can also decrease power systems stability in comparison to the case without WPPs under some disturbances. Therefore, calculating the penetration limit and margin is significantly important to system planning and operations.

2.3.2 Energy Storage System

An energy storage system (ESS) can store electrical energy during times of low demand at low energy cost and the stored energy can be released back to power systems during times of high demand at high energy cost or when there is a shortage in the generated capacity to meet demand. There are many energy storage technologies that have been used in power systems, each with its own different characteristics. In fact, ESS

can greatly balance the variability and intermittency of WPPs; so it is very useful in enhancing power systems stability, especially considering some disturbances [59-61].

In [59], the authors describe a power system stabilizer by utilizing the fast control of charging and discharging an ESS to improve the stability of an electric power system. This paper [60] presents a novel analytical method for studying the capability of an ESS installed in a power system to sufficiently damp the power system oscillations. It clearly and simply explains why and how an ESS can effectively suppress power system oscillations. In [61], it is shown that an ESS controlled via a robust control technique is an effective way of improving the low voltage ride-through (LVRT) capability and transient stability of fixed-speed wind turbines. The authors in [62] show the use of ESS (such as pumped-hydro storage (PHS) and compressed air energy storage (CAES)) to increase wind farm transient stability. Experiments with a 60-MW wind farm (FSIG or DFIG), show that ESS performance is better than that of a static var compensator (SVC); and ESS is more effective for FSIG than for DFIG. It increases the critical clearing time considerably and shortens the post-fault voltage recovery duration of a wind farm.

The important factors of an ESS for power systems are the construction cost, running cost, the round trip efficiency (RTE), storage capacity, discharge cycles, and lifetime. Based on these characteristics, each of these technologies is suitable for certain applications. The advantages and disadvantages of these technologies are as follows:

1. Battery Storage: There are several types of battery storage (lead acid, nickel cadmium, sodium sulphur, and lithium ion) in the industry and sizes range from 100W to several MW with round trip efficiency (60~80%). The main advantages include a very quick response time

(about 20 milliseconds) and less construction time [63]. However, the disadvantages include expensive the cost, periodic maintenance, and a limited life cycle.

2. Flywheel Storage: Flywheel storage uses the kinetic charge and discharge capability of a spinning wheel, and the round trip efficiency is about 80~85% [64]. The main advantages are less maintenance, long life cycle, quick recharge capability, and higher power density. On the other hand, the main disadvantages are small storage size and large stand-by losses.
3. Compressed Air Energy Storage (CAES): CAES uses the off-peak power to store energy by compressing air into a reservoir. The stored air is released, heated via combustion with a small amount of any type of fuel, and passed through turbines to generate electricity at peak. The round trip efficiency is around 73~79% [65]. The main advantages are high storage capacity, large size, quick start-up time, and easy geological requirements. However, the main disadvantages are the need for high energy input during the power production process and possible emission of greenhouse gas.
4. Pumped Hydro Storage (PHS): PHS can use or produce electricity through adjusting water between the base level reservoir and higher level reservoir, and the round trip efficiency is about 70~80% [65]. The main advantages are huge energy, large power capacity (up to 2000 MW), and the ability to store energy for a very long time (up to

six months). However, the main disadvantages are very high construction cost ($1,000/kW) and limited location with specific geographic, geologic, and environmental topography.

5. Hydrogen Storage (HS): HS consists basically of an electrolyzed unit that generates hydrogen (H2) using off-peak power. Hydrogen is compressed and stored in a storage system. Upon demand, the stored chemical energy in hydrogen is converted to electricity using a fuel cell. The round trip efficiency is around 60~85% [65]. The main advantages are zero CO2 emissions, cheaper storage for a longer time, higher energy density, and easier implementation in different size ranges from KW to several MW. However, the main disadvantages are the high flammability of hydrogen, high construction costs, and low efficiency.
6. Super-Capacitor Storage (SCS): SCS is also known as an electrochemical capacitor or electrical double-layer capacitor, and it is about 1,000 times smaller than traditional capacitors. SCS stores electrical energy in the electrical double layer at an electrode/electrolyte interface. The main advantages are high power density, long life cycle, quick recharge capability, easy installation, and higher efficiency [66]. Yet, the main disadvantages are very expensive cost (about five times of the same size of lead-acid batteries), low energy density, and power electronics requirement.

7. Superconducting Magnetic Energy Storage: SMES stores energy in a magnetic field by circulating a DC current through a superconducting coil which is cooled to -269 ºC and makes the resistance disappear. The main advantages are very high efficiency (around 98%) [66], very quick energy transfer (within 17 milliseconds), and unlimited charge and discharge cycles. On the other hand, the main disadvantages are high cost, low energy density, refrigeration losses, and AC-DC-AC losses.

Generally, it has been proven, in theories and experiments, that ESS can considerably improve the transient stability of WPPs. Considering storage capacity, response time, life time, and costs, the engineers can select suitable ESS to assist wind farms.

2.3.3 Reactive Power Compensation

The increasing effect of WPPs will influence the dynamic behavior of power systems by interacting with conventional generation and loads. Due to the inherent characteristics of wind turbines, no uniform power production causes variations in system voltage and frequency. Moreover, WPPs usually cannot produce enough reactive power, like the conventional synchronous generators. In this case, wind farms with FSIG connect to the medium voltage distribution systems directly, which represents a large percentage of the wind energy conversion systems around the world.

This is known as wind farm to weak grid connection, and its main problems are poor voltage regulation at the point of common coupling (PCC) and poor voltage stability.

Therefore, wind farms usually need high reactive power compensation to improve the voltage stability and transient performance during integration into the grid and the

operation of wind turbine groups. Generally, flexible AC transmission systems (FACTS) devices, such as static var compensator (SVC), static reactive compensator (STATCOM), dynamic voltage restorer (DVR), dynamic reactive compensation, etc., installed with wind farms can inject reactive power into the system, which helps in maintaining a better voltage stability.

The work in [67] describes how CCT of wind farms was increased based on reactive power compensation techniques. This paper [68] presents the design of a linear and a nonlinear coordinating controller between an SVC and the wind farm inverter at the point of interconnection. Results show that the voltage stability of the entire power system during small and large disturbances is improved. The simulation [69] results show that the stability margin of an FSIG can be significantly greater when there is extra reactive power compensation available from a DFIG in the vicinity. This paper [70] examines the use of STATCOM as a dynamic reactive power compensator at PCC to maintain stable voltage by protecting a DFIG-based wind farm interconnected to a weak distribution system during and after the disturbances. The results show that STATCOM mitigates the effects of transient disturbances, three-phase short circuit fault, step load change, voltage swelling and sagging in the system, and, hence, improves the stability and performance of the wind farm.

Therefore, reactive power compensation with wind farms has proven to be an effective, easy method to improve voltage stability, power quality, and operational characteristics of wind farms. Yet, the optimal location and reactive power compensation strategy may need more attention and will need to be considered on a case-by-case basis.

2.3.4 Wind Power Forecasting

The variability, intermittency, and non-displaced characteristics of WPPs can cause a stability problem. Power systems, in particular, need more operating reserve and more time to prepare for solving the intermittency of WPPs. Therefore, the electric industry depends on the wind power forecast to be exact. A more accurate forecast model of wind farms not only facilitates the integration of wind power with the grid but also forewarns the power system operators by providing weather alerts, thus improving system stability. It also aids in power system operations planning and economic dispatch:

- Prepare for upcoming high ramp rates of WPP by dispatching the generation and transmission systems to ensure supply reliability.
- Provide prediction information to plan for an ancillary services market in support of the intermittent wind power.
- Reduce operating reserve.
- Enable dispatching of quick-start generators in advance.
- Enable maximum WPP output by optimal operation scheduling.

Developing forecasting models is an overwhelming task due to the random and stochastic nature of wind. Generally, wind power forecasting includes several concepts [71]:

1. Definition: An average power $P_{t+k|\,t}$ is the expected power of a wind farm at time instant t for a look-ahead time t+k. The time step k represents the time resolution of the forecasts. The length of the time step depends on the length of the time horizon.

2. Forecast Objectives: They are defined by their applications. Power plant scheduling, power balancing, determination of wind speed and power, grid operation, and congestion management can be the applications.
3. Forecast Horizons: Depending on the time horizon, wind power forecasting can be categorized into three types: very short term, short term, and long term.
4. Forecast Data: The data required for wind power prediction are collected from wind farms via the Supervisory Control and Data Acquisition (SCADA) systems installed at each wind turbine, and data for weather forecasting can be obtained from National Weather Service Forecast Models.
5. Forecast Accuracy: The quality of wind power forecasting is determined by its accuracy. Mean absolute error (MAE), standard deviation of absolute error (STD), mean square error (MSE), root mean square error (RMSE), etc., are used to evaluate the prediction accuracy.

Building an accurate wind power forecasting model is a challenging task because of the need to cater to the high dimensional and random nature of wind. Wind power forecasting techniques are classified into three main groups: Physical Approach, Statistical Approach, and Learning Approach.

1. Physical Approach: It is comprised of several different physical processes, which translate the numerical weather prediction (NWP)

wind speed forecast at a certain grid point to a power forecast for a WT farm site at WT hub height. The mathematical description of the physical processes relevant to the translation is contained in each sub-module, including wind conditions at the site and the hub height of the turbines, wind turbine power curve, etc. [72].

2. Statistical Approach: The relation between historical measurements, meteorological predictions, and power output is realized through statistical models whose parameters are estimated from the historical data. After that, the statistical models can be used to obtain the power output in the time series without taking into account any physical phenomena [73].
3. Learning Approach: Artificial intelligence (AI) techniques (neural networks, fuzzy logic, etc.) are developed to learn the relationship between input data (NWP model predictions) and output data (power output). Subsequently, it uses algorithms that implicitly describe highly complex, nonlinear relationships between these data, unlike explicit statistical analysis used in the statistical approach [74].

However, it is difficult to compare the different techniques based on the available results because of the existing application differences (flat, complex terrain, altitude, land, offshore, etc.). The ultimate goal is to enhance the prediction accuracy and to develop models that can be the basis for predictive control. Generally, wind power forecasting plays an important role in enhancing the stability, efficiency, and reliability of modern power systems; and its importance is gradually increasing.

2.3.5 System Operations in High Wind Penetration Conditions

The high penetration of WPPs will profoundly affect the electric power industry and place greater demands on system operations. A number of studies [12-17] have been performed over the past decade to analyze the operational impacts that can occur at high penetration of WPPs. Some steps (most are system operations) can be taken to improve the ability to integrate the increasing amounts of wind capacity into power systems and the system stability. These include the following:

1. Improve WPP Models: Good models are a prerequisite to identifying and solving problems.
2. Improve WPP Operating Characteristics: For example, the ability of low voltage ride-through or the ability to provide an inertial response in a stability-constrained system can be critical to the reliable operation of power systems.
3. Upgrade and Expand Transmission Systems: Additional new transmissions will be required to tap these remote wind resources and bring them to market.
4. Make Better Use of Physically Available Transmission Capacity (in contrast with contractually): Hourly analysis of line loadings often shows that a line is heavily loaded for a very limited number of hours in the year. Development of a flexible-firm transmission product, which makes the unused capacity available for other transactions when the line is lightly loaded, could be accomplished with minor modifications to current practices. Improved

requirements of tracking power flow and dispatch method are greatly needed to use transmission system more effectively.

5. Incorporate Wind and WPP Output Forecasting into Utility Control Room Operations: This will also be the key to the future success of wind energy and can offer several advantages to system operators. The operating impact with the largest cost is determined to be in the unit-commitment time frame. Day-ahead WPP output forecasting offers significant opportunity to reduce the cost and risk associated with the uncertainty in the day-ahead time frame.
6. Improve the Capacity for Balancing the System: As additional wind capacity is added, greater regulation, load following, and quick-start capability will be required from the remaining generators. Operating reserve often needs to be increased correspondingly. The optimal generation mix will vary with the amount of wind in the system.
7. Evaluate Wind Integration Operating Impacts and Security Margin, Especially Stability, Reliability, and Frequency Control: The magnitude and frequency of occurrence of changes in the net load on the system in the time frames of interest (e.g., seconds, minutes, hours), before and after the addition of WPP, must be well understood to determine the additional requirements on the balance of the generation mix.
8. Better Use Flexible Resources: The most effective use of flexible resources including ESS, dispatchable hydropower and pumped

storage plants, reactive power compensation, FACTS, etc., should be considered.

9. Improve in Protection: Improved setting of the initial "pick-up" values for breakers makes them work in a more orderly fashion when a fault or power flow changes occur because of intermittency in wind power generation.
10. Islanded Operation in Distribution Systems.
11. Adopt Power Market Rules and Tariff Provisions More Appropriate for Weather-Driven Resources: Imbalance penalties that may discourage the behavior of fossil generators cannot be used to affect the behavior of a wind-driven resource. Weather-driven resources should pay the costs they incur, rather than be penalized for behavior they cannot control.
12. Consolidate Balancing Areas into Larger Entities or Access a Larger Resource Base Through the Use of Dynamic Scheduling or Some Form of ACE Sharing: These results [12] are corroborated by the New York State wind integration study which determined that the combined operation of the 11 zones in the New York State power system reduces hourly load variability by 5% and 5-minute load variability by 55%. Hourly wind variability is reduced by 33%, and 5-minute wind variability is reduced by 53% with state-wide operations. Hourly system variability is further reduced by 10%, and

5-minute system variability is reduced by 15% when wind and load are considered together.

13. Learn How to Best Operate a System with a High Penetration of Wind Energy: Some evidence proves that system operators will become more familiar with wind after working with it. For example, The Western Farmers Electric Cooperative recently conducted an analysis with the National Renewable Energy Laboratory on the operational impact of wind on its system. Initially, the system operators could not maintain the CPS-1 frequency standard at its pre-wind level. With experience, they became familiar with the wind system and brought CPS-1 into its pre-wind range [13].

This list is not exhaustive, and the items on the list are not mutually exclusive. Some combination of these items may significantly increase the ability of the grid to absorb increasing quantities of wind generation and system stability.

2.4 Interconnection Requirements and Grid Code

Wind plants are in a unique position for interconnection to the transmission grid system. As wind plants have grown to sizes that rival some conventional generation systems, the impact of these large plants on the electric grid has become an increasingly important issue. IEEE 1547 of 2003 and UL-1741 standards for interconnection and testing only apply to plants with an aggregate capacity of 10 MVA or less [86]. Small wind farms and small groups of turbines may fall into this category; but as wind farms have continually increased above this rate, new standards and regulations should be

developed. The Federal Energy Regulatory Commission issued Order 661 in 2005 to standardize interconnection of large wind energy systems.

1. IEEE 1547 Standards

   The standards developed by IEEE 1547 and further developed in UL-1741 focus on standardizing the interconnection of distributed resources (DR) of all types with electric power systems (EPS). IEEE 1547 is divided into four subsections that define the criteria and requirements for interconnection. Section 1547.1 contains the standardized testing required to verify that the equipment relevant to the interconnection is meeting the regulations put forth in the main section. Section 1547.2 is the technical background required to understand the concepts of 1547; it contains standard technical descriptions, schematics, guidance, and examples. Section 1547.3 develops standard monitoring procedures and identifies how important interconnection information will be exchanged. Lastly, Section 1547.4 develops standards for islanding conditions. UL-1741 is the expansion of IEEE 1547 and includes all DR connections and safety standards for interconnection equipment. Important standards developed that are relevant to small wind systems [87] include:

   A. Voltage regulation must not occur at the point of common coupling (PCC).
   B. Synchronization at the PCC may not cause more than ±5% voltage fluctuation on the EPS and must meet flicker requirements.

C. The EPS bus protectors must be energized to 50% before the DR can be connected. Inversely, the DR must not energize the EPS when it is de-energized.

D. Adding the DR cannot cause the network equipment to exceed loading and fault interrupting capacity.

E. Any aggregate DR connected to the grid that exceeds 250 KVA must be monitored.

F. Accessible breakers must be in place between DR and EPS.

G. Interconnection equipment must be able to withstand a voltage increase of 22% of rated values.

These are just a few important examples of the specific standards and requirements that are established by IEEE 1547.

2. FERC-661 Standards

The reason that FERC-661 was established was because the large wind farms are becoming important in transmission systems, and the same standards used for conventional generation plants do not work and result in unnecessary costs for wind systems. FERC-661 covers facilities that exceed 20 MW of production [88]. The ruling prevents unnecessary requirements from being applied to wind generators. It also assumes that all wind plants are nonsynchronous which is not true. The rulings of FERC often try to coincide with international standards, such as the International Electronic technical Commission ruling TC88, since many countries are ahead of the U.S. in the development of

standards. Many groups were involved in the ruling including the American Wind Energy Association (AWEA), North America Electric Reliability Council (NERC), and many transmission providers, manufacturers, and other research groups. The main areas discussed are low voltage ride-through (LVRT) capability, power factor design criteria, supervisory control and data acquisition (SCADA) capability, wind plant interconnection modeling, and self-study of interconnection.

3. Low Voltage Ride-Through Capability

   The commission rule is that the LVRT standard has to meet the requirements shown in Figure 2.5, but only if the System Impact Study (SIS) provided by the transmission provider requires them to be met. Also, the point of interconnection is adopted as the standard measurement of the voltage. The study uses a three-phase fault because it is the most severe. High voltage ride-through was rejected [88]. The wind generation plant must have low voltage-through capability down to 15% of the rated line voltage for 0.625 seconds; and it must be able to operate continuously at 90% of the rated line voltage, measured at the high voltage side of the wind plant substation transformers.

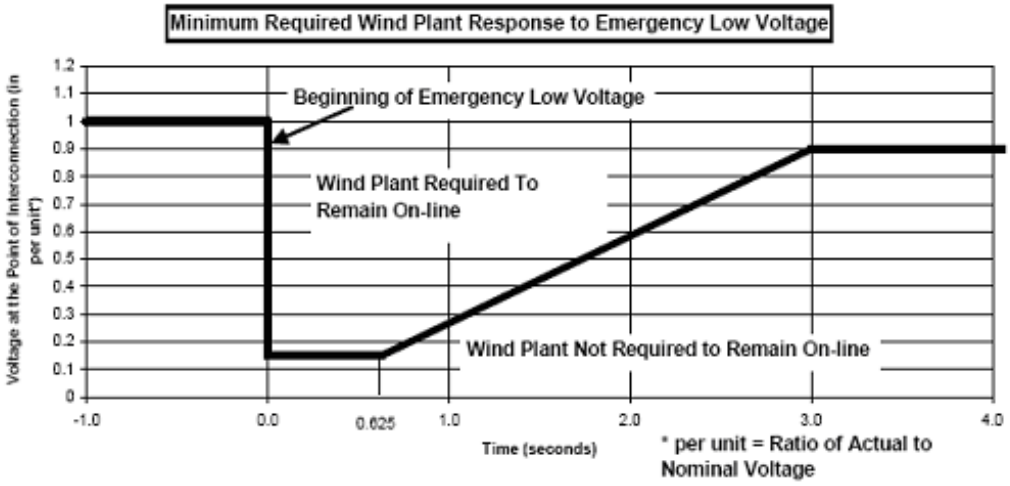

Figure 2.5. Proposed low voltage ride-through standards in [88].

4. Power Factor Design Criteria (Reactive Power)

   The Commission rules that the power factor must be within 0.95 lagging or leading at PCC. However, it is only required if the SIS shows that it is necessary. The Commission requires that the transmission provider shows it has reactive power capability for the wind plant interconnection customer.

5. SCADA Capability

   The Commission has adopted a requirement for the wind plant interconnection customer to have SCADA capability, and the necessary information is to be worked out with the transmission provider. It rejects the assertion that the transmission provider has full authority and that they cannot control the wind plant via SCADA.

6. Wind Plant Modeling

The Commission recommends that developers, manufacturers, transmission providers, and other interested groups work to improve and validate wind turbine models but has determined that the commission is not the appropriate avenue to make decisions on models.

6. Self-Study of Interconnection Feasibility

The Commission ruled that wind plant interconnection customers may satisfy the Interconnection Request using a single aggregate generator to represent the entire wind plant system because it is impossible for the wind plant to model individual turbines as they are too dynamic by themselves. Therefore, they can enter the queue with a satisfactory single generator model report and receive the base case data. Within six months, the WP interconnected customer must complete a detailed data specification so that the SIS can be completed.

In general, the Commission provides a set of guidelines but often leaves the actual requirements to be decided on a case-by-case basis between the transmission provider and the WP interconnection customer. FERC-661 is a flexible ruling that gives a lot of power to the parties that are involved, but it holds that the interconnection customer can appeal a decision by the transmission provider to the Commission. The Commission states that the ruling is to help facilitate wind power systems and preserve them from being unduly discriminated against. It also emphasizes work in the technical community to develop common regulations and standards that will lead to growth of wind energy and

bring down manufacturing and operating costs while ensuring the stability and reliability of all systems involved.

2.5 Small Signal Stability Analysis Model

The stability of power systems is a very complex issue because the nonlinear high-order differential equations which describe the dynamic components are very difficult to solve. When the disturbance is relatively small and power systems return to the initial steady state, the stability is defined as small signal stability. Therefore, the nonlinear high-order differential equations can be degraded to the ordinary first-order differential equations in small signal stability analysis to reduce the difficulties involved in solving them [35-37].

Power systems can be represented by a set of differential and algebraic equations (2.1). Here, x and y are the vectors of state and algebraic variables, respectively. Linearization of Equation (2.1) at an initial operating point $(\mathbf{x}_0, \mathbf{y}_0)$, which is obtained by the load flow calculations at this initial operating point, is given as [35]:

$$\begin{bmatrix} \mathbf{\Delta \dot{x}} \\ 0 \end{bmatrix} = \begin{bmatrix} \mathbf{A\,B} \\ \mathbf{C\,D} \end{bmatrix} \begin{bmatrix} \mathbf{\Delta x} \\ \mathbf{\Delta y} \end{bmatrix} \tag{2.5}$$

where

$$\mathbf{A} = \begin{bmatrix} \frac{\partial f_1}{\partial x_1} \cdots\cdots \frac{\partial f_1}{\partial x_n} \\ \vdots \\ \frac{\partial f_n}{\partial x_1} \cdots\cdots \frac{\partial f_n}{\partial x_n} \end{bmatrix}; \mathbf{B} = \begin{bmatrix} \frac{\partial f_1}{\partial y_1} \cdots\cdots \frac{\partial f_1}{\partial y_m} \\ \vdots \\ \frac{\partial f_n}{\partial y_1} \cdots\cdots \frac{\partial f_n}{\partial y_m} \end{bmatrix}; \mathbf{C} = \begin{bmatrix} \frac{\partial g_1}{\partial x_1} \cdots\cdots \frac{\partial g_1}{\partial x_n} \\ \vdots \\ \frac{\partial g_m}{\partial x_1} \cdots\cdots \frac{\partial g_m}{\partial x_n} \end{bmatrix}; \mathbf{D} = \begin{bmatrix} \frac{\partial g_1}{\partial y_1} \cdots\cdots \frac{\partial g_1}{\partial y_m} \\ \vdots \\ \frac{\partial g_m}{\partial y_1} \cdots\cdots \frac{\partial g_m}{\partial y_m} \end{bmatrix}. \tag{2.6}$$

n = the column number of the matrix; m= the row number of the matrix;

$$\mathbf{A} = [n \times n], \mathbf{B} = [n \times m], \mathbf{C} = [m \times n], \mathbf{D} = [m \times m], \begin{bmatrix} \mathbf{A\,B} \\ \mathbf{C\,D} \end{bmatrix} = [(n+m) \times (n+m)];$$

$$\mathbf{x} = \left[x_{1,} x_{2,} \cdots x_n \right]^T \quad and \quad \mathbf{y} = \left[y_{1,} y_{2,} \cdots y_m \right]^T;$$

$$\mathbf{f}(\mathbf{x},\mathbf{y}) = \begin{bmatrix} f_1(\mathbf{x},\mathbf{y}) \\ \vdots \\ f_n(\mathbf{x},\mathbf{y}) \end{bmatrix} \quad and \quad \mathbf{g}(\mathbf{x},\mathbf{y}) = \begin{bmatrix} g_1(\mathbf{x},\mathbf{y}) \\ \vdots \\ g_m(\mathbf{x},\mathbf{y}) \end{bmatrix};$$

Eliminating the algebraic variables and using the ordinary first-order differential equations:

$$\begin{cases} \mathbf{\Delta \dot{x} = A_{sys} \Delta x} \\ \mathbf{A_{sys} = A - BD^{-1}C} \end{cases} \tag{2.7}$$

$\mathbf{A_{sys}}$ is the state matrix of the system, and the eigenvalues ($\lambda_{1,}$ $\lambda_{2,} \sim \lambda_n$) of the state matrix can be obtained by solving the state equation (2.8).

$$\det(\mathbf{A_{sys}} - \lambda \mathbf{I}) = 0 \tag{2.8}$$

$$\lambda_i = \sigma_i \pm j\omega_i, \quad f_i = \omega_i / 2\pi, \quad i \in 1, \cdots, n. \tag{2.9}$$

λ_i is the ith eigenvalue of the system and only if all eigenvalues are on the left-half plane of four quadrants ($\sigma_i < 0$), the system is stable in a small signal sense. If one of the eigenvalues isn't on the left-half plane ($\sigma_i \geq 0$), the system is unstable in a small signal sense. Small signal stability analysis is the method that analyzes the stability margin of the dynamic system via calculating the eigenvalues of the state matrix. The farther the eigenvalues are on the left-half plane, the more stable the system.

The damping ratio is a measure of how rapidly the oscillations in the system decay following a disturbance. Here, the damping ratio of the ith eigenvalue is defined in Equation (2.10):

$$\xi_i = \left| \sigma_i / \sqrt{(\sigma_i^2 + \omega_i^2)} \right|, \ if \ \sigma_i < 0 \ and \ \omega_i \neq 0 \tag{2.10}$$

If the damping ratio is very small, the system oscillates for a long time to reach to the initial steady state; and the small signal stability is not acceptable. If the damping ratio is large enough, the system quickly goes to the initial steady state because the oscillation is well damped and the small signal stability is improved. Therefore, an optimization problem can be formulated to maximize the objective function:

$$F= \text{Max}\left\{\min(\xi_i)\right\},\ \ if\ \ \sigma_i < 0,\ \ \omega_i \neq 0\ \ and\ \ i \in 1,\cdots,n, \tag{2.11}$$

This will assure that the minimum damped eigenvalue is still heavily damped in the system's small signal stability analysis so that the oscillation quickly disappears. In a wind power integration system, some low-frequency oscillations are more cause for concern. Therefore, the optimization could also be adjusted to increase the damping ratio of the special low-frequency eigenvalues. In this dissertation, a particle swarm optimization (PSO) method is selected to optimize the low-frequency oscillation of DFIGs in Chapter 4.

CHAPTER 3
WIND TURBINES WITH DOUBLY FED INDUCTION GENERATORS

The difference among wind generator technologies (FSIG, DFIG, and PMSG) is based mostly on the electrical generation part (generator, power converter, and control algorithm) whereas the mechanisms to control the prime mover are generally similar. These mechanisms usually use mechanical brakes and blade pitch control to avoid runaway conditions and to keep the mechanical stresses on the mechanical components within the design tolerance for operating conditions. The pitch angle control is usually used in a high-wind-speed region to keep the aerodynamic power within limits so that the output power and rotor speed can be kept within their boundary limits. The advantages, disadvantages, and the impacts of the three wind generator technologies were discussed in Chapter 2.3.1. Chapter 3, however, will focus on wind turbines with DFIGs. Modern wind turbines with DFIGs usually include four subsystems: wind turbine, induction generator, converter system, and grid connection, as shown in Figure 3.1. This chapter will discuss the detailed mathematical models for each subsystem.

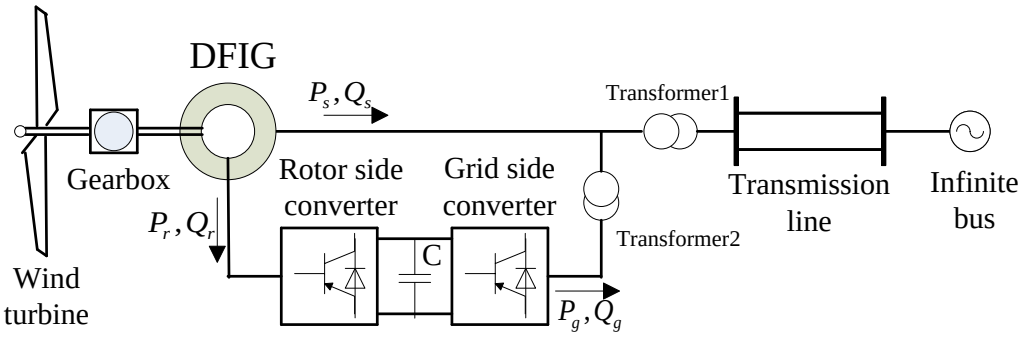

Figure 3.1. Wind turbine DFIG system in [26].

3.1 Wind Turbine Model

Aerodynamic power control of a wind turbine is based on the aerodynamic properties of the wind turbine rotor blade. There are two forces that act on the rotor disc: 1) edge force that builds up shaft torque (orthogonal to the free wind direction) and 2) thrust that imposes unwanted load on the turbine (parallel to the free wind direction). Methods for improving the aerodynamic properties of wind turbines are not the subject of this dissertation. In general, the mechanical power delivered to the shaft is a complex function of wind speed, blade pitch angle, and shaft speed [75].

$$P_m = 0.5\rho A_r v_w^3 C_p(\lambda, \beta) \tag{3.1}$$

where $\rho, A_r, v_w, \lambda, \beta, C_p$ are the air density, the area swept by the turbine blades, the wind speed, the tip-speed-ratio, the blade pitch angle, and the power coefficient, respectively. The power coefficient is a function of both tip-speed-ratio and the blade pitch angle and is given as $C_p(\lambda, \beta)$ curves which are provided by the wind turbine manufacturers. The tip-speed-ratio is defined in

$$\lambda = \omega_t R / v_w \tag{3.2}$$

where R is the blade length in m, and ω_t is the wind turbine rotor rotational speed in rad/s. In this dissertation, the mathematical representation of the $C_p(\lambda, \beta)$ curves used for the 3.6 MW wind turbine are obtained by curve fitting, given in [76]:

$$C_p(\lambda, \beta) = \sum_{i=0}^{4} \sum_{j=0}^{4} a_{ij} \beta^i \lambda^j \tag{3.3}$$

where the coefficients a_{ij} are given in [76]. At one certain wind speed, there is a unique wind turbine rotor rotational speed to achieve the maximum power coefficient ($C_{p\max}$)

to absorb the maximum mechanical power from the wind. If the wind speed is below the rated wind speed, the wind turbine operates in the variable speed mode; and the rotor rotational speed is adjusted by DFIG active power control so that C_p tracks at the $C_{p\max}$ point. In this operating mode, the pitch control does not function; and the pitch angle is usually fixed to zero. However, if the wind speed increases above the rated value, the pitch control works to increase the blade pitch angle in order to reduce the mechanical power absorbed from the wind for protecting the wind turbine system. In this dissertation, it is assumed that the wind turbine does not function in the high wind speed condition such that neglecting the pitch angle change and setting the power coefficient to the maximum value according to the unique wind speed are reasonable.

The shaft system of the wind turbine can usually be represented either by a two-mass system [75-77] or by a single lumped-mass system [78-81]. In the two-mass model, two separate masses are used to represent the low-speed rotational turbine and the high-speed rotational generator; and the connecting resilient shaft is modeled as a spring and damper, shown in Figure 3.2. The electromechanical dynamic equations [76] are then given by

$$2H_t p\omega_t = T_m - D_{tg}(\omega_t - \omega_r) - T_{tg} \tag{3.3}$$

$$2H_g p\omega_r = T_{tg} + D_{tg}(\omega_t - \omega_r) - T_e \tag{3.4}$$

$$pT_{tg} = K_{tg}(\omega_t - \omega_r) \tag{3.5}$$

where $p = d/dt$; $T_m, T_e, T_{tg}, \omega_t, \omega_r, H_t, H_g, D_{tg}, K_{tg}$ are the mechanical torque, the electrical torque, the internal torque, the turbine rotor speed, generator rotor speed, the inertia constants of the turbine and the generator, the damping coefficient of the shaft between

two masses, and the shaft stiffness, respectively. In Figure 3.2, Nt/Ng is the gear ratio of the gearbox.

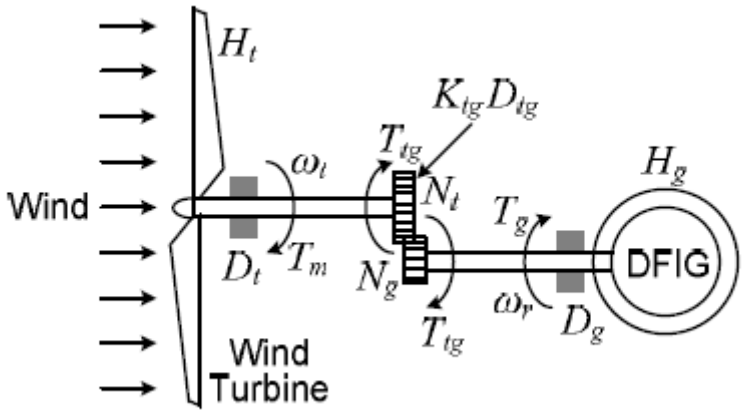

Figure 3.2. Wind turbine-DFIG shaft system represented by a two-mass model in [26].

In the single lumped-mass model [78], the shaft system is simply modeled as a single lumped mass with the lumped inertia constant H_m, calculated by

$$H_m = H_t + H_g \tag{3.6}$$

The electromechanical dynamic equation is then given by

$$2H_m p\omega_m = T_m - D_m\omega_m - T_e \tag{3.7}$$

where ω_m is the rotational speed of the lumped-mass system and $\omega_m = \omega_t = \omega_r$, D_m is the damping of the lumped system. The author [82] theoretically proves that there should be no low-frequency oscillations via the single lumped-mass model of a wind turbine. However, low-frequency oscillations of WTG were actually observed in many reports. Therefore, the single lumped-mass model might be insufficient to represent the dynamic behavior of a WTG system; therefore, it may not be a good choice for performing a stability analysis of a WTG. In this dissertation, a two-mass system model of a WTG was selected for investigation.

3.2 Induction Generator Model

The induction generator in this dissertation is a single-cage wound rotor induction machine. In terms of the instantaneous variables shown in Figure 3.1, the stator and rotor equations can be written as follows, in matrix form:

$$v_{sabc} = r_s i_{sabc} + p\lambda_{sabc} \tag{3.8}$$

$$v_{rabc} = r_r i_{rabc} + p\lambda_{rabc} \tag{3.9}$$

Applying synchronously rotating reference frame transformation [83] to Equations (3.8) and (3.9), the voltage and the flux linkage equations become:

$$v_{ds} = r_s i_{ds} - \omega_s \lambda_{qs} + p\lambda_{ds} \tag{3.10}$$

$$v_{qs} = r_s i_{qs} + \omega_s \lambda_{ds} + p\lambda_{qs} \tag{3.11}$$

$$v_{dr} = r_r i_{dr} - (\omega_s - \omega_r)\lambda_{qr} + p\lambda_{dr} \tag{3.12}$$

$$v_{qr} = r_r i_{qr} + (\omega_s - \omega_r)\lambda_{dr} + p\lambda_{qr} \tag{3.13}$$

$$\lambda_{ds} = L_s i_{ds} + L_m i_{dr} \tag{3.14}$$

$$\lambda_{qs} = L_s i_{qs} + L_m i_{qr} \tag{3.15}$$

$$\lambda_{dr} = L_m i_{ds} + L_r i_{dr} \tag{3.16}$$

$$\lambda_{qr} = L_m i_{qs} + L_r i_{qr} \tag{3.17}$$

where $v_{ds}, v_{qs}, v_{dr}, v_{qr}, i_{ds}, i_{qs}, i_{dr}, i_{qr}, \lambda_{ds}, \lambda_{qs}, \lambda_{dr}, \lambda_{qr}, \omega_s, \omega_r, r_s, r_r$ are the d/q axis stator voltages, the d/q axis rotor voltages, the d/q axis stator currents, the d/q axis rotor currents, the d/q axis stator flux linkages, the d/q axis rotor flux linkages, the synchronous reference speed, the generator rotor speed, the stator resistors, and the rotor resistor, respectively. Also, $L_s = L_{ls} + L_m, L_r = L_{lr} + L_m, ; L_{ls}, L_{lr}, L_m$ are the stator leakage inductance, the rotor

leakage inductance, and the mutual inductance, respectively. The stator transient voltage equations in [84] become:

$$e'_{ds} = -\omega_s \lambda_{qr} L_m / L_r \tag{3.18}$$

$$e'_{qs} = \omega_s \lambda_{dr} L_m / L_r \tag{3.19}$$

where e'_{ds}, e'_{qs} are the d and q axis stator transient voltages, respectively. Substituting (3.18) and (3.19) into (3.16) and (3.17), they can be gotten:

$$i_{dr} = \frac{e'_{qs}}{L_m \omega_s} - \frac{L_m i_{ds}}{L_r} \tag{3.20}$$

$$i_{qr} = \frac{-e'_{ds}}{L_m \omega_s} - \frac{L_m i_{qs}}{L_r} \tag{3.21}$$

In order for the rotor mmf to be in synchronism with the stator mmf, the frequency of the rotor current, ω_{rf} must satisfy the slip frequency constraint: $\omega_{rf} = \omega_s - \omega_r = s\omega_s$. The flux linkage variables are now eliminated by substituting (3.18), (3.19), (3.20), and (3.21) into (3.12) and (3.13), as:

$$pe'_{ds} = s\omega_s e'_{qs} - \frac{r_r e'_{ds}}{L_r} - r_r \omega_s i_{qs} \frac{L_m^2}{L_r^2} - \omega_s v_{qr} \frac{L_m}{L_r} \tag{3.22}$$

$$pe'_{qs} = -s\omega_s e'_{ds} - \frac{r_r e'_{qs}}{L_r} + r_r \omega_s i_{ds} \frac{L_m^2}{L_r^2} + \omega_s v_{dr} \frac{L_m}{L_r} \tag{3.23}$$

Substituting (3.14), (3.15), (3.20), and (3.21) into (3.10) and (3.11), results in:

$$\begin{aligned} \frac{L_m^2 - L_s L_r}{L_r} pi_{ds} = -v_{ds} + r_s i_{ds} - \frac{r_r e'_{qs}}{L_r \omega_s} - \left(\omega_r - \omega_s\right) e'_{ds} / \omega_s \cdots \\ \cdots + r_r \omega_s^2 i_{ds} \frac{L_m^2}{L_r^2} + \omega_s^2 v_{dr} L_m / L_r - L_s \omega_s i_{qs} - L_m \omega_s i_{qr} \end{aligned} \tag{3.24}$$

$$\frac{L_m^2 - L_s L_r}{L_r} p i_{qs} = -v_{qs} + r_s i_{qs} + \frac{r_r e'_{ds}}{L_r \omega_s} - \left(\omega_r - \omega_s\right) e'_{qs} / \omega_s \cdots$$
$$\cdots + r_r i_{qs} \frac{L_m^2}{L_r^2} + v_{qr} L_m / L_r + L_s \omega_s i_{ds} + L_m \omega_s i_{dr} \tag{3.25}$$

Equations (3.22), (3.23), (3.24), and (3.25) will be used later in small signal stability analysis. Also, the per-unit electromagnetic torque equation is given by:

$$T_e = \lambda_{ds} i_{qs} - \lambda_{qs} i_{ds} = \lambda_{qr} i_{dr} - \lambda_{dr} i_{qr} = L_m (i_{qs} i_{dr} - i_{ds} i_{qr}) \tag{3.26}$$

Neglecting the power losses associated with the stator and rotor resistances, the active and reactive stator powers are given by:

$$P_s = \frac{3}{2}(v_{ds} i_{ds} + v_{qs} i_{qs}) \tag{3.27}$$

$$Q_s = \frac{3}{2}(v_{qs} i_{ds} - v_{ds} i_{qs}) \tag{3.28}$$

The active and reactive rotor powers are given by:

$$P_r = \frac{3}{2}(v_{dr} i_{dr} + v_{qr} i_{qr}) \tag{3.29}$$

$$Q_r = \frac{3}{2}(v_{qr} i_{dr} - v_{dr} i_{qr}) \tag{3.30}$$

3.3 Rotor-Side Converter and Grid-Side Converter Model

The rotor windings of a DFIG are connected to the grid through four-quadrant AC-DC-AC converters based on insulated gate bipolar transistors (IGBTs). Above synchronous speed, the converters operate as a generator of active power delivering power to the grid parallel to the stator windings of a DFIG. Below synchronous speed, they absorb active power from the grid into the rotor circuit. The converters compose of two Pulse width modulation converters (PWM) connected back-to-back by a DC link.

The rotor side converter (RSC) injects an AC voltage at slip frequency to the rotor circuit. The objective of the RSC is to govern both the stator-side active and reactive powers independently. The grid side converter (GSC) works as a controlled voltage source by generating an AC voltage at power frequency and keeps the DC link voltage constant. The reactive power control by the RSC and GSC is necessary to keep the voltage within the desired range when the DFIG feeds into a weak power system with insufficient local reactive compensation. The main advantages of a DFIG are that it can operate in a wider wind speed range and produce or consume reactive power by controlling the grid-side converter.

The overall vector control scheme of the RSC and GSC circuit was investigated in [82] and is shown in Figure 3.3. In the RSC, in order to achieve independent control of the stator active power Ps (by means of speed control) and reactive power Qs (by means of rotor current regulation), the instantaneous three-phase rotor currents i_{rabc} are sampled and transformed to d-q components i_{dr} and i_{qr} in the stator-flux oriented reference frame. Subsequently, Qs and Ps (thus the generator rotor speed ω_r) can be represented as functions of the individual current components. Therefore, the reference values of i_{dr} and i_{qr} can be determined directly from the Qs and ω_r commands. The actual d-q current signals of the rotor (i_{dr} and i_{qr}) are then compared with their reference signals to generate the error signals, which are passed through two PI controllers to form the voltage signals of the rotor (v_{dr1} and v_{qr1}). The two voltage signals (v_{dr1} and v_{qr1}) are compensated by the corresponding cross-coupling terms to form the d-q voltage signals (v_{dr} and v_{qr}). They are then used by the PWM module to generate the IGBT gate control signals to drive the IGBT converter.

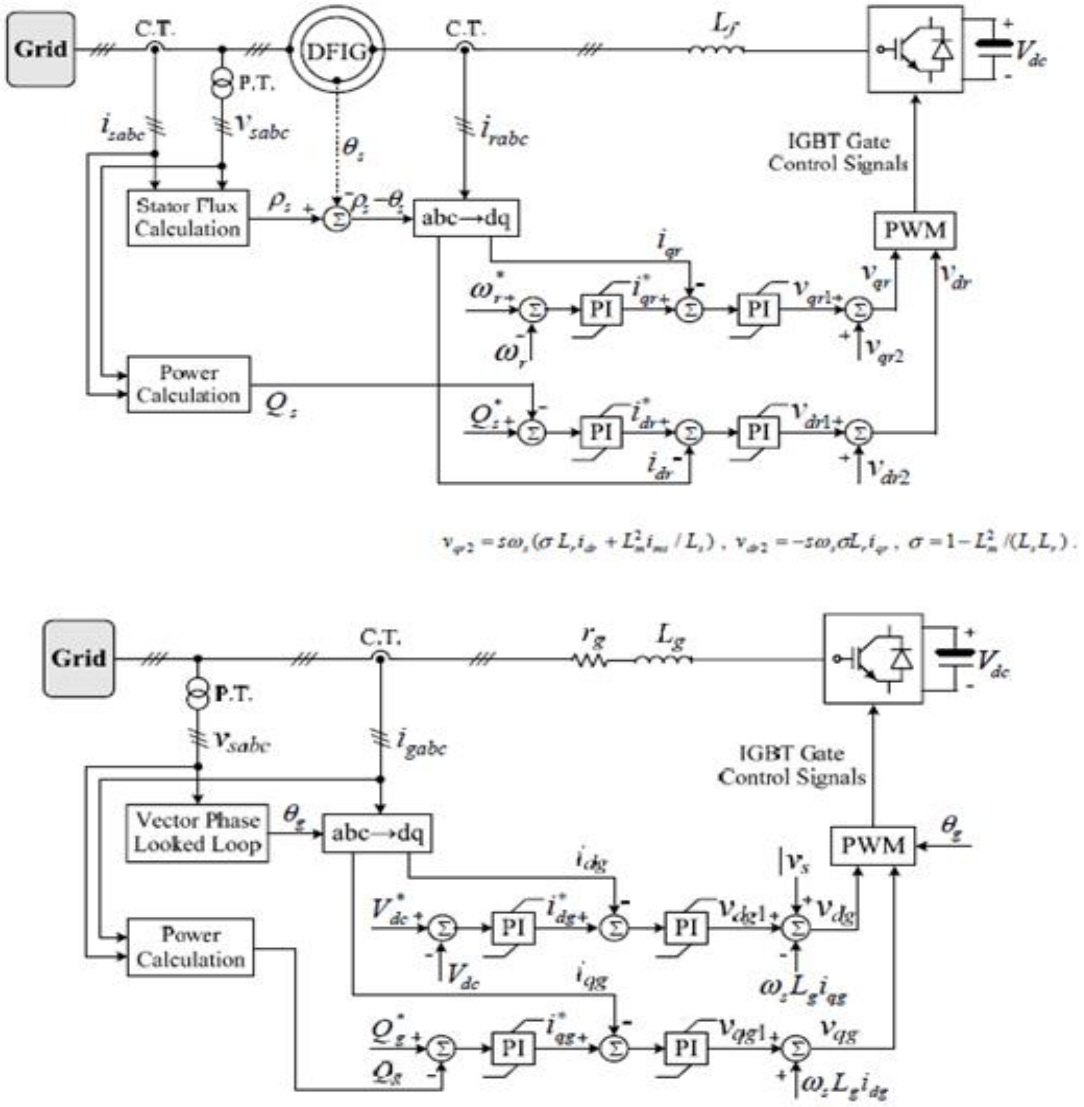

Figure 3.3. Overall vector control scheme of the RSC and GSC of a DFIG in [26],

In the GSC, in order to achieve independent control of the DC-link voltage and the GSC reactive power (V_{dc} and Qg), they are compared with their reference values to form the error signals, which are passed through the PI controllers to generate the reference signals for the d-axis and q-axis current components of the GSC. The instantaneous AC-side, three-phase current of the GSC is sampled and transformed into d-axis and q-axis current components i_{dg} and i_{qg} by applying the synchronously rotating reference frame transformation. The actual signals (i_{dg} and i_{qg}) are then compared with

the corresponding reference signals to form the error signals, which are passed through two PI controllers to form the voltage signals of the GSC (v_{dg1} and v_{qg1}). They are compensated by the corresponding cross-coupling terms to form the d-q voltage signals (v_{dg} and v_{qg}). They are then used by the PWM module to generate the IGBT gate control signals to drive the IGBT converter. The RSC and GSC control block diagram, based on Figure 3.3 and [82], is shown in Figure 3.4; and the equations follow:

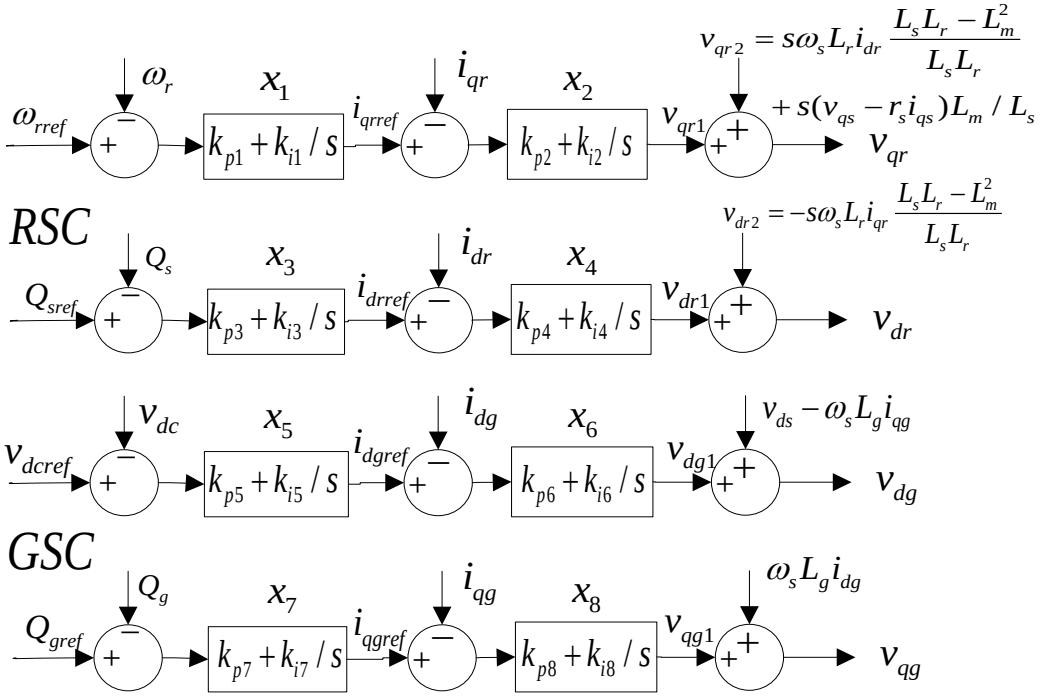

Figure 3.4. The RSC and GSC control block diagram.

$$px_1 = \omega_{rref} - \omega_r \tag{3.31}$$

$$i_{qrref} = k_{p1}(\omega_{rref} - \omega_r) + k_{i1}x_1 \tag{3.32}$$

$$px_2 = i_{qrref} - i_{qr} = k_{p1}(\omega_{rref} - \omega_r) + k_{i1}x_1 - i_{qr} \tag{3.33}$$

$$\begin{aligned} v_{qr} = v_{qr1} + v_{q2} = k_{p2}k_{p1}(\omega_{rref} - \omega_r) + k_{p2}k_{i1}x_1 - k_{p2}i_{qr} + k_{i2}x_2 \cdots \\ \cdots s\omega_s L_r i_{dr}(L_s L_r - L_m^2)/(L_s L_r) + s(v_{qs} - r_s i_{qs})L_m / L_s \end{aligned} \tag{3.34}$$

$$px_3 = Q_{sref} - Q_s \tag{3.35}$$

$$i_{drref} = k_{p3}(Q_{sref} - Q_s) + k_{i3}x_3 \tag{3.36}$$

$$px_4 = i_{drref} - i_{dr} = k_{p3}(Q_{sref} - Q_s) + k_{i3}x_3 - i_{dr} \tag{3.37}$$

$$\begin{aligned} v_{dr} = v_{dr1} + v_{dr2} = k_{p4}k_{p3}(Q_{sref} - Q_s) + k_{p4}k_{i3}x_3 - k_{p4}i_{dr} \cdots \\ \cdots + k_{i4}x_4 - s\omega_s L_r i_{qr}(L_s L_r - L_m^2)/(L_s L_r) \end{aligned} \tag{3.38}$$

$$px_5 = v_{dcref} - v_{dc} \tag{3.39}$$

$$i_{dgref} = k_{p5}(v_{dcref} - v_{dc}) + k_{i5}x_5 \tag{3.40}$$

$$px_6 = i_{dgref} - i_{dg} = k_{p5}(v_{dcref} - v_{dc}) + k_{i5}x_5 - i_{dg} \tag{3.41}$$

$$\begin{aligned} v_{dg} = v_{dg1} + v_{ds} - \omega_s L_g i_{qg} = k_{p6}k_{p5}(v_{dcref} - v_{dc}) + k_{p6}k_{i5}x_5 \cdots \\ \cdots - k_{p6}i_{dg} + k_{i6}x_6 + v_{ds} - \omega_s L_g i_{qg} \end{aligned} \tag{3.42}$$

$$px_7 = Q_{gref} - Q_g \tag{3.43}$$

$$i_{qgref} = k_{p7}(Q_{gref} - Q_g) + k_{i7}x_7 \tag{3.44}$$

$$px_8 = i_{qgref} - i_{qg} = k_{p7}(Q_{gref} - Q_g) + k_{i7}x_7 - i_{qg} \tag{3.45}$$

$$\begin{aligned} v_{qg} = v_{qg1} + \omega_s L_g i_{dg} = k_{p8}k_{p7}(Q_{gref} - Q_g) + k_{p8}k_{i7}x_7 \cdots \\ \cdots - k_{p8}i_{qg} + k_{i8}x_8 + \omega_s L_g i_{dg} \end{aligned} \tag{3.46}$$

The RSC and GSC are connected by a large capacitor (C) to decouple. The parameter ω_{rref} is the reference for the generator rotor speed which is determined by WT power speed characteristics for maximum power extraction [26]. Parameters $Q_{sref}, Q_{gref}, and v_{dcref}$ are the reference set points of stator and GSC reactive power and the capacitor voltage; and they are set to 0, 0, and 4KV, respectively. Parameters $k_{pi}, k_{ii}, x_i \ (i = 1, \cdots, 8),\ v_{dg}, v_{qg,} i_{dg}, i_{dg}, L_g, s$ are the proportional gains/integrating

gains of PI controllers, the state variables, the d/q axis voltage/current/inductance of the GSC winding, and the slip, respectively. By neglecting losses and harmonics, the power balance equation (between real power of the RSC and real power of the GSC) is given by:

$$P_r - P_g = Cv_{dc} Pv_{dc} \approx Cv_{dcref} Pv_{dc} \tag{3.47}$$

3.4 Interfacing with Power Grid

Considering the single machine connected to the infinite bus (SMIB) system as an example, shown in Figure 3.1, the voltage equation can be obtained:

$$V_s \angle\theta - V_{grid} \angle 0 = jx_{TL}(-I_s - I_g) \tag{3.48}$$

where $V_{grid} \angle 0$ is the voltage of the infinite bus; $V_s \angle\theta$ is the terminal voltage of the DFIG stator winding; x_{TL} is the combined reactance of the transformer and transmission line, which is given by $x_{TL} = x_T + x_L$, and I_s, I_g are the currents of the DFIG stator winding and the GSC. Neglecting losses and applying the d/q frame transformation to the point at which the DFIG connects with the grid and the GSC connects with the stator winding, the voltage equations are given by:

$$\begin{bmatrix} v_{ds} \\ v_{qs} \end{bmatrix} = \begin{bmatrix} \cos\theta \\ -\sin\theta \end{bmatrix} V_{grid} - \begin{bmatrix} 0 & -x_{TL} \\ x_{TL} & 0 \end{bmatrix} \begin{bmatrix} i_{ds} + i_{dg} \\ i_{qs} + i_{dg} \end{bmatrix} \tag{3.49}$$

$$\begin{bmatrix} v_{ds} \\ v_{qs} \end{bmatrix} = \begin{bmatrix} v_{dg} \\ v_{qg} \end{bmatrix} + \begin{bmatrix} 0 & -x_{tg} \\ x_{tg} & 0 \end{bmatrix} \begin{bmatrix} i_{dg} \\ i_{qg} \end{bmatrix} \tag{3.50}$$

where x_{tg} is the combined reactance of the transformer and the GSC winding between the GSC and the stator winding, and more details can be found in [27]. By linearizing Equations (3.49) and (3.50):

$$\begin{bmatrix} \Delta v_{ds} \\ \Delta v_{qs} \end{bmatrix} = -\begin{bmatrix} 0 & x_{TL} \\ -x_{TL} & 0 \end{bmatrix} \begin{bmatrix} \Delta i_{ds} + \Delta i_{dg} \\ \Delta i_{qs} + \Delta i_{dg} \end{bmatrix} \tag{3.51}$$

$$\begin{bmatrix} \Delta v_{ds} \\ \Delta v_{qs} \end{bmatrix} = \begin{bmatrix} \Delta v_{dg} \\ \Delta v_{qg} \end{bmatrix} + \begin{bmatrix} 0 & -x_{tg} \\ x_{tg} & 0 \end{bmatrix} \begin{bmatrix} \Delta i_{dg} \\ \Delta i_{qg} \end{bmatrix} \tag{3.52}$$

3.5 Small Signal Stability Analysis with WT-DFIG

In Chapter 2, it was shown that a power system can be represented by a set of differential and algebraic equations (2.1):

$$\begin{cases} \dot{\mathbf{x}} = \mathbf{f(x, y)} \\ \mathbf{0} = \mathbf{g(x, y)} \end{cases}$$

In the SMIB-DFIG system, the 16 differential equations include (3.3), (3.4), (3.5), (3.22), (3.23), (3.24), (3.25), (3.31), (3.33), (3.35), (3.37), (3.39), (3.41), (3.43), (3.45) and (3.47); and the ten algebraic equations include (3.20), (3.21), (3.34), (3.38), (3.42), (3.46), (3.51) and (3.52). Linearizing, and substituting the algebraic equations into the differential equations, it can get the state equation (2.7): $\mathbf{\Delta \dot{x} = A_{sys} \Delta x}$

The column vector of 16 state variables is:

$$\mathbf{x}=[e'_{ds}, e'_{qs}, i_{ds}, i_{qs}, x_1, x_2, x_3, x_4, x_5, x_6, x_7, x_8, v_{dc}, \omega_t, \omega_r, T_{tg}].$$

The column vector of ten other variables is:

$$\mathbf{y}=[v_{ds}, v_{qs}, v_{dr}, v_{qr}, v_{dg}, v_{qg}, i_{dr}, i_{qr}, i_{dg}, i_{qg}].$$

Variables $P_r, P_g, Q_s, Q_g, \omega_{rref}, Q_{sref}, and\ v_{dcref}$ are dependent variables and are easily replaced by the state and other variables and the initial values/set points. In per unit, the mechanical torque T_m and the electrical torque T_e are easily replaced by:

$$T_m = P_m / \omega_t \ and \ T_e = L_m(i_{qs} i_{dr} - i_{ds} i_{qr}) \tag{3.52}$$

The damping ratios of the eigenvalues of the state equation can be solved by the approach shown in Chapter 2. Therefore, the optimization problem can be formulated to maximize the objective function:

$$F= \text{Max}\left\{\min(\xi_i)\right\},\ \ if\ \ \sigma_i < 0,\ \ \omega_i \neq 0\ \ and\ \ i \in 1,\cdots,n, \tag{2.11}$$

There are 16 control variables in Figure 3.4: K_{ii} and K_{pi} of DFIG PI controller parameters, i=1,...,8 because there are eight PI gains in one DFIG model.

Constraints: K_{ii} and K_{pi} are in the range $[K_{iimin}, K_{iimax}]$ and $[K_{pimin}, K_{pimax}]$, respectively.

Through optimization calculation of one special operating point, it hopes to find the optimal values of K_{ii} and K_{pi} to make the damping ratios to be large enough so that the small signal stability and the transient performance of a DFIG system will be improved. In wind power integration systems, low-frequency oscillations are of more cause for concern. Therefore, the optimization could also be adjusted to increase the damping ratio of the special low-frequency eigenvalues. This will ensure that the low frequency oscillations (frequency in 0.5~1.5Hz) are well damped. In this dissertation, particle swarm optimization (PSO) will be the optimization method used to optimize the low-frequency oscillation of a DFIG system; and it will be introduced in Chapter 4.

3.6 Impact of Crow-bar Activation

In a DFIG system, in order to produce electrical power at constant voltage and frequency for the utility grid over a wide operating range from sub-synchronous to super-synchronous speed, the power flow between the rotor circuit and the grid must be controlled, both in magnitude and in direction. When the stator voltage suddenly drops to a low value during a fault, high rotor currents can be induced correspondingly. Such over-current transients may occur when fluxes are forced to change suddenly. Even

though these currents only exist for a quite short period of time, they may damage or even destroy the RSC. In order to prevent the over-current transients, a crow-bar protection is activated; and the rotor winding is short-circuited through one small resistance. Under this condition, the machine no longer operates as a DFIG but works as a conventional induction machine which has no control over real power and reactive power. This is one of the simplest and the lowest cost techniques to improve DFIG transient performance, and it was analyzed in [18-20] and [89-91].

During the transients of the crow-bar activation [18], a DFIG may operate anywhere from absorbing active power (motor) to supplying active power (generator), depending on the pre-disturbance speed of the rotor. Moreover, absorption of reactive power depends on the deviation from the synchronous speed. The simulation results in [18] show that the turbine is operating in steady state at sub-synchronous speed; then during the transients, the DFIG behaves as a decelerated induction motor and consumes a significant amount of P and Q. If the turbine is operating in steady state at super-synchronous speed, the DFIG can still produce P and consumes Q during the transients. The effects of crow-bar impedance and the RSC restarting are explained below:

- Effect of Crow-bar Impedance: If the crow-bar impedance is very small or near zero, the rotor current will show a large oscillatory response during the transients of the crow-bar activation; and even if the RSC tries to resume its control many times, system voltage will oscillate to collapse. However, when a small impedance (such as $2R_r$) is inserted, oscillations are sufficiently damped and the machine remains stable. It behaves like an over-speeding induction machine and consumes a large amount of Q when the crow-bar

protection is active. Further increase in crow-bar impedance (such as $200R_r$) would make rotor currents that are too low, which will lead to unnecessary electrical torque reduction and over-speeding of the turbine during the disturbance. In [18], the crow-bar impedance (from $10R_r$ to $100R_r$) was found to result in a satisfactory performance.

- Effect of the RSC Restarting: During the transients of the crow-bar activation, the machine loses control of real and reactive power; and it may absorb a large amount of Ps and Qs. This does not have a good effect on grid safety, and the RSC should be restarted as soon as the rotor currents decrease to a safe value to prevent instability. However, restarting the RSC very soon, especially during the voltage sag, may cause the converter to trip again at the fault clearance due to significant voltage (hence flux) change, leading to high induced currents. Therefore, even though a fast restart of the RSC may result in increased power quality, serious analysis should be required in order to provide reliable operation. In [18], it is observed that the machine can result in a satisfactory performance if the RSC restarts after the fault clears 200ms later.

With the quick development of DRs, grid code requires higher requirements of the capability of LVRT. Therefore, many experts try to find new control algorithms or power electronic circuit designs to improve WPP's LVRT capability, not through the crow-bar activation. The work mainly focuses on optimizing control parameters, new control algorithms for converters, advanced DC-link designs, adding ESS, adding PSS to WPP, etc. These are not the key points of this dissertation, so no more details will be discussed.

CHAPTER 4
OPTIMIZATION OF WIND TURBINES WITH DOUBLY FED INDUCTION GENERATORS

Generally, mathematical optimization usually includes finding the best available values (maximum or minimum) of a given objective function for a defined domain with regard to a set of constraints, which is widely applied in every walk of life in modern society, especially in power systems. How to operate power systems to achieve high performance in a more stable, reliable, secure, efficient, and more economical manner under various constraints is referred to as power system optimization. It is mainly divided into optimal power flow (economic dispatch/resource schedule), optimal reactive power compensation, optimal generation planning/capacity/location, optimal distribution, optimal power systems stabilizer design, optimal electrical equipment design, etc. Essentially, power system optimization is still a mathematical optimization problem; however, the solution sometimes isn't a strict mathematical solution because it has many practical constraints and requires an accurate, robust, and relatively short computational time.

4.1 Introduction to Optimization of a Wind Turbine Generator

Generally, optimization of a wind turbine generator is included in optimal electrical equipment design; and it usually focuses on real power output, reactive power output, the transient performance/system stability, equipment safety, and fault ride-through capability. Optimal real power output usually pays more attention to wind turbine blade pitch angle control, generator rotor speed control (according to wind turbine power speed characteristics for maximum power extraction), gearbox ratio, and converter

control. Equipment safety can be enhanced by reducing the over-current/over-voltage in converters or generator rotor winding and the mechanical torque fluctuation in the gearbox. The reactive power output/transient performance/system stability/fault ride-through capability can be addressed through advancement of converters/circuits controls in order to realize the specific goals. This dissertation will focus on improving the transient performance/system stability via adaptive optimal PI gains control of DFIG converters based on small signal stability analysis. The process will be divided into two steps. The first step is optimization of PI gains values of DFIG converters, and it will be illustrated in this chapter. The second step is adaptive optimization control according to different operating points, and it will be explained in Chapter 5.

In Chapters 2 and 3, the optimization problem can be formulated to maximize the objective function:

$$\text{F= Max}\left\{\min(\xi_i)\right\},\ \ if\ \ \sigma_i < 0,\ \ \omega_i \neq 0\ \ and\ \ i \in 1,\cdots n, \tag{2.11}$$

$\xi_i = \sigma_i + \omega_i, and\ \xi_i$ is the eigenvalue of system state equation $\mathbf{\Delta\dot{x} = A_{sys}\Delta x}$, (2.7). Control variables K_{ii} and K_{pi} are DFIG PI gain controller parameters, i=1,...,8 (16 control variables). Equation 2.11 makes sure that the minimum damped eigenvalue is heavily damped in system small signal stability analysis. Constraints of K_{ii} and K_{pi} are in the range $[K_{iimin}, K_{iimax}]$ and $[K_{pimin}, K_{pimax}]$, respectively.

This is a typical multi-variable optimization problem, and there are no fast and easy solutions because of the large number of control variables.

4.2 Classification of Mathematical Optimization Techniques

Generally, there are two different types of techniques for solving optimization problems.

1. Gradient techniques: they can move toward convergence through iterative calculations according to one specific direction, such as gradient direction. The typical techniques [92] include Newton's method, Quasi-Newton methods, Gradient descent method, Reduced gradient method, etc. The main disadvantage of this type of techniques is that the computational time may be excessively high because it usually needs the second order derivatives when it attempts to determine the specific direction [93-94].
2. Search techniques: they also attempt to search and determine the convergence point in a search space, even though the specific direction to the convergence point is unknown [95]. This type of technique has a lower computational time due to lack of a second order derivatives calculation when compared to the gradient techniques.

More importantly, the gradient techniques have worse performance when the generating units practically have non-convex input-output characteristics due to prohibited operating zones, valve-point loadings, inequality constraints, non-continuous operating characteristics of some electrical equipment, and the huge dimensionality. The main classification of mathematical optimization techniques is shown in Figure 4.1.

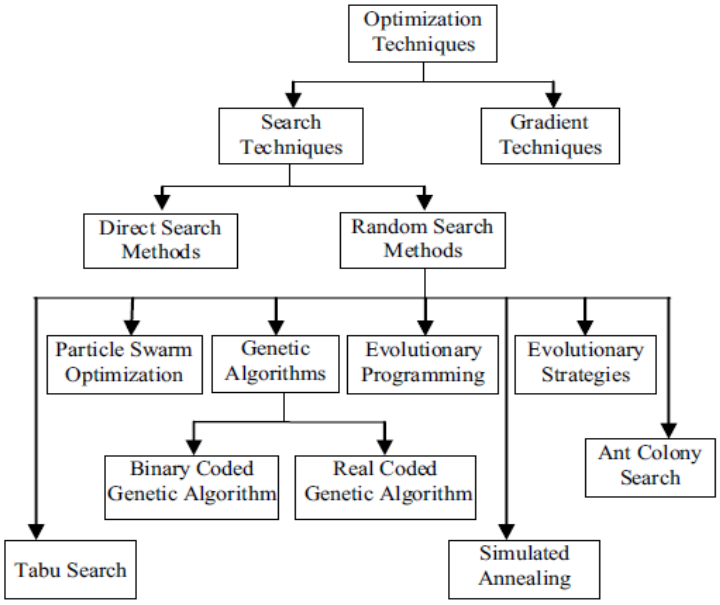

Figure 4.1. Classification of mathematical optimization techniques.

The search techniques can be categorized into direct search (DS) and random search (RS). In the past 30 years, random search (RS) has been greatly developed to solve these problems. It is a family of numerical optimization method that does not require a gradient so it can be used on functions that are non-continuous or non-differentiable, as opposed to the DS method. RS is attributed to Rastrigin [96] who made an early presentation on RS along with basic mathematical analysis. RS works well with iteratively moving to better positions in the search space which are sampled from a hypersphere surrounding the current position. RS mainly includes tabu search (TS), genetic algorithm (GA), evolutionary programming (EP), evolutionary strategies (ES), particle swarm optimization (PSO), ant colony search (ACS), hybrid search methods, etc. GA, EP, ES, PSO, and ACS are all sub-fields of evolutionary computing. The first three methods belong to evolutionary algorithms, and the latter two methods belong to swarm intelligence.

Tabu search, created by Fred W. Glover in 1986 [97] and formalized in 1989 [98-99], is a **local search** method used for mathematical optimization. It uses a local or neighborhood search procedure to iteratively move from one potential solution to an improved solution in the neighborhood of the initial solution, until some stopping criterion has been satisfied. The disadvantages of TS are that it is easy to become stuck in poor-scoring areas or areas where many solutions are equal because of its local search procedures and the selection of the initial solution. The authors in [100] combined PSO and TS have created a novel hybrid TS-PSO algorithm which conducts both a global and a local search in each iterations, so that the probability of finding the optimal solution significantly increases.

Genetic algorithm became popular through the work of John Holland in the early 1970s, particularly through his book, *Adaptation in Natural and Artificial Systems* (1975) [101]. The algorithm consists of search and optimization procedures that are based on the principle of natural genetics and natural selection. In GA [102], a population of strings (the genotype of the genome), which encode candidate solutions (called individuals) to an optimization problem, evolved toward better solutions. Traditionally, solutions are represented in binary form as strings of 0s and 1s, but other encodings are also possible. The evolution usually starts from a population of randomly generated individuals and happens in generations. In each generation, the fitness of every individual in the population is evaluated and multiple individuals are stochastically selected from the current population (based on their fitness) and then modified (recombined and possibly randomly mutated) to form a new population. The new population is then used in the next iteration of the algorithm. Commonly, the algorithm terminates when either a maximum

number of generations has been produced or a satisfactory fitness level has been reached for the population. Real-coded GA is mainly applied to solve real parameter optimization problems, and it is easier when compared to the binary-coded GA [103]. If the population size requirement is large for large strings, the computational complexity of the algorithm greatly increases [104].

Evolution strategies were created in the early 1960s, further developed in the 1970s, with later contributions by Ingo Rechenberg and Hans-Paul Schwefel and his co-workers [105]. ES uses natural problem-dependent representations, primarily mutation and selection, as search operators and is designed particularly to solve problems in the real-value domain. It uses self-adaptation to adjust control parameters of the search. De-randomization of self-adaptation has led to the contemporary Covariance Matrix Adaptation Evolution Strategy. As with evolutionary algorithms [106], the operators are applied in a loop. An iteration of the loop is called a generation. The sequence of generations is continued until a termination criterion is met. As far as real-valued search spaces are concerned, a mutation is normally performed by adding a normally distributed random value to each vector component. The step size or mutation strength is often governed by self-adaptation. Individual step sizes for each coordinate or correlations between coordinates are either governed by self-adaptation or by covariance matrix adaptation [107].

Evolutionary programming is a mutation-based evolutionary algorithm applied to discrete search spaces. David Fogel extended the initial work of his father, Larry Fogel, for real-parameter optimization problems [108]. Real-parameter EP is actually similar in principle to ES. Normally distributed mutations are performed in both algorithms. Both

algorithms encode mutation strength or variance of the normal distribution for each decision variable. A self-adapting rule is used to update the mutation strengths. EP begins its search with a set of solutions initialized randomly in a given bounded space. Thereafter, EP is allowed to search anywhere in real space, similar to the real-parameter GAs. Each solution is evaluated to calculate its objective function value. EP [109] can be summarized into two major steps: 1) mutate the solutions in the current population and 2) select the next generation from the mutated and the current solutions. These two steps can be regarded as a population-based version of the classical generate-and-test method, where mutation is used to generate new solutions (offspring), and selection is used to test which of the newly generated solutions should survive to the next generation. One disadvantage of EP in solving some of the multimodal optimization problems is its slow convergence to a good, near optimum solution [110]. The generate-and-test formulation of EP indicates that mutation is a key search operator which generates new solutions from the current ones. The new EP with Cauchy mutation significantly outperforms the classical EP (CEP), and the new EP is denoted as “fast EP” (FEP) [111].

Ant colony search was initially proposed by Marco Dorigo in 1992 in his Ph.D. thesis [112], and the goal of the first algorithm was to search for an optimal path in a graph based on the behavior of ants seeking a path between their colony and a source of food. The original idea has since diversified to solve a wider class of numerical problems; and as a result, several problems have emerged, drawing on various aspects of the behavior of ants. ACS is not commonly applied in optimization problems of power systems; therefore, it is not investigated in detail. GA, EP, ES, and PSO are commonly

used to solve optimization problems of power systems, especially in economic dispatch, optimal power systems stabilizer design, optimal electrical equipment design, etc.

4.3 Introduction of Particle Swarm Optimization

Particle swarm optimization (PSO) is an evolutionary computing technique introduced by Kennedy, Eberhart, and Shi in 1995 [113]. The searching starts from a group of initial positions (particles or solutions) in the space in order to increase the possibility of finding the optimal solution. It usually includes four steps: initialization, evaluation, stopping criterion, and updating velocities and positions. Compared with other evolutionary algorithms, such as GA, TS, and EP, PSO possesses many attractive properties, such as memory and constructive cooperation, so it has more of a chance at finding a better solution and discovering a reasonable quality solution much faster [114-116]. Moreover, PSO is difficult to degrade when the parameters being optimized are highly correlated, as reported in [26]. Therefore, in this dissertation, PSO will be used to solve the optimization problem in Equation 2.11. The searching procedure for PSO is as follows:

Step 1: Initialization

If there are P variable parameters (K_{ii}, K_{pi}) of DFIG PI gain values to be considered to optimize (the upper and lower bounds, X_{max} and X_{min}, respectively), should be initially specified. In the searching space, L particles{ $X_{i(0)}$, i=1, 2, …, L} can be generated randomly where $X_{i(0)}$={ $X_{i,j(0)}$, j=1, 2, …, P} is the initial group of particles. The velocity for the position updating should also be initialized, and the bound of the velocity is:

$$v_{j,max} = \frac{x_{j,max} - x_{j,min}}{N}, v_{j,min} = -v_{j,max}, j = 1, 2, ..., P. \tag{4.1}$$

The upper and lower bounds of member j particles are $X_{j,max}$ and $X_{j,min}$. The maximum and minimum velocities of member j particles are $v_{j,max}$ and $v_{j,min}$. The interval of the dimension (normally between 10 and 20) is N. Then the initial velocities, $v_{(0)}=\{v_{i,j(0)}$, i=1,2, …,L, j=1, 2, …, P}, are generated randomly between $[v_{j,min}, v_{j,max}]$.

Step 2: Evaluation

Evaluate the fitness value (F) in Equation 2.11 to make sure that the minimum damped eigenvalue is heavily damped in system small signal stability analysis.

$$If\ (\ F(x^{*}_{i,j}) < F(x_{i,j}(t+1))\ ), \text{then}:$$

$$Update\ the\ particle's\ best\ known\ position: x^{*}_{i,j} = x_{i,j}(t+1);$$

$$If\ (\ F(x^{**}_{j}) < F(x^{*}_{i,j})\ ), then$$

$$Update\ the\ swarm's\ best\ known\ position: x^{**}_{j} = x^{*}_{i,j}.$$

The best position which particle i has achieved so far, is $x^{*}_{i,j}$ which is called pbest; and x^{**}_{j} is the best position obtained by any particle among the group. It is the potential solution to the problem and is called gbest.

Step 3: Stopping criterion

If the stopping criterion is met, then stop, otherwise continue to Step 4. Here, the stopping criteria may be the maximum number of iterations (50) or the fitness value larger than a specified positive value (0.4).

Step 4: Updating velocities and positions

The velocity updating is given as:

$$v_{i,j}(t+1) = wv_{i,j}(t) + c_1 r_1 (x^{*}_{i,j} - x_{i,j}(t)) + c_2 r_2 (x^{**}_{j} - x_{i,j}(t)) \tag{4.2}$$

if $v_{i,j}(t+1) > v_{j,max}$, $v_{i,j}(t+1) = v_{j,max}$

if $v_{i,j}(t+1) < v_{j,min}$, $v_{i,j}(t+1) = v_{j,min}$

The position updating is given as:

$$x_{i,j}(t+1) = x_{i,j}(t) + v_{i,j}(t+1) \tag{4.3}$$

if $x_{i,j}(t+1) > x_{j,max}$, $x_{i,j}(t+1) = x_{j,max}$

if $x_{i,j}(t+1) < x_{j,min}$, $x_{i,j}(t+1) = x_{j,min}$

where i=1,…,L (the number of particles in each group, we set L = 50), j=1,…,P (the Interval of the dimension, we set P=25); w is the weighting factor of velocity (normally between 0.5 and 1.5, we set w=0.9); c_1 and c_2 are the accelerating constants (normally between 1 and 3, we set $c_1=c_2=2$); and r1 and r2 are random numbers between 0 and 1. Go to Step 2.

CHAPTER 5
OPTIMAL VALUES PREDICTION AND ARTIFICIAL NEURAL NETWORKS

In Chapter 4, a particle swarm optimization algorithm was discussed to solve for the optimal values of a DFIG's PI gains. However, this approach requires significant computational time; and it couldn't be directly used in on-line control. Second, these optimal parameter values only match one special operating point; and at another wind speed operating point, the initial optimal parameter values may be not optimal values in the new operating point. Therefore, a possible solution is to forecast these optimal values quickly based on historical data. So, the optimal values were calculated according to different wind speed operating points (from 8m/s to 14m/s); and a data set where one group of optimal values (PI gains of a DFIG) match one special wind speed value was obtained. Using this data set as historical data, an artificial neural network (ANN) can be constructed and trained. After that, this ANN can obtain the capacity to quickly predict the optimal values according to one wind speed. This dissertation realizes real-time optimization of a DFIG via training an ANN to forecast the optimal values and transfer much of the calculation off line.

5.1 Introduction to Prediction

Generally, a prediction or forecast is a statement about the way things will happen in the future, often, but not always, based on experience or knowledge. Although guaranteed information about the future is, in many cases, impossible, a prediction is necessary to allow plans to be made about possible development. This is widely used in many fields, including personal behavior, social events, business strategic planning, game

theory, finance, fiction, statistics, science, etc. Even in power systems, load forecast/generation prediction plays a very important role.

In science, a prediction is a rigorous and quantitative statement about what will happen under specific conditions. For example, if an apple falls from a tree, it will be attracted towards the center of the earth by gravity with a specified and constant acceleration; and it cannot go toward the sky. The scientific method is built on testing statements that are logical consequences of scientific theories. This is done through repeatable experiments or observational studies.

In statistics, a prediction is a part of statistical inference. One particular approach to such inference is known as predictive inference, but the prediction can be undertaken within any of the several approaches to statistical inference. In many applications, if models can be expressed as transfer functions or in terms of state-space parameters, the smoothed, filtered, and predicted data estimates can be calculated [117].

In this dissertation, the optimal values prediction is a problem of numerical prediction. Generally, the numerical prediction can be solved through regression analysis /regression equation/multiple regression, exponential smoothing, iterative reweighted least squares, adaptive load forecasting, stochastic time series models, fuzzy logic, neural networks, or knowledge-based expert systems. Various methods have their advantages, disadvantages, and limitations; but these details will not be discussed here because of space limitations. Using neural networks to make optimal values predictions will be discussed in later sections.

5.2 Introduction to Artificial Neural Networks

Artificial neural networks (ANN) or simulated neural networks (SNNs) are composed of interconnecting artificial neurons (programming constructs to model how the human brain performs a particular task). An ANN may either be used to gain an understanding of biological neural networks or to solve artificial intelligence problems without necessarily creating a model of a real biological system [118-120]. It was first proposed by Warren McCulloch, Walter Pitts in 1940 [121] and was greatly enhanced by Bernard Widrow, Ted Hoff, Teuvo Kohonen, David Rumelhart, etc., between the 1950s and 1990s. Recently, it has been widely used in space, electronics, insurance, transportation technologies, etc.

An ANN is an interconnected group of artificial neurons that use a mathematical or computational model for information processing based on a connective approach to computation. In most cases, an ANN is an adaptive system that changes its structure based on external or internal information that flows through the network. In more practical terms, an ANN is essentially a mathematical model of a nonlinear statistical data modeling tool or decision making tool. It is a powerful and simple algorithm to approximate nonlinear functions or to solve problems where the input-output relationship is neither well defined nor easily computable. After selection of a suitable model, comes training and learning the algorithm (historical data needed) and evaluation. The ANN provides the ability to quickly forecast the desired output when inputs are known. The normal procedure using an ANN is shown as [120]:

Step 1: Model selection

Selection of an appropriate model usually depends on the data representation and the application. Overly complex models tend to lead to problems with learning. In feed-forward networks, an ANN is often arranged as an input layer, one or more hidden layers, and an output layer, see Figure 5.1.

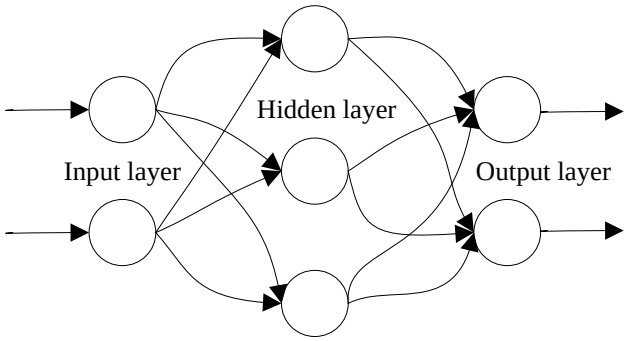

Figure 5.1. The construction of an ANN.

Step 2: Training and learning algorithm

According to the historical data, including inputs and desired outputs, the learning process adjusts the ANN constructs, the weights, and the biases by comparing the errors between the ANN-produced outputs and the desired outputs in each iteration until the stopping criteria are met. Here, the stopping criteria may be the maximum number of iterations (50) or when the errors are smaller than a specified positive value (0.001).

Step 3: Evaluation

An ANN is evaluated by using historical data. If the model and learning algorithm are selected appropriately, the resulting ANN can be extremely robust; and it can accurately predict the output value in a wider input range. If the error between the ANN prediction and the historical data is significant, the ANN model needs be adjusted appropriately.

5.3 Construction of an ANN Based on DFIG Optimal PI Gain Values Prediction

Artificial neural network techniques are also widely used in wind power/wind speed forecasting and some control algorithms in power systems. Recently, they have also been used in the control of wind turbine generator systems. The authors in [122] present a fuzzy logic technique to compensate the PI controller signals of a variable speed wind generation system to feed a utility grid maintaining unity power factor at all conditions and supply to an autonomous load. The fuzzy logic could help optimize the efficiency and enhance the performance. An ANN is also used to design an interface neurons-controller for the coordinated reactive power control between a large wind farm (DFIG) and a static synchronous compensator in [123]. It effectively enhances the fault ride-through capability of the wind farm.

In this dissertation, the input data set (wind speed v_w) and the output data set (optimal PI gain values K_{ii} and K_{pi}) are from the calculation results of PSO based on small signal stability analysis in some operating points. PSO couldn't be applied at every operating point, so it was necessary to pay attention to the ANN prediction. After sufficient data training and a learning process, an ANN could forecast the optimal PI gain parameters (K_{ii} and K_{pi}) at any wind speed rather quickly, so that the real-time optimization will be realized. The ANN construction should be suitable and efficient so that it can predict the optimal values fast and accurately. A two-layer feed-forward ANN model in which the first layer has one input (wind speed v_w) and ten tansig neurons, and the second layer has one purelin neuron (tansig and purelin are transfer functions of ANN) was commonly used in [124]. One ANN construction is designed to forecast only one

optimal parameter. The mathematical function of the ANN is given by Equation 5.1, and the construction is shown in Figure 5.2.

$$K = \left[\sum_{i=1}^{10} \left[\left(\frac{2}{\left(1+e^{\left(-2\left(IW_i * v_w + B1_i\right)\right)}\right)} - 1 \right) * LW_i \right] \right] + BL \tag{5.1}$$

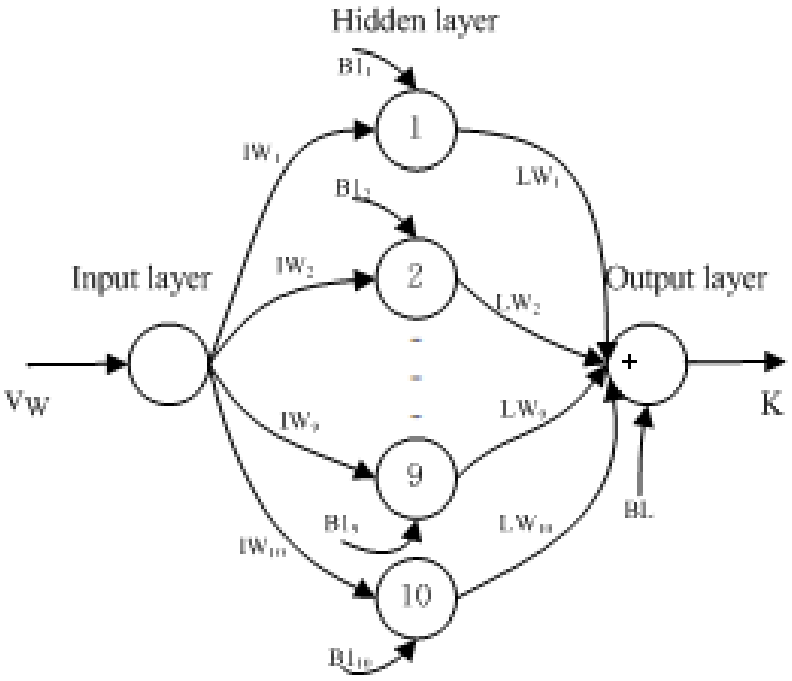

Figure 5.2. The construction of ANN for DFIG optimal PI gain forecast.

After sufficient historical data training, these constant parameters (IW_i, Bl_i, LW_i, and BL [125]) of the ANN can be easily obtained. After the construction has been identified, the ANN can quickly forecast the optimal PI parameter at any wind speed.

5.4 Design of an ANN Controller

In control engineering, the PI (proportional-integral) controller is a basic feedback controller which drives the plant with a weighted sum of the error (the difference between the output (PV) and desired set point (SP)) and the integral of that value. The diagram of a PI controller is provided in Figure 5.3. The integral term in a PI controller makes the

steady-state error to be zero for a ramp input. However, the disadvantage is that it causes a phase lag such that the phase margin (a measure of stability) decreases. Therefore, the gain parameters (K_i and K_p) must be carefully selected and designed.

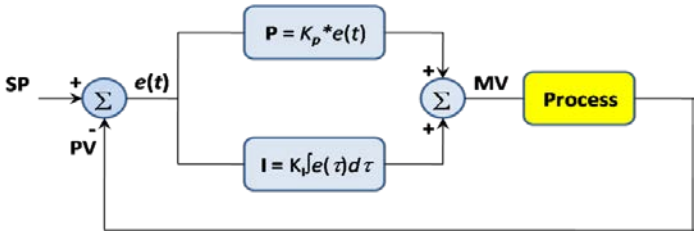

Figure 5.3. Diagram of PI controller block.

In a traditional PI controller of converters, K_i and K_p are constant. In this dissertation, an ANN controller was designed to dynamically adjust the gain value according to the wind speed so that PI gain parameters can always be optimum based on small signal stability analysis under various wind speed conditions. This requires additional time to train the ANN which can be done off line. After the construction has been accomplished, this ANN can very quickly forecast the optimal value; and it can be used in the real-time optimization online. There are a total of 16 parameters (K_i and K_p) in the DFIG converter resulting in 16 ANN controllers to be designed. The diagram of an ANN controller is shown in Figure 5.4. Equation 5.1 and the parameters (IW_i, Bl_i, LW_i, and BL) were used to build the ANN controller in an RSC PI control circuit in PSCAD™, as shown in Fig. 5.5. The ANN optimal DFIG model maintained optimal transient performance in all wind speed ranges via ANN controllers by dynamically adjusting PI gain parameters. In the simulation, the adjustment of ANN controllers did not reduce the robustness of the system.

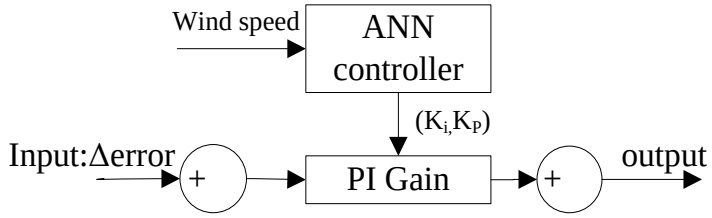

Figure 5.4. Diagram of an ANN controller block.

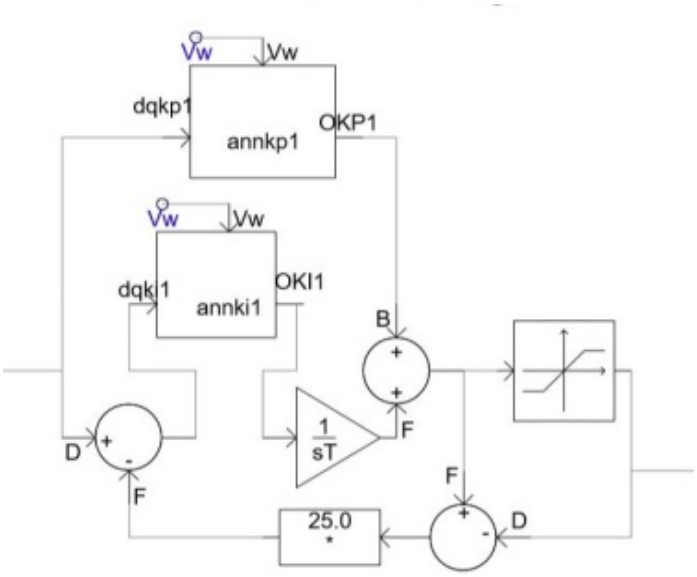

Figure. 5.5. The ANN controller for K_{p1} and K_{i1} in PSCAD.

5.5 Summary

This chapter firstly introduces the basic concept-prediction which is widely applied in many fields, including power systems (load forecast/generation prediction). Next, attentions are focused on numerical prediction in statistics and science, and the standard methods used in numerical prediction (regression analysis /regression equation/multiple regression, exponential smoothing, iterative reweighted least-squares, adaptive load forecasting, stochastic time series models, fuzzy logic, neural networks and knowledge based expert systems) are mentioned. Subsequently, the introduction of artificial neural network is provided. After three basic steps (model selection, training and learning algorithm, and evaluation), an ANN can quickly and accurately solve the

problem of numerical prediction. Then, a two-layer feed-forward ANN construction is designed and trained to predict the DFIG's optimal PI gain values. Finally, the traditional PI controller is introduced and an ANN controller is designed to dynamically adjust the PI gain value so that the PI gain parameters can always be optimum based on small signal stability analysis under various wind speed conditions. Therefore, the ANN controller in essence realizes the real-time optimization online because the large amount of computational time is handled in PSO optimization and ANN training which is done offline.

CHAPTER 6
FLOWCHART AND SYSTEM STUDY

In Chapter 6, the flowchart of the ANN optimal DFIG model design procedure used in this dissertation will be discussed. Then, some system studies will be provided, such as the single machine (DFIG) connected to the infinite bus system and the multi-machine system. After that, a voltage analysis of the DFIG in a distribution system will be discussed.

6.1 Flowchart of the ANN Optimal DFIG Model Design

There are five main steps for the ANN optimal DFIG model design procedure in Figure 6.1.

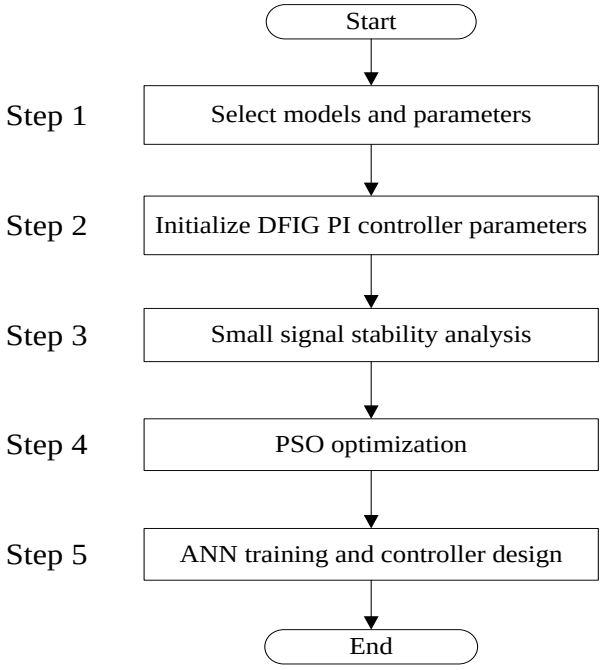

Figure 6.1. The five steps of the ANN optimal DFIG model design procedure.

1. *Select models and parameters:* Choose the appropriate test system, including the DFIG, and set the appropriate parameters for PSO taking into

consideration the accuracy required and the computation budget. Beginning with the most simple configuration, the single machine (DFIG) connected to the infinite bus system was selected.

2. *Initialize DFIG PI controller parameters:* Specify the DFIG's PI gain parameters and select an appropriate operating point. In optimization theory, selecting the appropriate initial point will save a lot of time in locating the optimal point.
3. *Analyze small signal stability:* The small signal stability analysis has been done for this test system with DFIGs and the objective function (Equation 2.11) has been gotten.
4. *Optimize the PSO:* Use the PSO to search for the optimal PI gain parameters based on the objective function at different operating point to get the historical data.
5. *Train the ANN and design the controllers:* Train the ANN using the historical data and design the ANN controllers to adaptive control the PI gain. The ANN optimal DFIG model will equivalently have real-time optimization capability, and it can always be in an optimal state based on small signal stability analysis whenever the wind speed changes. A detailed flowchart is provided in Figure 6.2.

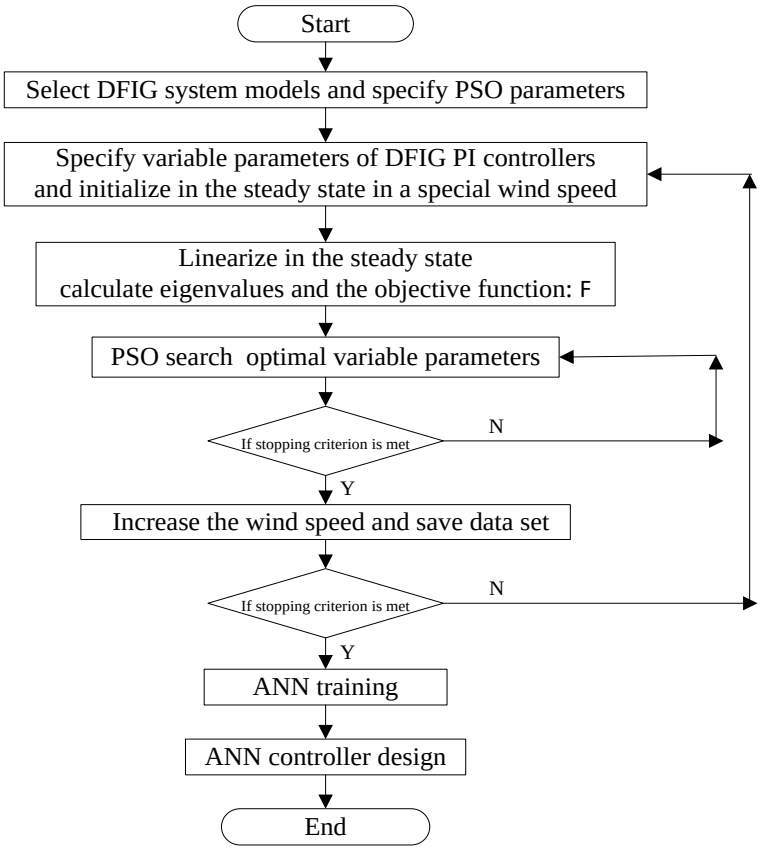

Figure 6.2. The flowchart for an ANN optimal DFIG model design procedure.

6.2 System Study for the Single Machine (DFIG) Connected to the Infinite Bus System

In Figure 3.1, the single machine (DFIG) connected to the infinite bus system (SMIB) is shown. The parameters of the test system follow [82] and are shown in Table 6.1, including power grid, wind turbine and DFIG. The PI gain parameters of the initial DFIG model are shown in Table 6.2. The lower bounds of PI gain parameters are shown in Table 6.3. The upper bounds of PI gain parameters are shown in Table 6.4. The main parameters of PSO algorithm are shown in Table 6.5.

Table 6.1. The parameters of SMIB test system.

Power Grid:	
Voltage Level	34.5 kV
Frequency	60 Hz
Combined reactance of the transformer and transmission line	x_{TL} = 0.05 p.u.
Wind Turbine:	
Rated capacity	3.6 MW
Number of blades	3
Rotor diameter	104 m
Swept area	8495 m^2
Inertia constant of the turbine	H_t = 4.29 s
Inertia constant of the generator	H_g = 0.9s
Damping coefficient of the shaft between two masses	D_{tg} = 1.5
Shaft stiffness	K_{tg} = 296.7
DFIG:	
Rated capacity	3.6 MW
Rated stator voltage	4.16 kV
Stator resistor	r_s = 0.0079 p.u.
Rotor resistor	r_r = 0.025 p.u.
Stator leakage inductance	L_{ls} = 0.07937 p.u.
Rotor leakage inductance	L_{lr} = 0.40 p.u.
mutual inductance	L_m = 4.4 p.u.
Combined reactance of the transformer and the GSC winding between the GSC and the stator winding	x_{tg} = 0.05 p.u.
Capacitor	C = 0.02 F
Transformer:	
Rated capacity	5.0 MW
Winding 1 voltage	4.16 kV
Winding 2 voltage	34.5 kV
Positive sequence leakage reactance	0.01 p.u.

Table 6.2. The PI gain parameters of the initial DFIG model.

k_{p1}	k_{p2}	k_{p3}	k_{p4}	k_{p5}	k_{p6}	k_{p7}	k_{p8}
0.2	0.7	1.0	2.0	0.5	1.5	0.05	1.5
k_{i1}	k_{i2}	k_{i3}	k_{i4}	k_{i5}	k_{i6}	k_{i7}	k_{i8}
1.00	0.333	10.00	25.00	1.00	161.29	20.0	161.29

Table 6.3. LB: the lower bounds of PI gain parameters.

k_{p1}	k_{p2}	k_{p3}	k_{p4}	k_{p5}	k_{p6}	k_{p7}	k_{p8}
0.02	0.1	0.1	0.0	0.1	0.1	0.002	0.1
k_{i1}	k_{i2}	k_{i3}	k_{i4}	k_{i5}	k_{i6}	k_{i7}	k_{i8}
0.005	0.1	5	5	0.2	50	5	50

Table 6.4. UB: the upper bounds of PI gain parameters.

k_{p1}	k_{p2}	k_{p3}	k_{p4}	k_{p5}	k_{p6}	k_{p7}	k_{p8}
1	5	5	5	3	5	0.5	5
k_{i1}	k_{i2}	k_{i3}	k_{i4}	k_{i5}	k_{i6}	k_{i7}	k_{i8}
1	50	150	150	5	300	100	310

Table 6.5. The parameters of PSO algorithm.

Number of particles	L = 50
Interval of the dimension	P = 25
Weighting factor of velocity	w = 0.9
Accelerating constants	c1 = c2 = 2

6.2.1 Eigenvalue Analysis and ANN Design of the SMIB System

Using the data of the SMIB system and the initial DFIG model, the small signal stability analysis is completed when the wind speed is 11m/s. The eigenvalues of the state matrix in Table 6.6 can be obtained.

Table 6.6. The eigenvalues of the initial DFIG model of SMIB.

	σ+jω	ξ	f
λ1,2	-0.301±j0.49	0.52	0.078
λ3,4	-0.196±j3.83	0.051	0.61
λ5,6	-0.21±j6.91	0.030	1.10
λ7,8	-12.07±j89.91	0.133	14.30
λ9,10	-60.47±j393.2	0.152	62.58
λ11	-8320	1	0
λ12	-243.37	1	0
λ13	-65.22	1	0
λ14	-31.94	1	0
λ15	-15.85	1	0
λ16	-1.62	1	0

Table 6.7. The eigenvalues of the fix-optimal DFIG model of SMIB.

	σ+jω	ξ	f
λ1,2	-0.43±j0.503	0.65	0.080
λ3,4	-0.74±j3.96	0.18	0.63
λ5,6	-1.47±j6.85	0.21	1.09
λ7,8	-31.47±j93.18	0.32	14.83
λ9,10	-99.76±j396.4	0.24	63.08
λ11	-9865	1	0
λ12	-162.78	1	0
λ13	-84.43	1	0
λ14	-57.59	1	0
λ15	-4.37	1	0
λ16	-0.38	1	0

Then, the PSO can be used to obtain the optimal parameters of the DFIG PI gains at the fixed wind speed (11m/s). Therefore, the parameters in Table 6.8 can be used to set the PI

gains of the DFIG and obtain the fix-optimal DFIG model (the DFIG is only optimized at the fixed wind speed 11m/s) which will be used in the simulation.

Table 6.8. The PI gain parameters of the fix-optimal DFIG model of SMIB.

k_{p1}	k_{p2}	k_{p3}	k_{p4}	k_{p5}	k_{p6}	k_{p7}	k_{p8}
0.08	5.04	4.11	5.23	3.46	4.92	0.23	4.52
k_{i1}	k_{i2}	k_{i3}	k_{i4}	k_{i5}	k_{i6}	k_{i7}	k_{i8}
0.13	2.12	149.25	50.31	4.88	222.22	98.04	303.03

After that, the eigenvalues of the fix-optimal DFIG model in Table 6.7 can be determined. Comparing the values of λ_1~λ_{10} indicates that all eigenvalues are on the left-half phase plane, and the systems are both stable in a small signal sense. There are mainly three oscillation modes in λ_1~λ_{10}; and λ_{11}~λ_{16} belong to a non-oscillation mode, which can be ignored. Low frequency oscillations of λ_1~λ_6 are near 0.05~1.1Hz, and they cause mechanical mode associated with turbine and shaft dynamics. λ_7~λ_8 cause electric-mechanical mode associated with rotor electrical (q-flux) and mechanical (speed) dynamics near 14.5Hz. λ_9~λ_{10} cause electrical mode associated with stator dynamics near 62Hz. The damping ratios of $\lambda_{1,2,\ 7,8,9,10}$ are not very small, and the damping ratios of $\lambda_{3,4,5,6}$ are very poor (0.051, 0.030) in the initial DFIG model so that the system may have a severe problem of low frequency oscillation. The eigenvalue frequencies of the fix-optimal DFIG model slightly change while the eigenvalue damping ratios greatly increase, especially in 0.6Hz and 1.1Hz. They almost increase 4~7 times so that the damping ratios are big enough, low frequency oscillation will almost disappear in the simulation. In Figure 6.3, only the curves of eigenvalues (λ_1, $\lambda_{3,}$ λ_5, $\lambda_{7,}$ λ_9) in the upper phase plane have been plotted in the phase plane. The eigenvalues of the fix-optimal DFIG model are farther away in the left-half phase plane than the initial DFIG model.

Therefore, the fix-optimal DFIG model will have a better stability than the initial DFIG model in small signal stability analysis.

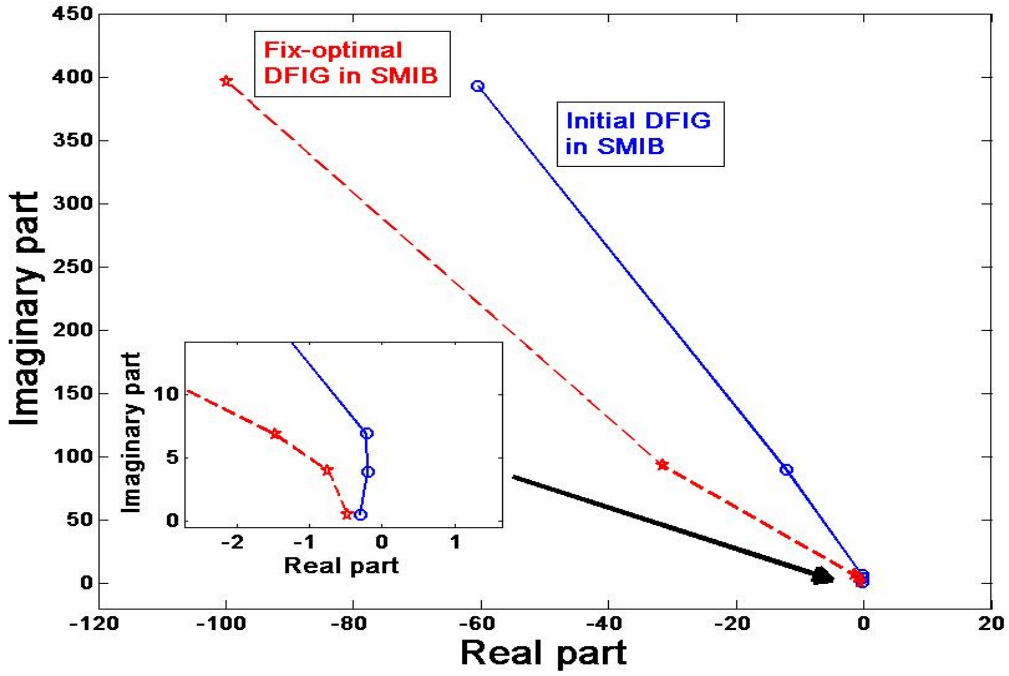

Figure 6.3. The curves of eigenvalues of the initial and fix-optimal DFIG model of SMIB in phase plane.

Next, PSO will be used to obtain all of the optimal parameters of DFIG PI gains in different wind speeds (from 8m/s to 14m/s); and parts of the data are shown in Table 6.9 because of space limitations. Dividing the different wind speeds with smaller intervals and using PSO will result in more data. After more data training (The mathematical function of the ANN is given by Equation 5.1, and the construction is shown in Figure 5.2.), the ANN will be able to more accurately predict the optimal parameters. In this dissertation, 50 data sets will be produced and used (input/wind speed-output/optimal values of $k_{p,}$ k_i) to train the ANNs and develop the ANN construction and parameters. There are 16 ANNs in one DFIG model because one ANN can only predict one value of k_p or k_i.

Table 6.9. The optimal parameters of DFIG PI gains of SMIB in different wind speeds.

	vw=8.5	vw=9.0	vw=9.5	vw=10	vw=10.5	vw=11	vw=11.5	vw=12.0	vw=12.5	vw=13	vw=13.5	vw=14
kp1	0.0742	0.0764	0.0775	0.0791	0.0821	0.0808	0.0812	0.08542	0.0818	0.0884	0.0891	0.0923
kp2	4.5632	4.3841	4.8653	4.4671	4.8624	5.0125	4.9983	5.3246	5.4768	5.2102	5.0964	4.8959
kp3	4.2984	3.9263	3.6079	4.2156	4.3458	4.0374	3.8995	3.7621	4.2537	4.3124	4.1578	3.9958
kp4	3.7842	4.545	5.3127	5.0481	5.5841	4.9865	4.8230	5.1568	5.3999	5.4652	5.2413	5.0235
kp5	2.1697	2.4521	1.8829	2.6398	3.1504	3.0423	2.9608	2.7841	3.5462	3.2976	2.6588	2.8982
kp6	6.0229	5.5304	5.2999	4.7823	5.1444	4.9242	4.9995	3.9813	4.7067	4.2118	5.0879	4.7207
kp7	0.2718	0.2148	0.3125	0.2921	0.2141	0.2032	0.2274	0.3384	0.2102	0.3520	0.2695	0.2462
kp8	4.1149	4.6118	5.1034	5.9362	5.9981	4.5025	4.9946	4.7646	4.9588	4.2866	4.1465	4.8921
ki1	0.0811	0.1236	0.0678	0.1705	0.2141	0.1313	0.1948	0.1741	0.0631	0.0813	0.0766	0.1593
ki2	2.5006	2.1058	1.8463	2.3120	2.4289	2.0028	2.1227	1.9627	2.3462	2.0502	2.2276	2.4791
ki3	120.74	143.21	136.95	127.61	143.08	149.25	148.65	141.99	131.46	140.38	147.26	145.85
ki4	36.5715	27.2735	41.6522	38.5624	44.2536	49.97	40.3426	48.2014	42.3562	39.4568	42.3934	46.1052
ki5	3.9407	4.2995	3.7628	4.9257	4.3865	4.8843	4.9576	4.5521	4.9879	4.2996	4.0523	4.7803
ki6	275.35	234.31	250.52	268.19	250.156	222.22	243.83	287.46	238.84	273.07	220.18	240.67
ki7	96.313	89.98	91.98	87.467	93.79	98.04	88.16	97.48	87.854	83.72	94.976	88.02
ki8	254.32	269.89	268.83	281.28	278.54	300.03	255.46	279.51	287.06	266.61	298.27	288.56

Only the construction and parameters of ANN for k_{p1} are reproduced here because of space limitations. Using MATLAB® Neural Network Toolbox™ and the data set of k_{p1} in Table 6.9, it is not difficult to obtain the parameters (IW_i, Bl_i, LW_i, and BL) of this ANN:

$$IW=\left[-13.77;\ -14.40;\ -13.70;\ -13.91;\ -13.92;\ 13.96;\ 13.99;\ -14.07;\ -13.94;\ -13.29\right];$$

$$BI=\left[14.23;\ 10.28;\ 8.27;\ 4.889;\ 2.074;\ 1.816;\ 4.681;\ -7.648;\ -10.965;\ -14.694\right];$$

$$LW=[-0.1358;-0.3932;\ 0.1374;\ -0.09057;\ -0.08974;\ 0.2121;\ 0.00611;\ -0.1805;\ 0.04522;\ 0.5262]^{T};$$

$$BL=\left[0.671231\right]$$

The forecast result of test data showed output = 0.97*Target+0.0024. The construction of the ANN and the main parameters are shown in Figure 6.4. Data has been divided randomly. The Levenberg-Marquardt algorithm, also known as the damped least-squares

method, has been used in the training; and MEX has been used for more memory efficiency. The best validation performance index, Mean squared error (MSE), was 2.6669e-07 in Figure 6.5. After sufficient historical data training, the data error between the PSO calculation and the ANN prediction was less than 0.0015, as shown in Figure 6.6. Therefore, the ANN has the capability to accurately predict the optimal parameter in a wide range of wind speeds.

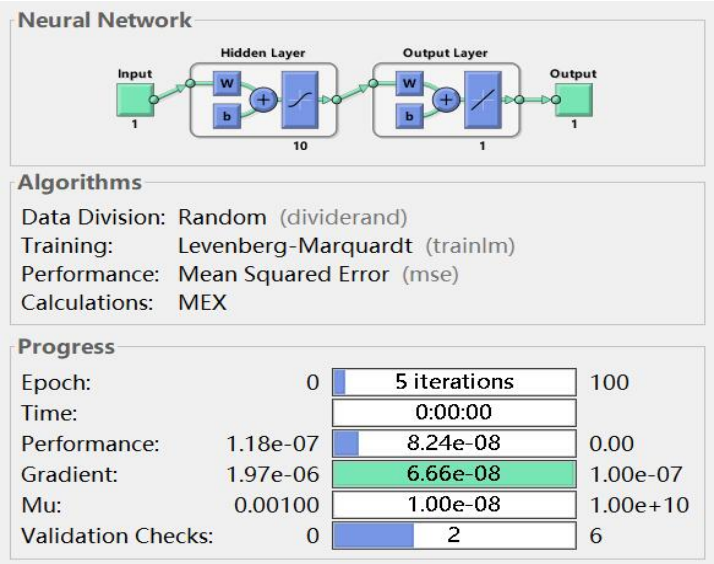

Figure 6.4. The important data of the ANN.

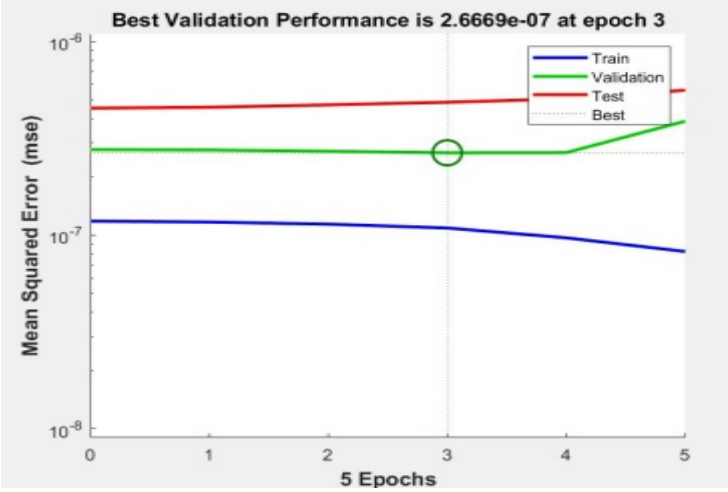

Figure 6.5. The MSE of the ANN.

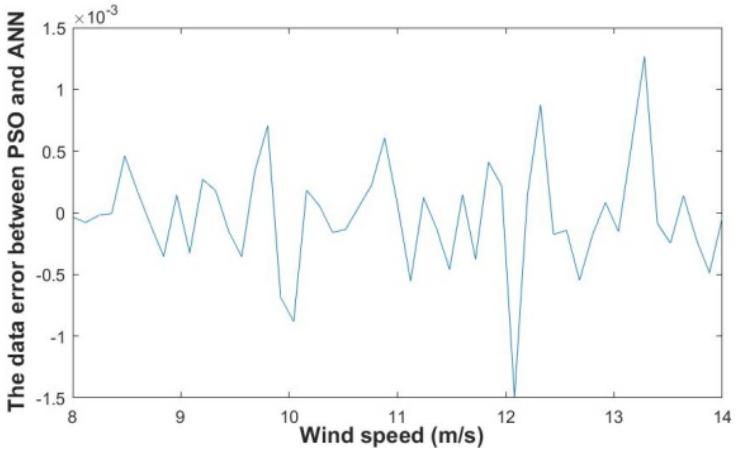

Figure 6.6. Data error between the PSO calculation and the ANN forecast.

Equation 5.1 and the parameters (IW_i, Bl_i, LW_i, and BL) were used to build the ANN controller in an RSC PI control circuit in PSCAD™, as shown in Fig. 5.5. The ANN optimal DFIG model maintained optimal transient performance in all wind speed ranges via ANN controllers by dynamically adjusting PI gain parameters. In the simulation, the adjustment of ANN controllers did not reduce the robustness of the system. The simulation results of these three models will be compared next.

6.2.2 Simulation Analysis of the SMIB System

The SMIB shown in Figure 3.1 is simulated via PSCAD software to prove the transient performance improvement by comparing three models: 1) the initial DFIG model, 2) the fix-optimal DFIG model (only optimizing PI parameters at wind speed=11m/s based on small signal stability analysis), and 3) the ANN optimal DFIG model. All of the data comes from Chapter 6.2.1. The main differences among the three models are the PI controller parameters. The disturbances are given as follows:

1. At t=0 second, the wind speed is 11m/s and GSC/RSC controllers are not working at first.

2. At t=0.001 second, GSC and RSC start. The purpose of this simulation is to prove the cut-in impact of DFIG.
3. At t=4 seconds, the three-phase short circuit happens in the transmission line near the infinite bus and clears at t=4.7 second. **In this fault, the voltage of a DFIG connected to the grid decreases to 0.5 p.u.** in order to investigate the low voltage ride-through capability of DFIG.
4. At t=10 second, the wind speed has a step change from 11m/s to 13m/s to check the wind step change impact of DFIG.

The results of the three models' rotor speed, real power, mechanical torque, connection point voltage, DC-link capacitor voltage, and rotor q axis current, are shown in Figure 6.7-6.12, respectively. Comparing the results between the ANN optimal model and the initial model, it can be verified that the advantages of the ANN optimal model are numerous during the disturbances of cut-in, short circuit fault, and wind speed step change, especially considering T_m, P_o, I_{qr}, and v_{dc}. The low frequency oscillations are greatly reduced. The indices, such as eigenvalues, damping ratios, peak values, dynamic impacts, and settling times, as well as stability of the ANN optimal model, are improved significantly compared to the initial model. The peak value reductions are very useful to reduce WT stochastic output and the impact to the grid. It will be useful to protect electrical windings for overvoltage and overcurrent. The oscillation of T_m is greatly damped to improve the safety of WT's gearbox which is the most easily damaged equipment. The oscillations of I_{qr} and v_{dc} are reduced significantly, thus contributing to better safety of the rotor winding and DC-link capacitor. The connection point voltage of

the ANN optimal model recovers to 0.995p.u. two seconds faster than the initial model, and it is imperative to grid voltage stability.

Comparing the results between the fix-optimal model and the ANN optimal model, they almost have the same transient performances for the cut-in and short circuit fault disturbances. However, for the wind speed step change disturbance, which is the most common disturbance, the peak/trough values of ω_r, P_o, $T_{m,}$ and I_{qr} of two models are varied from 1.181 to 1.109p.u., from -3.2 to -2.10MW, from 0.57 to 0.25p.u., and from -0.67 to -0.38p.u., respectively. This means that the ANN optimal model holds an obvious advantage when the wind speeds change frequently and rapidly. This is particularly important since this disturbance may occur thousands of times in one day; and, therefore, improving the transient performance subject to speed changes is crucial. This is the most important contribution of this dissertation.

Although the value of the v_{dc} peak of the ANN optimal model is 4.80KV during the cut-in disturbance, this value is still in an appropriate range, especially comparing it to the trough of the initial model where v_{dc} decreases to 2.75KV. The reason may be that the ANN controllers are highly sensitive. However, this is not a noticeable drawback of the ANN optimal model.

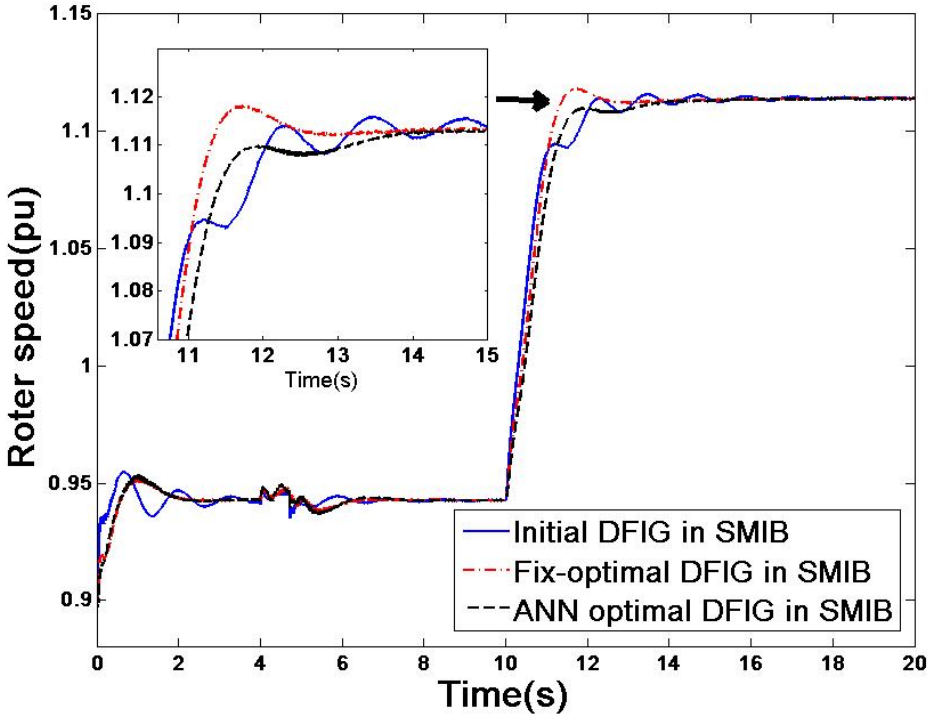

Figure 6.7. Simulation results of rotor speed ω_r.

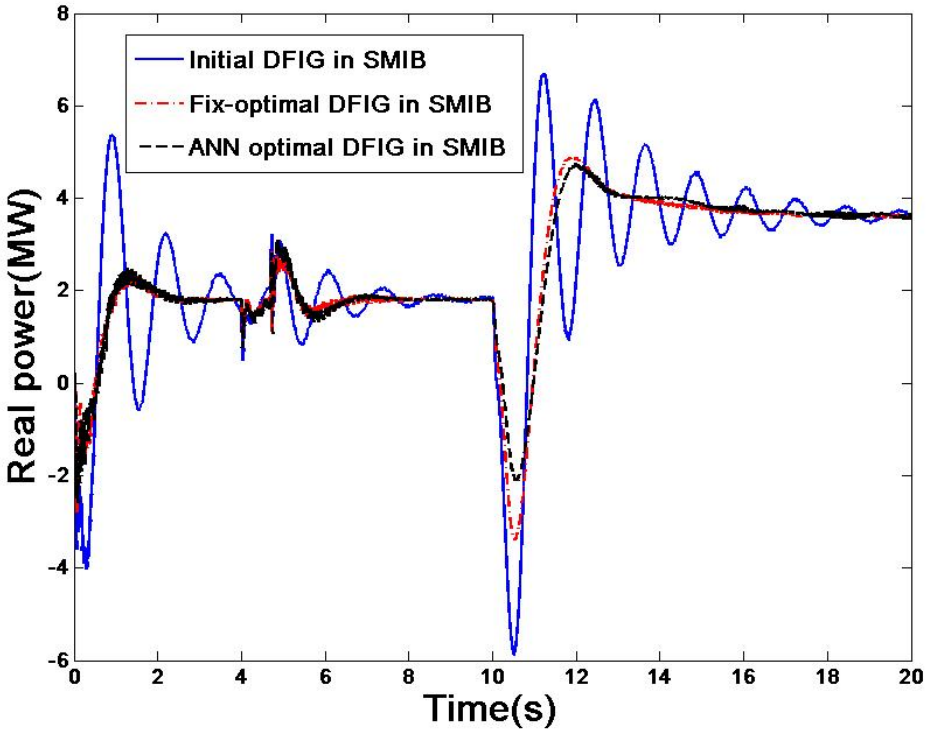

Figure 6.8. Simulation results of real power P_o.

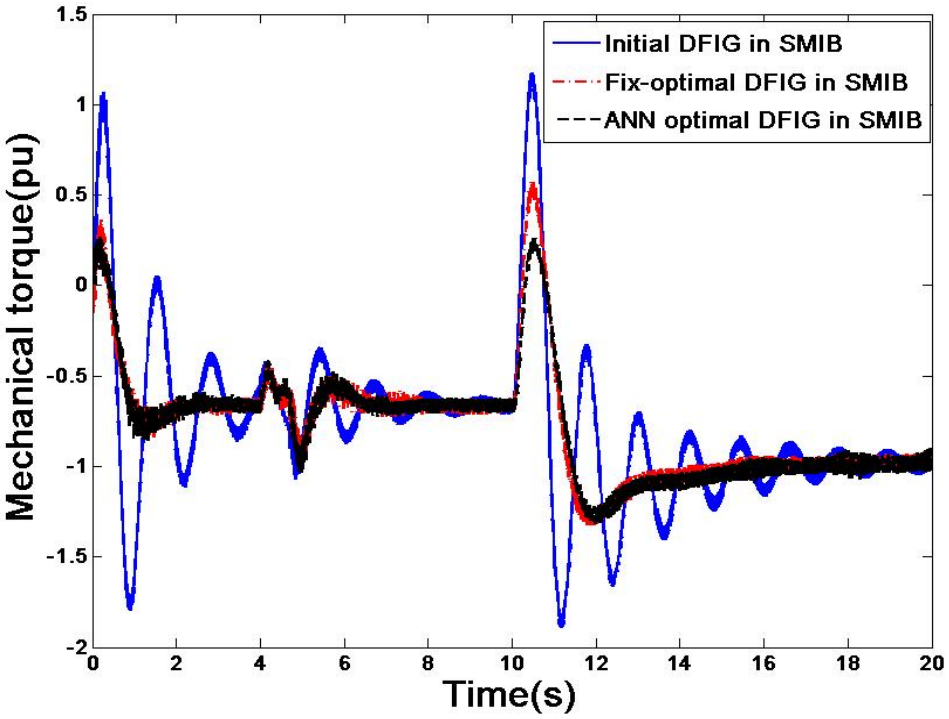

Figure 6.9. Simulation results of mechanical torque T_m.

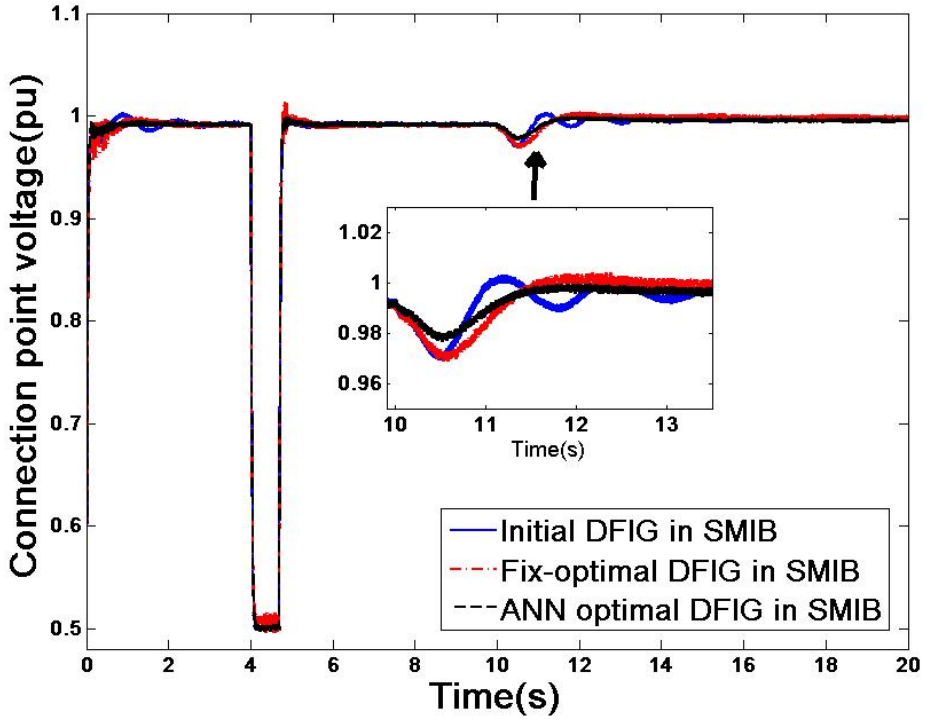

Figure 6.10. Simulation results of connection point voltage v_s.

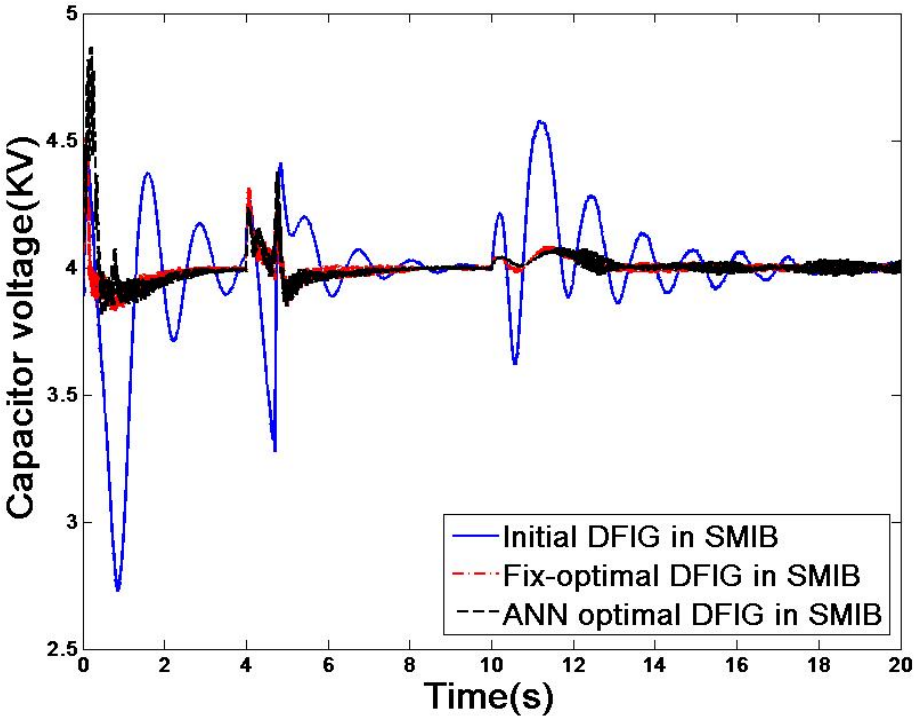

Figure 6.11. Simulation results of DC-link capacitor voltage v_{dc}.

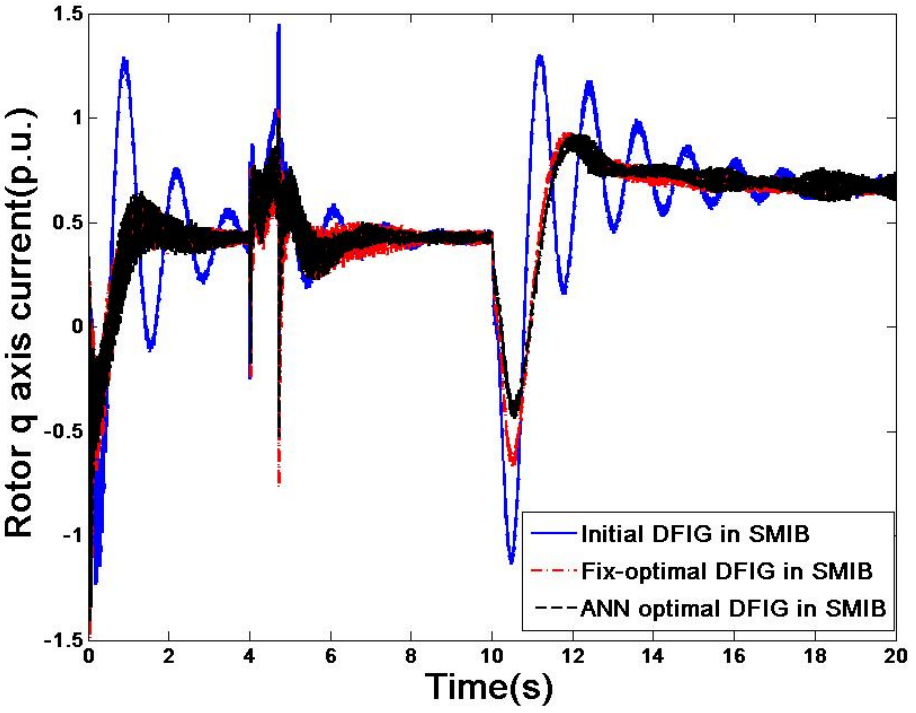

Figure 6.12. Simulation results of rotor q axis current I_{qr}.

6.3 System Study for the Single Machine (DFIG) Connected to the Weak Grid (SMWG)

Short circuit ratio (SCR) is the measure of the generator stability characteristics. It is the ratio of field current required to produce rated no load armature voltage at rated frequency to armature current at the same frequency with armature terminals short circuited [130]. If the impacts of flux saturation and resistors are ignored and values are per unit, SCR$\approx 1/x_d$ which is the Thevenin equivalent reactance of the system. Usually, the larger the value of SCR is, the more stable the system is. The simplified equivalent circuit of DFIG connected an infinite bus is shown in Figure 6.13.

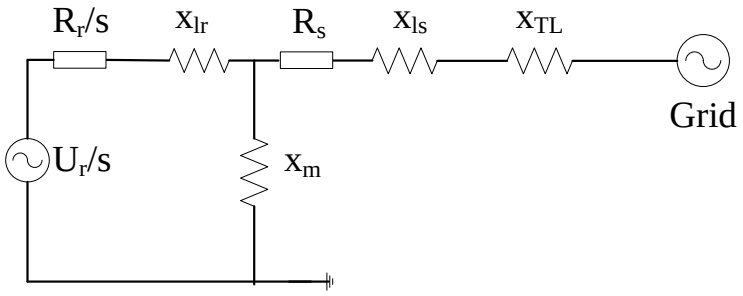

Figure 6.13. The equivalent circuit of DFIG connected an infinite bus.

If the rotor resistor is ignored, the Thevenin equivalent reactance of the system:

$$x_d = x_{TL} + x_{ls} + x_{lr} || x_m.$$

x_{ls}, x_{lr} and x_m are constant parameters of DFIG so that the transmission line impedance (x_{TL}) will mainly decide the value of short circuit ratio.

In Figure 3.1 and Chapter 6.2, the single machine (DFIG) is connected the infinite bus system with a transmission line x_{TL}=0.05p.u. and the SCR is about 2.01. This means that the DFIG is connected to a strong grid. In this section, a DFIG connected to a weak grid (SMWG) will be discussed later. SCR is about 1.26 when x_{TL} =0.35p.u. and the initial

DFIG system will lose the stability. After PSO, the fix-optimal DFIG model can keep the stability. It proves the important significance of the algorithm in this dissertation.

6.3.1 Eigenvalue Analysis and ANN Design of the SMWG System

Using the data of Chapter 6.2 with the only changed set of x_{TL}=0.15p.u. and the SCR is about 1.67, the same steps are performed as in Chapter 6.2 for a small signal stability analysis when the wind speed is 11m/s. The eigenvalues of the state matrix are in Tables 6.10 and 6.11.

Table 6.10. The eigenvalues of the initial DFIG model in SMWG.

	σ+jω	ξ	f
λ1,2	-0.193±j0.515	0.35	0.082
λ3,4	-0.103±j4.90	0.021	0.78
λ5,6	-0.209±j7.73	0.027	1.23
λ7,8	-10.13±j101.54	0.10	16.16
λ9,10	-33.79±j442.6	0.077	70.45
λ11	-5478	1	0
λ12	-143.71	1	0
λ13	-45.34	1	0
λ14	-14.47	1	0
λ15	-3.46	1	0
λ16	-0.92	1	0

Table 6.11. The eigenvalues of the fix-optimal DFIG model in SMWG.

	σ+jω	ξ	f
λ1,2	-0.26±j0.572	0.41	0.091
λ3,4	-0.54±j4.84	0.11	0.77
λ5,6	-1.14±j8.04	0.14	1.28
λ7,8	-21.38±j99.52	0.21	15.84
λ9,10	-66.42±j437.9	0.15	69.71
λ11	-6823	1	0
λ12	-165.82	1	0
λ13	-38.21	1	0
λ14	-21.38	1	0
λ15	-1.79	1	0
λ16	-0.42	1	0

Then, the PSO can be used to obtain the PI gain parameters of the fix-optimal DFIG model in SMWG in Table 6.12.:

Table 6.12. The PI gain parameters of the fix-optimal DFIG model in SMWG.

k_{p1}	k_{p2}	k_{p3}	k_{p4}	k_{p5}	k_{p6}	k_{p7}	k_{p8}
0.092	5.358	3.821	4.587	3.241	4.495	0.214	4.837
k_{i1}	k_{i2}	k_{i3}	k_{i4}	k_{i5}	k_{i6}	k_{i7}	k_{i8}
0.108	1.644	135.48	46.48	5.062	214.60	89.76	295.61

Comparing the results of DFIG in SMIB, all eigenvalues are still on the left-half phase plane; but they move closer to the right-half phase plane than the eigenvalues in the SMIB (as can be clearly seen in Figure 6.14). This means that the weak grid reduces the stability of the DFIG system. The eigenvalue frequencies of λ_1~λ_8 in Table 6.10 show a slight increase, but the frequency of λ_9~λ_{10} almost increases 13.6% from 62Hz to 70Hz. This shows that the weak grid has a bigger impact on the electrical mode associated with stator dynamics. The eigenvalue damping ratios of λ_1~λ_8 reduce a little, but the damping ratios of λ_9~λ_{10} almost reduce 50% from 0.152 to 0.077. This also indicates that the weak grid greatly increases the oscillation of the electrical mode. Comparing the values in Tables 6.10 and 6.11, the optimal parameters change the frequencies slightly; but the increase to the damping ratios is larger, especially λ_3~λ_6 (5 times) and λ_9~λ_{10} (2 times). This shows that the optimal parameters can partly weaken the influence of the weak grid, but the weak grid obviously has a stronger impact on this system than the optimal parameters. If the grid is too weak (such as x_{TL} is too large), the system would lose the stability. It will be found in next simulation Chapter 6.3.2. At here, the fix-optimal DFIG model in SMWG will have better stability than the initial DFIG model in SMWG. Next, the PSO will be promoted to obtain all of the optimal parameters of the DFIG PI gains in different wind speeds (from 8m/s to 14m/s). Part of the data is shown in Table 6.13 due to space limitations. Then, using the ANN training functions to get the ANN's construction and parameters, the ANN controllers can be designed in SMWG. The simulation results of these different models will be presented next.

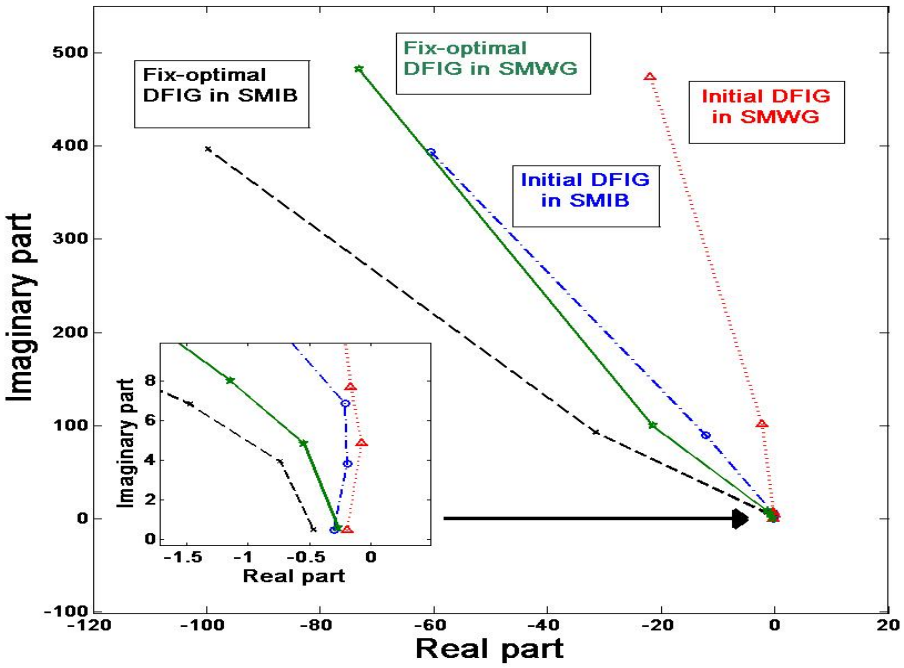

Figure 6.14. The curves of eigenvalues of the initial and fix-optimal DFIG in SMWG in phase plane.

Table 6.13. The optimal parameters of DFIG PI gains of SMWG in different wind speeds.

	vw=8.5	vw=9.0	vw=9.5	vw=10	vw=10.5	vw=11	vw=11.5	vw=12.0	vw=12.5	vw=13	vw=13.5	vw=14
kp1	0.0814	0.0857	0.0831	0.0819	0.0884	0.0921	0.0946	0.1035	0.1104	0.1153	0.1087	0.1045
kp2	4.8721	4.7964	4.9321	4.9677	5.1863	5.3576	5.2864	5.4625	5.4398	5.2156	5.3087	5.1923
kp3	4.4235	4.2078	4.0573	3.9756	4.0285	3.8208	3.9554	3.8032	3.9501	4.1046	4.0821	4.0498
kp4	3.9422	3.9912	4.2312	4.0481	4.3262	4.5874	4.6243	4.8163	4.8642	5.0152	5.1485	5.0966
kp5	2.7745	2.8756	2.5432	2.6987	2.9005	3.2412	3.1023	2.9841	3.0671	3.2768	3.1047	3.1538
kp6	5.8594	5.7164	5.4658	5.1028	4.8563	4.4947	4.3469	4.1886	4.3476	4.6453	4.8271	4.9534
kp7	0.2645	0.2436	0.2714	0.2833	0.2405	0.2136	0.2297	0.2547	0.2368	0.2687	0.2802	0.2763
kp8	4.0546	4.2473	4.5386	4.8846	5.0321	4.8374	4.9235	5.1203	4.9554	4.8764	4.8009	4.9245
ki1	0.0921	0.1056	0.1146	0.1215	0.1187	0.1083	0.1241	0.1315	0.1216	0.1410	0.1521	0.1452
ki2	2.3312	2.0486	1.9564	1.8775	1.7366	1.6442	1.5670	1.8671	2.0679	2.1141	2.3252	2.2431
ki3	112.45	128.74	146.31	120.45	130.22	135.48	146.12	139.63	132.40	142.81	146.23	139.33
ki4	38.7541	32.3510	30.8952	35.4612	40.5462	46.48	48.1277	43.5562	40.3113	37.4665	35.7839	42.3301
ki5	4.1221	4.3565	4.8125	4.9961	5.0974	5.0622	5.1044	4.9533	4.7885	4.6754	4.5023	4.7355
ki6	245.56	230.23	240.62	266.77	243.35	214.60	207.36	225.86	233.49	255.17	244.38	235.88
ki7	95.34	90.45	86.44	80.52	85.63	89.76	90.46	94.65	91.16	87.11	81.35	85.76
ki8	246.77	274.91	290.37	298.18	282.14	295.61	280.93	275.28	270.34	268.42	278.87	290.36

6.3.2 Simulation Analysis of the SMWG System

The SMWG system is the same as in Figure 3.1, while x_{TL} is increased to represent the weak grid. PSCAD is used as the simulation tool to prove the transient performance improvement by comparing four models: the initial DFIG model (DFIG A) in SMIB, the initial DFIG model in SMWG, the fix-optimal DFIG model (DFIG B) in SMWG, and the ANN optimal DFIG model (DFIG C) in SMWG. All of the other data and the disturbances are the same as in Chapter 6.2.

In the simulation with the initial DFIG model, the weaker the grid is, the more system stability is weakened. When x_{TL} increases from 0.05p.u. to 0.12p.u., the transient

performance of the initial DFIG model in SMWG changes slowly; when x_{TL} increases from 0.12p.u. to 0.3p.u., the transient performance begins to accelerate change; when x_{TL} increases from 0.3p.u. to 0.35p.u., the losing stability has been caught in Figure 6.15. The real power largely fluctuates because of wind speed change, and it doesn't converge to the initial steady state. However, in the simulation with the ANN optimal DFIG model, the stability could be kept. The real power bears some serious oscillations because of faults and wind speed change, but it finally goes back to the steady state. This proves that the stability of the ANN optimal DFIG model has been improved more than the initial DFIG model. It also proves the conclusion reached in Chapter 6.3.1, that the optimal parameters can partially weaken the influence of the weak grid; but the weak grid obviously has a stronger impact on this system than the optimal parameters. Naturally, the actual power grid cannot be so weak; and many technologies exist to solve the problem. Therefore, the weak grid ($x_{TL=}$ 0.15p.u.) is selected to do more simulation at here.

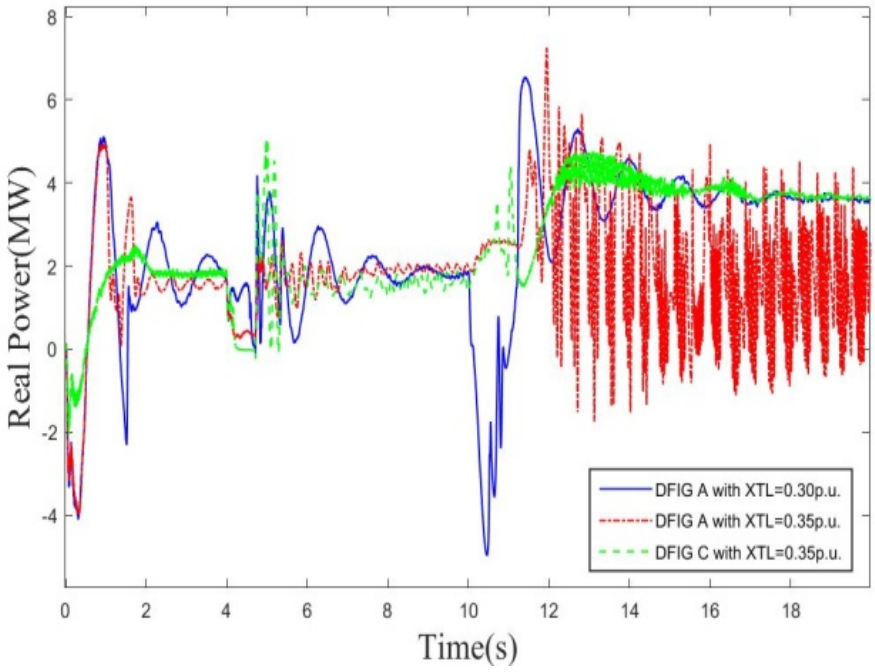

Figure 6.15. Simulation results of real power of DFIG in SMWG with different x_{TL}.

The results of the four models' rotor speed, real power, mechanical torque, connection point voltage, DC-link capacitor voltage, and rotor q axis current, are shown in Figure 6.16-6.21, respectively. Comparing the results between the initial DFIG model in SMIB and the initial DFIG model in SMWG, the transient performances are very close, such as ω_r, T_m, P_o. The peak values of I_{qr}, v_{dc}, and v_s in the initial DFIG model in SMWG are a little bigger than the initial DFIG model in SMIB because of the weak grid. Comparing the results of the latter three models, it is easy to reach the same conclusion as in Chapter 6.2. The fix-optimal DFIG and ANN optimal DFIG models perform better during the disturbances of cut-in, short circuit fault, and wind speed step change, especially considering T_m, P_o, I_{qr}, and v_{dc}. The low frequency oscillations and the peak value are greatly reduced. They demonstrate almost the same transient performance for the cut-in

and short circuit fault disturbances. In the wind speed step change disturbance, the peak/trough values of ω_r, P_o, $T_{m,}$ and I_{qr} of two models are varied from 1.122 to 1.112p.u., from -3.3 to -2.78 MW, from 0.55 to 0.41p.u., and from -0.85 to -0.62p.u., respectively. This provides the ANN optimal model with an obvious advantage when the wind speeds change frequently and rapidly. Although the effect of these improvements is not as good as the effect in Chapter 6.2, it proves that the weak grid obviously has a stronger impact on this system than the optimal parameters.

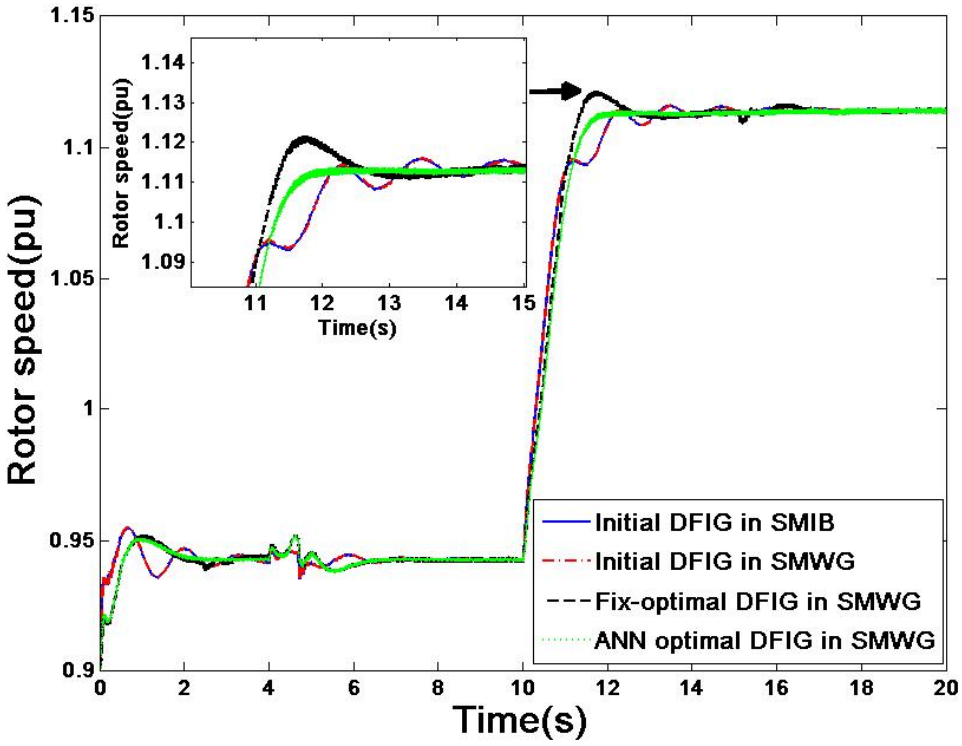

Figure 6.16. Simulation results of rotor speed ω_r in SMWG.

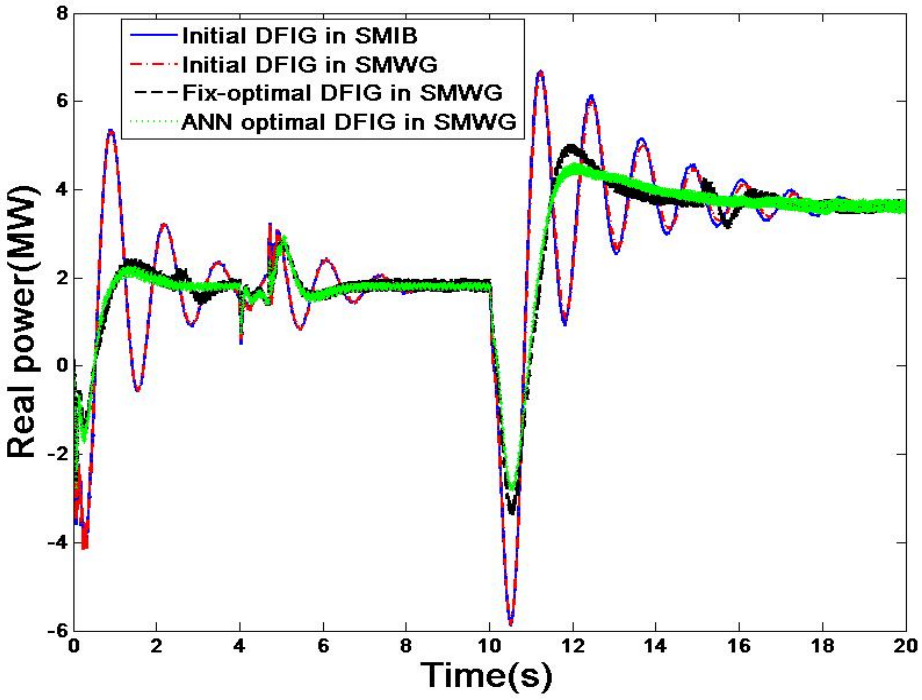

Figure 6.17. Simulation results of real power P_o in SMWG.

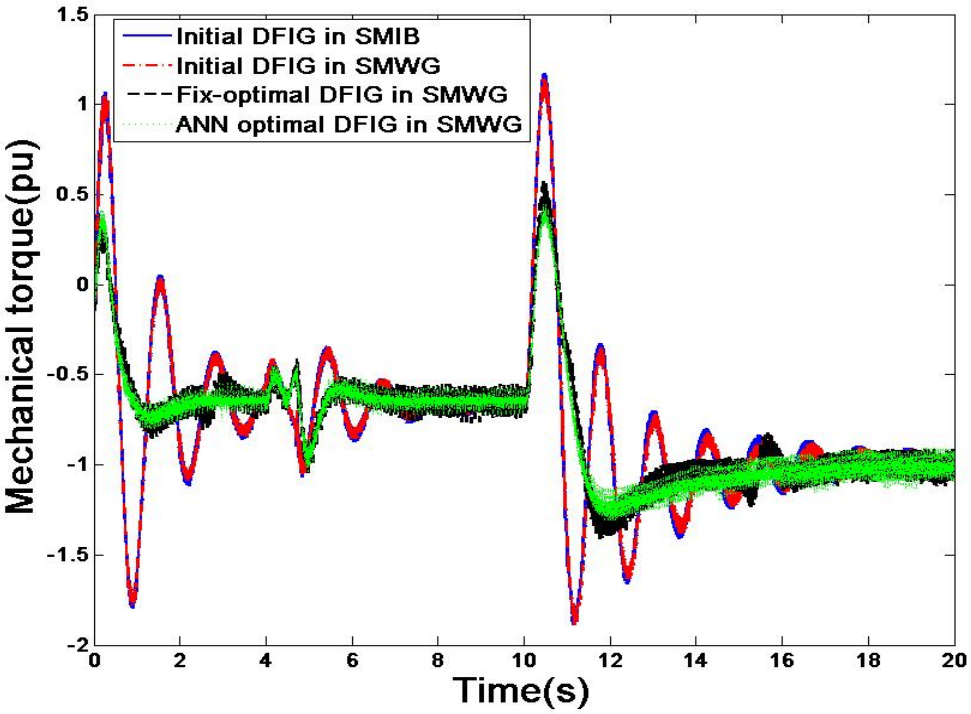

Figure 6.18. Simulation results of mechanical torque T_m in SMWG.

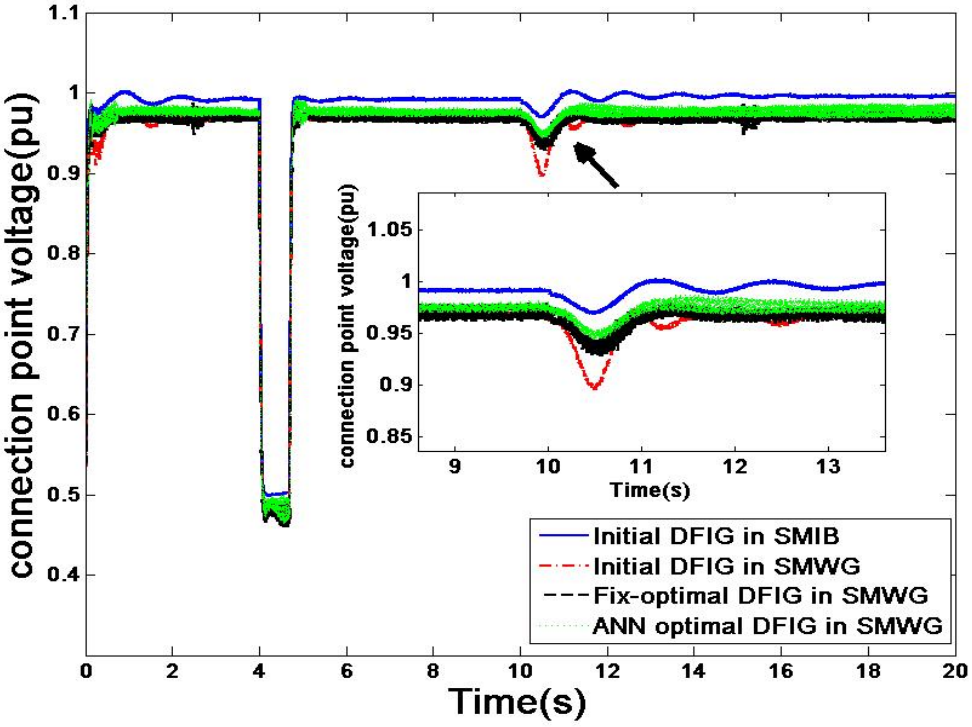

Figure 6.19. Simulation results of connection point voltage v_s in SMWG.

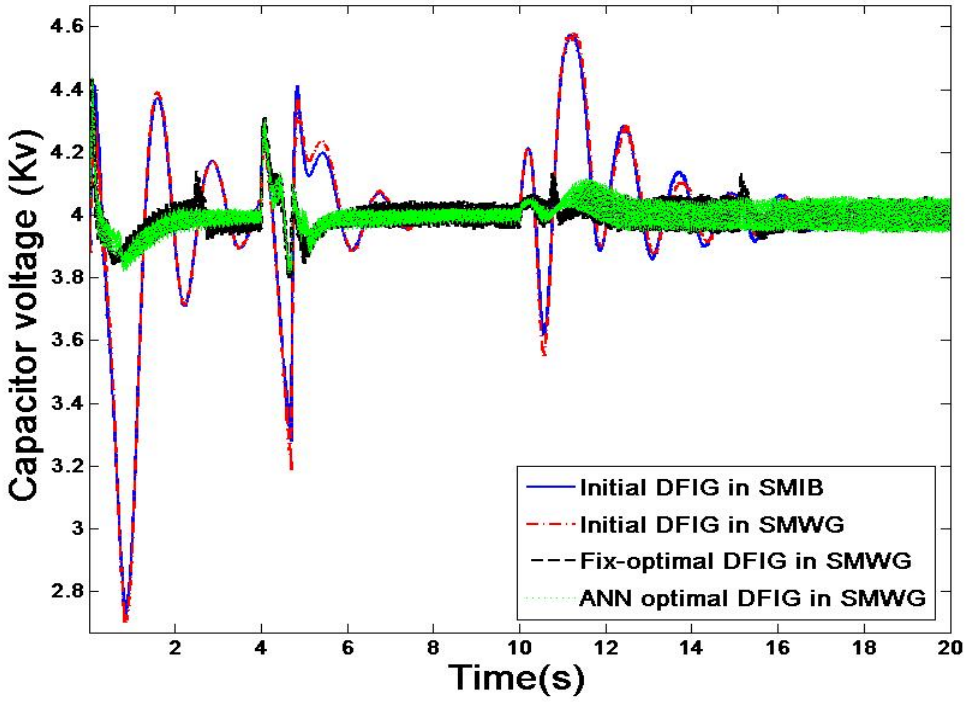

Figure 6.20. Simulation results of DC-link capacitor voltage v_{dc} in SMWG.

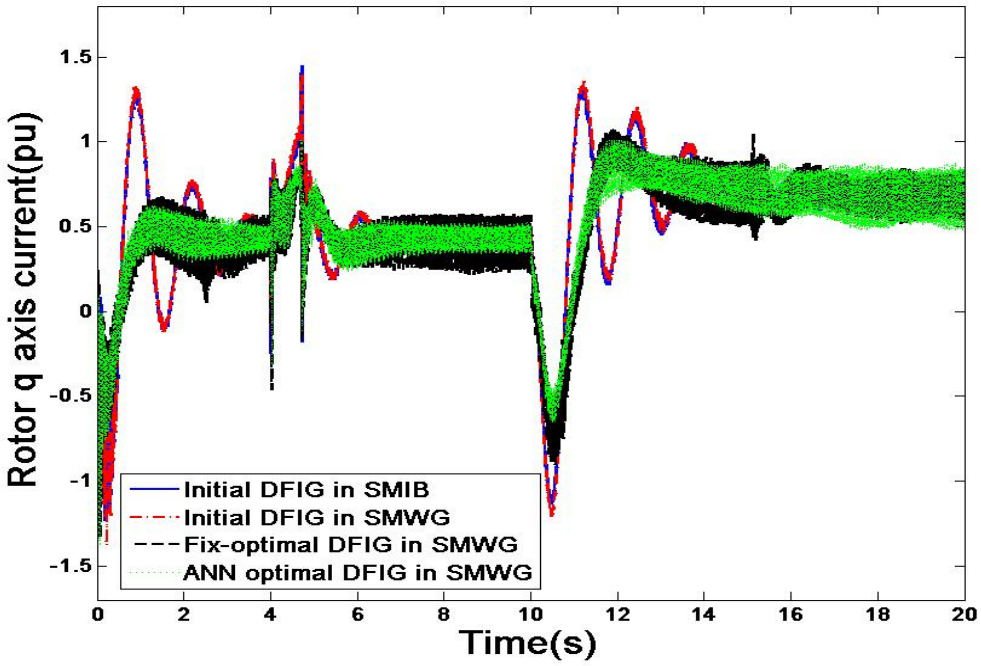

Figure 6.21. Simulation results of rotor q axis current I_{qr} in SMWG.

6.4. System Study for the Multi-machine DFIG and Synchronous Generator Connected to the Grid System (MMS)

In Chapter 6.3, it already found that the ANN optimal DFIG has a better transient performance in SMIB and SMWG systems. In this chapter, the MMS performance and the impacts between DFIG and SG will be discussed.

In Chapter 2.3.1, it was discussed that Power system transient stability is noticeably degraded at high penetration levels due to the high reactive power demand of wind generators under some disturbances. Therefore, high penetration wind levels not only stop improving power system stability in comparison to low penetration levels, but can also decrease power systems stability in comparison to the case without WPPs under some disturbances. Therefore, calculating the penetration limit and margin is significantly important to system planning and operations. In here, fives cases have been planned to

provide more discussions. The multi-machine DFIG system (MMS) is shown in Figure 6.22, and it is similar to the IEEE 9-bus 3 generators system. Power grid data is shown in Table 6.14. SG data is in Appendix I.

- Case 1: G1 is the initial DFIG; G2, G3 are SGs; Penetration is about 30%.
- Case 2: G1 is the ANN optimal DFIG; G2, G3 are SGs; Penetration is about 30%.
- Case 3: G1, G2 are the initial optimal DFIG; G3 is SG; Penetration is about 60%
- Case 4: G1, G2 are the ANN optimal DFIG; G3 is SG; Penetration is about 60%.
- Case 5: G1, G2, G3 are all the ANN optimal DFIG; Penetration is about 90%.

The disturbances are the same with Chapter 6.2.2 except for the fault disturbance. At t=4 seconds, the three-phase short circuit happens in the PCC bus 1 and **the short circuit resistance changes its value to make bus 1 voltage to satisfy grid code low voltage ride-through capability (LVRT) standard** which is shown in Figure 2.5 Chapter 2.4.

Table 6.14. The parameters of MMS test system.

Power Grid:	
Voltage level: Bus 1, 2, 3, 4, 5	34.5 kV
Bus 6, 7, 8	4.16 kV
Frequency	60 Hz
Transmission line	x_{12} = 0.05 p.u.
	x_{14} = 0.05 p.u.
	x_{25} = 0.05 p.u.
	x_{34} = 0.05 p.u.
	x_{35} = 0.05 p.u.
Load: $Load_1$, $Load_2$	6MW+j0.6Mvar
Wind Turbine, DFIG and transformer data are the same with Table 6.1.	
Synchronous generator(SG) data is in Appendix 1	

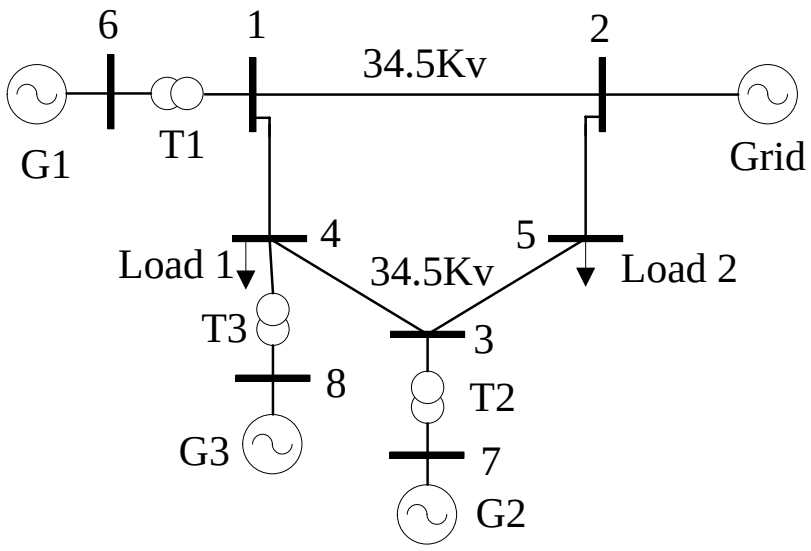

Figure 6.22. The multi-machine DFIG system (MMS).

6.4.1 Eigenvalue Analysis of the MMS System

Using the same steps in Chapter 6.2, small signal stability analysis for MMS system has been conducted. With the limit of space, only the results of Case 3 and Case 4 have been attached. The eigenvalues of the state matrix can be found in Tables 6.15 and 6.16 (only conjugate complex roots of DFIGs are shown) when wind speed is 11m/s.

Table 6.15. The eigenvalues of the initial DFIG model in MMS Case 3.

	σ+jω	ξ	f
λ1,2	-0.229±j0.42	0.479	0.067
λ3,4	-0.101±j2.07	0.048	0.33
λ5,6	-0.235±j6.81	0.034	1.08
λ7,8	-13.50±j91.44	0.146	14.55
λ9,10	-70.35±j387.2	0.178	61.62
λ11,12	-0.219±j0.47	0.42	0.075
λ13,14	-0.198±j4.19	0.047	0.67
λ15,16	-0.29±j7.29	0.040	1.16
λ17,18	-15.65±j93.36	0.165	14.86
λ19,20	-57.32±j391.4	0.144	62.29

Table 6.16. The eigenvalues of the ANN optimal DFIG model in MMS Case 4.

	σ+jω	ξ	f
λ1,2	-0.342±j0.45	0.61	0.071
λ3,4	-0.81±j2.51	0.31	0.40
λ5,6	-1.25±j6.62	0.19	1.05
λ7,8	-28.43±j93.81	0.29	14.93
λ9,10	-81.05±j384.8	0.21	61.24
λ11,12	-0.276±j0.48	0.50	0.076
λ13,14	-0.634±j4.46	0.14	0.71
λ15,16	-1.30±j7.15	0.18	1.14
λ17,18	-23.46±j95.26	0.24	15.15
λ19,20	-86.49±j389.7	0.22	62.02

Then, the PSO can be used to get the optimal parameters of the DFIG's PI gain in Tables 6.17 and 6.18:

Table 6.17. The PI gain parameters of the DFIG 1 in MMS Case 4.

k_{p1}	k_{p2}	k_{p3}	k_{p4}	k_{p5}	k_{p6}	k_{p7}	k_{p8}
0.082	5.18	3.95	5.19	3.11	4.78	0.20	4.71
k_{i1}	k_{i2}	k_{i3}	k_{i4}	k_{i5}	k_{i6}	k_{i7}	k_{i8}
0.114	1.87	140.52	48.15	5.05	228.67	91.72	296.26

Table 6.18. The PI gain parameters of the DFIG 2 in MMS Case 4.

k_{p1}	k_{p2}	k_{p3}	k_{p4}	k_{p5}	k_{p6}	k_{p7}	k_{p8}
0.095	5.45	3.70	4.75	3.31	4.64	0.22	4.65
k_{i1}	k_{i2}	k_{i3}	k_{i4}	k_{i5}	k_{i6}	k_{i7}	k_{i8}
0.127	1.74	145.16	47.35	5.52	221.75	94.48	292.51

Comparing the data in Tables 6.15 and 6.16, it can be seen that the eigenvalue frequencies had only a small fluctuation, but the eigenvalue damping ratios had an obvious increase in the fix-optimal DFIG model in MMS, especially $\lambda_{3,4,5,6,13,14,15,16}$. They almost increased about 3~5 times. In Figure 6.23, it is clear that the eigenvalues of the ANN optimal DFIG model in MMS moved further to the left-half phase plane than the

initial DFIG model in MMS. This means that the former has a better stability. This will be proven in next simulation part.

With the same method in Chapter 6.2, the use of small signal stability analysis will be promoted to get all of the optimal parameters of DFIG 1 and DFIG 2 PI gains in different wind speeds (from 8m/s to 14m/s). The data is shown in Table 6.19 and 6.20. Using the same ANN training method as in Chapter 6.2, the parameters and construction values for the ANNs can be obtained. As they are similar to the values in Chapter 6.2, no detail is provided here because of space limitations. Next, the simulation results of Case 1~5 will be compared.

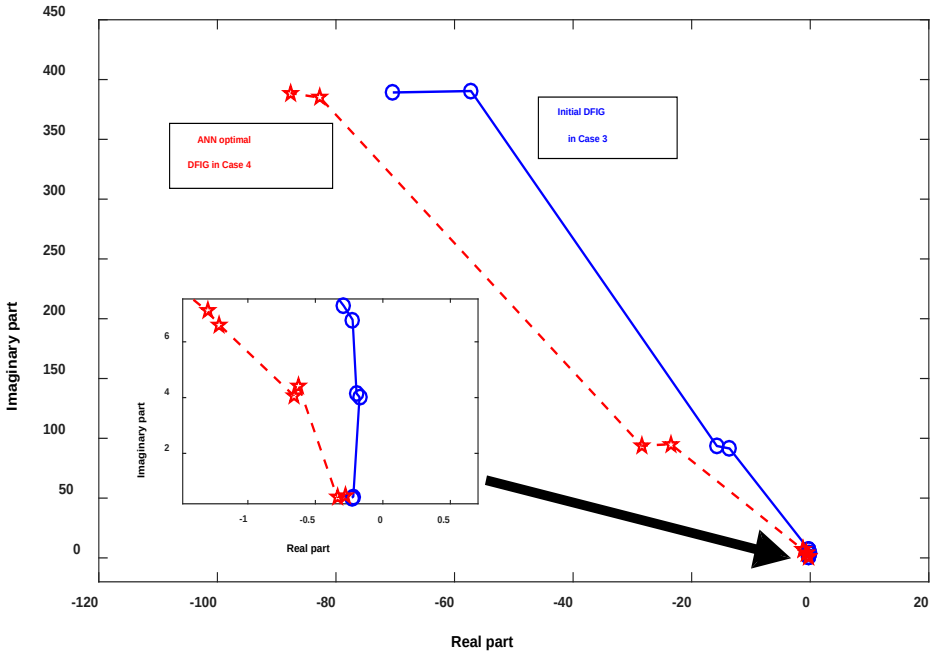

Figure 6.23. The curves of eigenvalues of the initial and optimal DFIGs in MMS in the phase plane.

Table 6.19. The optimal parameters of DFIG 1 PI gains in Case 4 for different wind speeds.

	vw=8.5	vw=9.0	vw=9.5	vw=10	vw=10.5	vw=11	vw=11.5	vw=12.0	vw=12.5	vw=13	vw=13.5	vw=14
kp1	0.0714	0.0762	0.0783	0.0815	0.0834	0.0821	0.0838	0.0859	0.0841	0.0879	0.0878	0.0913
kp2	4.3567	4.6541	4.8764	4.9257	5.0663	5.1231	5.2123	5.3164	5.4782	5.3621	5.1688	5.3518
kp3	4.0966	3.8675	3.5543	3.9016	4.0522	3.9663	3.8755	3.7041	4.1683	4.2251	4.1244	4.0964
kp4	3.9686	4.6554	5.5313	5.1987	5.5177	5.1932	4.9433	5.1246	5.2776	5.3217	5.1946	5.1575
kp5	2.2244	2.6131	2.4710	2.7812	3.0955	3.1641	3.2158	3.1646	3.4718	3.2637	3.0813	3.1776
kp6	5.8161	5.5432	5.3882	4.8844	4.9756	4.7284	4.6737	4.5874	4.9133	4.6349	4.8471	4.8122
kp7	0.2122	0.1967	0.2425	0.2474	0.2214	0.2177	0.2311	0.2457	0.2377	0.2465	0.2635	0.2462
kp8	4.3775	4.8225	5.1241	5.3326	5.0518	4.8883	4.7463	4.7955	4.8537	4.6922	4.5633	4.7508
ki1	0.0823	0.1033	0.0899	0.1158	0.1435	0.1272	0.1222	0.1451	0.1244	0.1335	0.1301	0.1452
ki2	2.0860	2.1078	1.8242	1.6807	1.8943	1.8272	2.0743	1.9725	2.1261	2.3502	2.6671	2.5224
ki3	126.37	135.86	143.42	147.75	139.81	140.96	144.25	136.35	131.65	144.23	146.66	144.56
ki4	33.2456	31.4178	40.5221	44.4615	49.6675	47.4535	44.2612	42.1910	40.9874	42.9821	47.1661	45.4531
ki5	4.2836	4.6186	4.8681	5.1267	5.3145	5.1757	5.0961	4.8932	4.7541	4.6836	4.6250	4.7468
ki6	254.43	235.54	227.87	247.45	243.53	238.44	234.66	250.71	243.85	255.51	249.62	242.25
ki7	92.723	84.437	86.120	85.663	89.645	93.237	90.532	95.944	89.343	85.611	89.854	88.264
ki8	264.46	286.63	297.74	303.32	300.86	297.72	284.43	278.66	281.57	293.54	296.63	301.45

Table 6.20. The optimal parameters of DFIG 2 PI gains in case 4 for different wind speeds.

	vw=8.5	vw=9.0	vw=9.5	vw=10	vw=10.5	vw=11	vw=11.5	vw=12.0	vw=12.5	vw=13	vw=13.5	vw=14
kp1	0.0724	0.0753	0.0795	0.0826	0.0866	0.0848	0.0833	0.0861	0.0843	0.0877	0.0881	0.0915
kp2	4.6756	4.5524	4.8964	4.9577	5.1663	5.2213	5.2771	5.3564	5.5882	5.3221	5.1568	5.0518
kp3	4.1566	3.8896	3.6543	3.7896	4.0322	3.9266	3.8055	3.7254	4.0883	4.2425	4.1344	4.0546
kp4	3.9866	4.5554	5.3531	5.1887	5.5477	5.2532	4.9833	5.1046	5.2977	5.3717	5.1846	5.0775
kp5	2.2544	2.6511	2.2910	2.8812	3.1055	3.1441	3.2058	3.0866	3.4478	3.2563	2.9813	3.0776
kp6	5.7861	5.4454	5.1882	4.6844	4.9557	4.7984	4.6537	4.5474	4.8533	4.6034	4.8671	4.8081
kp7	0.2152	0.1867	0.2525	0.2744	0.2314	0.2077	0.1931	0.2557	0.2277	0.2546	0.2663	0.2578
kp8	4.3577	4.8925	5.1541	5.4326	5.0818	4.6883	4.7463	4.7955	4.8837	4.6422	4.5063	4.8008
ki1	0.0881	0.1133	0.0802	0.1358	0.1635	0.1147	0.1322	0.1551	0.1044	0.1235	0.1366	0.1485
ki2	2.1060	2.0178	1.8042	1.7207	1.9043	1.8472	2.0343	1.9272	2.2261	2.4502	2.6266	2.5112
ki3	125.44	133.68	141.42	147.22	138.81	140.66	145.25	138.27	129.65	144.23	148.63	143.85
ki4	34.3324	32.3541	43.5221	46.4415	49.1166	48.35	45.2612	42.4110	40.2474	43.6821	48.2661	45.2331
ki5	4.2436	4.5386	4.9681	5.2767	5.0345	5.1557	5.0661	4.8532	4.7345	4.5636	4.6050	4.7235
ki6	255.24	237.54	225.77	250.45	240.53	230.44	235.66	256.37	240.85	265.51	248.62	238.52
ki7	91.472	85.453	82.612	85.663	88.865	92.37	90.232	95.442	90.543	84.611	89.554	88.524
ki8	265.74	285.63	297.85	302.32	305.86	298.42	286.43	272.66	280.85	291.54	297.46	301.87

6.4.2. Simulation Analysis of the MMS System

The MMS system is shown in Figure 6.22. PSCAD is used as the simulation tool to prove the transient performance improvement by comparing Case 1~5:

The simulation results of case 1~5 DFIG G1's real power, mechanical torque, connection point voltage, DC-link capacitor voltage, and rotor q axis current, are shown in Figure 6.24-6.28, respectively. Comparing the results, the transient performances of the ANN optimal DFIG model are obviously much better than the initial DFIG model as it has already been proved in Chapter 6.2.2. When the fault happens at t=4 seconds according to grid code, the connection point voltage Vs even drops to 0.05pu. This causes

some serious low frequency oscillations and the DC-link capacitor voltage V_{dc} almost drops to 0 in case 1 and case 3. Case 2 and 4 obviously have the capability to greatly reduce these low frequency oscillations. Moreover, they have some better transient performances when the wind speed changes. Therefore, it will focus on the discussion of cases 2, 4, and 5 in this part.

Cases 2, 4 and 5 present low penetration system, medium penetration system, and high penetration system, separately. It briefly discussed the different impacts of power systems stability of FSIG, DFIG and PMSG in Chapter 2.3.1. With the simulation results, it could compare the different impacts of DFIG and SG at different penetration conditions.

In case 5, there are only DFIGs, not any SGs. It is easy to find that it has a better performance in the wind speed change disturbance than cases 2 and 4 because DFIG holds a better decoupled effects than SG, but it bears some worse low frequency oscillations in the fault disturbance. Part of reasons may be that case 5 doesn't have any SGs so that DFIGs can't generate enough reactive power.

In the starting state, DFIG 1 of cases 2, 4, and 5 almost has the same performance, even though case 5 has a slight advantage in some peak/trough values.

In the fault state, the values of Po, Tm, Vdc and Iqr in cases 2 and 4 successfully wipe out the low frequency oscillations and this is the most advantage, comparing with case 5. With the increase of penetration, V_{dc} trough value significantly drops from 3.26Kv, 2.31Kv to 0.10Kv and T_m has a serious low frequency oscillation between 0.15pu (peak) and -1.14pu (tough). It is very bad for gearbox's safety. The main differences of case 2 and 4 are V_{dc} trough value (3.26Kv/2.31Kv) and P_o trough value

(1.94MW/0.67MW). Case 2 may have a little better performance in fault state than case 4, much better than case 5.

In the wind speed change state, case 5 obviously have a better performance than case 2 and 4. The peak/trough values of P_o, $T_{m,}$ and I_{qr} of case 5 and case 4 are 4.24MW/1.37MW, -0.56p.u./-1.28p.u., 1.08p.u./0.37p.u., 4.69MW/-2.52MW, 0.39p.u./-1.29p.u., 0.96p.u./-0.51p.u., respectively. Obviously, case 5 greatly reduces the gaps of peak/trough of P_o, $T_{m,}$ and I_{qr} so that it is very good for generators safety and system stability. Vs of case 5 recovers more quickly than case 4, even though it has a small oscillation. The only drawback of case 5 is that V_{dc} recovers from very low voltage so that it charges to a high voltage about 5.68Kv. Case 4 and case 5 have almost the same performance in this state.

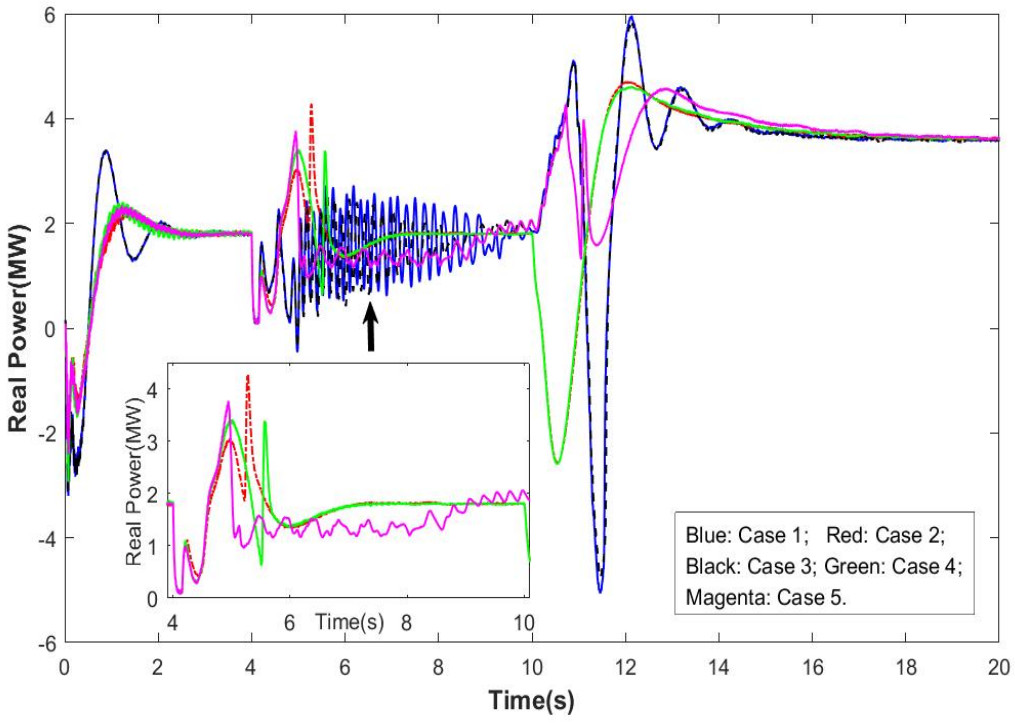

Figure 6.24. Simulation results of real power P_o in MMS.

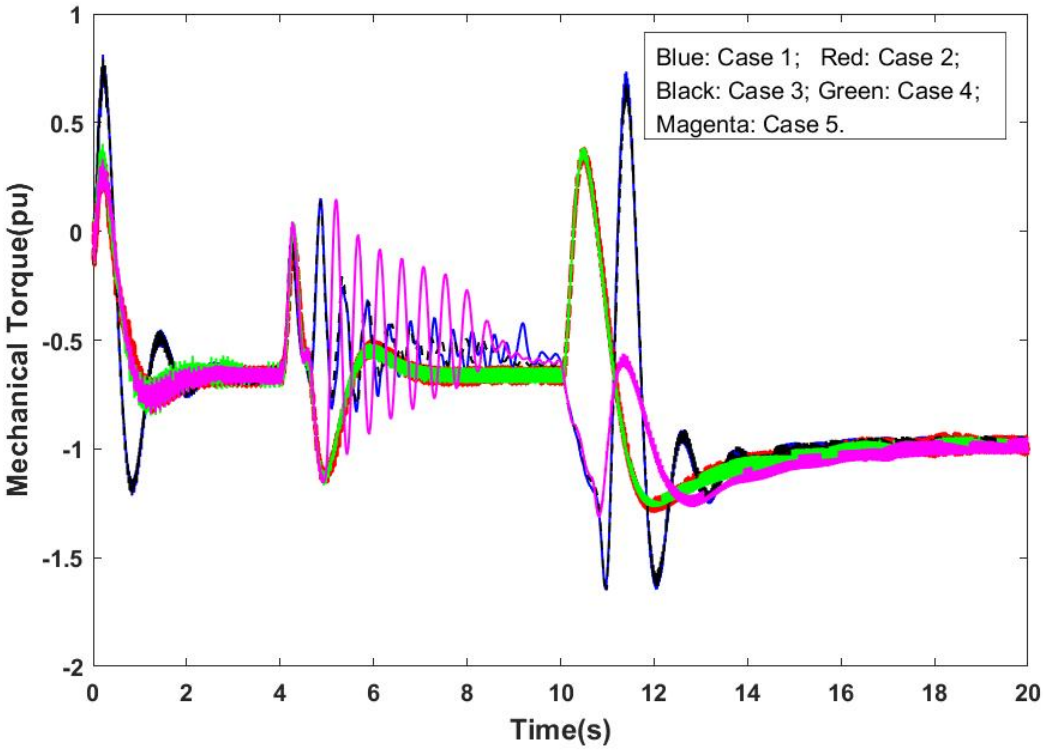

Figure 6.25. Simulation results of mechanical torque T_m in MMS.

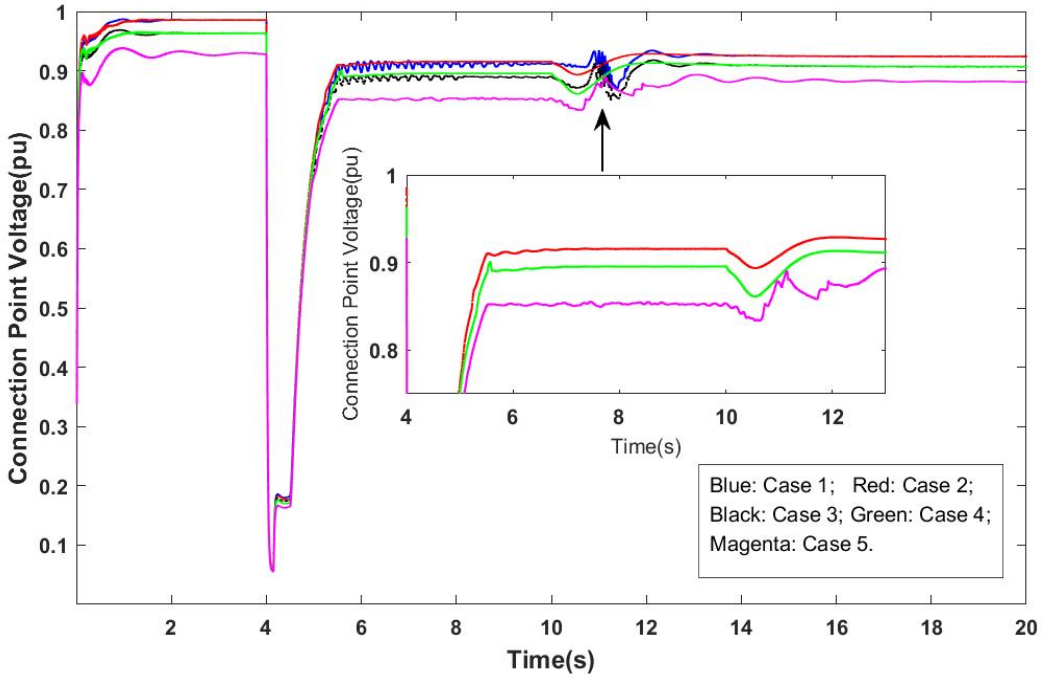

Figure 6.26. Simulation results of connection point voltage v_s in MMS.

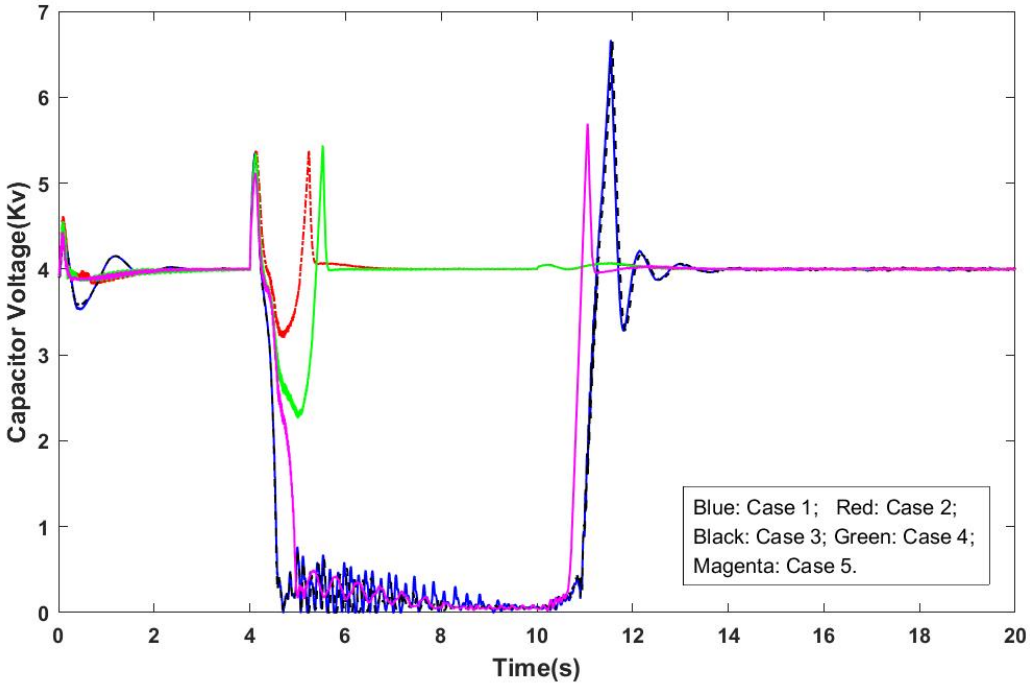

Figure 6.27. Simulation results of DC-link capacitor voltage v_{dc} in MMS.

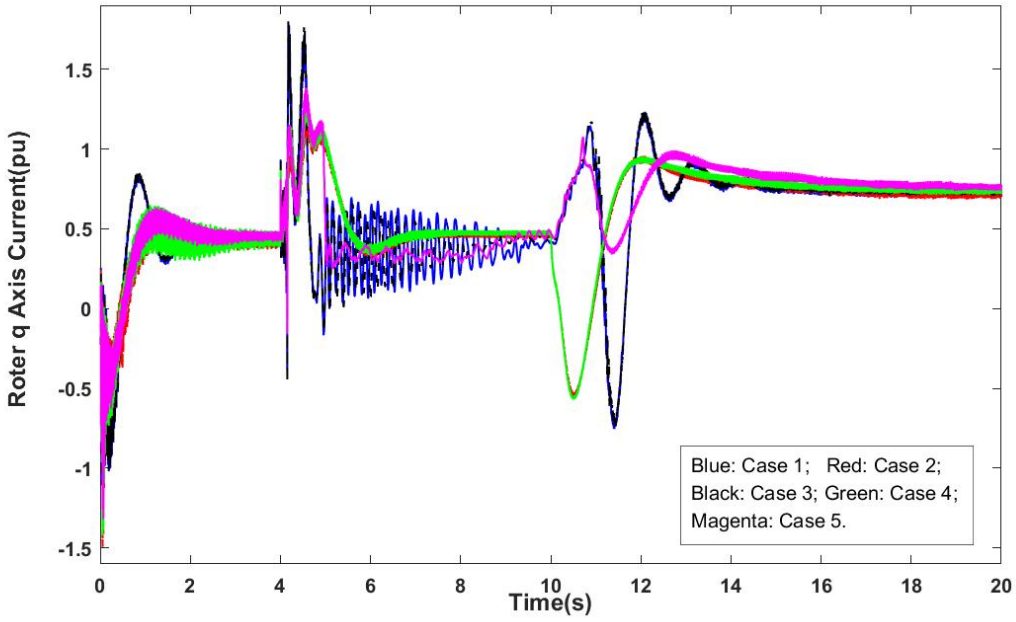

Figure 6.28. Simulation results of rotor q axis current I_{qr} in MMS.

6.5 System Study for DFIG in Distribution Systems

With the increase of wind power penetration in distribution systems, voltage fluctuation, flicker and harmonics in distribution systems become a hot topic. In general, reactive power compensations are very important to wind power in distribution systems. Lack of sufficient reactive power may result in voltages typically lower (0.05-0.1p.u.) than normal voltages in [9]. However, the worse disturbances in system operation occur during the cut-in and cut-off of wind power generators from the grid. In some autonomous power systems, the frequency and voltage level would decrease more than 1Hz and more than 0.05-0.1pu [126], respectively. This dissertation will simply discuss the voltage analysis of a moderate size system, i.e., the IEEE 34-bus test system [127], which includes WT-DFIGs. Simulation studies are carried out in DIgSILENT software [128] to investigate effect of WT-DFIGs on the steady-state and transient behavior of the distribution systems.

6.5.1 The Introduction of DFIG in IEEE 34-bus Distribution Test System

The IEEE 34-bus test system shown in Figure 6.29 is a typical radial-distribution system and the simulation system is constructed with DIgSILENT using detailed data in [127] and Appendix II.

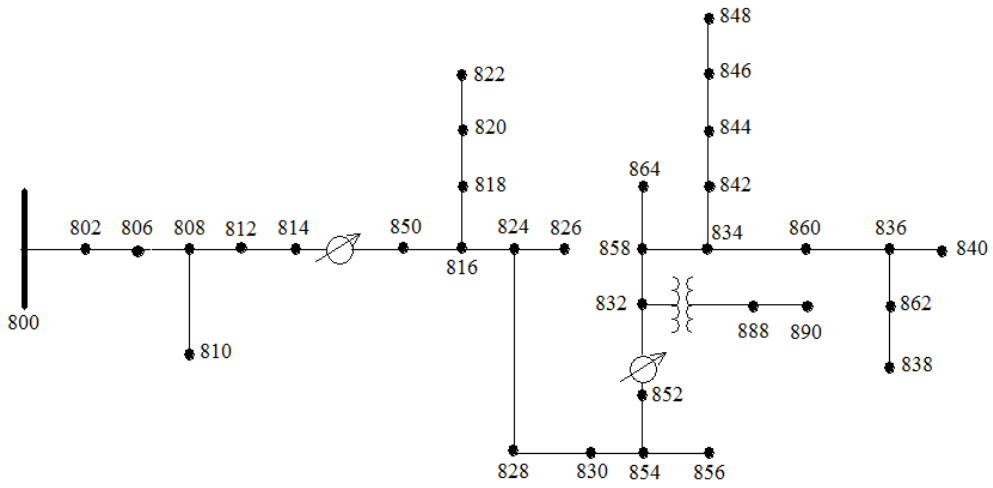

Figure 6.29. The IEEE 34-bus test system.

The system has two auto-regulators which regulate the voltage in ±0.05p.u. range and one auto-transformer which controls the voltage in ±0.05p.u. range. They are set to automatic-tap adjustment for the basic case position because their initial tap position has a significant role on the system voltage regulation. The distributed loads are handled as split loads with half on each bus. In the test system, bus 800 is connected to the grid and buses 890 and 844 are the load centers. The voltage at bus 890 is usually low because the line between bus 888 and 890 is relatively long. Several shunt capacitors are added at buses 844 and 848 to totally compensate for reactive power 0.75MVar. The two regulators work together to control bus 852 voltage and it plays an essential role in system voltage control. In light loading conditions given by [127], the total unbalanced load is 1.769MW and 1.044MVar; the grid loss is 0.27MW; the voltages at buses 852 and 890 are 0.965p.u. and 0.921p.u., respectively. Other bus voltages are in the range of 0.95-1.05p.u. Bus 890 is apparently the weakest bus.

6.5.2 Basic case study for one single DFIG connected to the test system

The average bus voltage $\bar{V}$ is usually used to evaluate the system voltage profile [129]. However, it does not reasonably reflect the system voltage unbalanced factor. A new index (system unbalanced voltage variance) is proposed to evaluate system voltage as follows:

$$\bar{V} = \sum_{i=1}^{N} \frac{V_{iA} + V_{iB} + V_{iC}}{3N} \tag{6.1}$$

$$s^2 = \sum_{i=1}^{N} \frac{(V_{iA} - 1.05)^2 + (V_{iB} - 1.05)^2 + (V_{iC} - 1.05)^2}{3N} \tag{6.2}$$

Where $V_{iA,}$ $V_{ib,}$ V_{iC} are the 3-phase voltages at bus i; N is the system bus number; $\bar{V}$ is the system average voltage; s^2 is the system unbalanced voltage variance (using 1.05 to replace $\bar{V}$ for a higher accuracy).

If a constant load (1.0MW, 0.1MVar) is added at the terminal bus 840 and reactive power compensation (0.30MVar) is added at bus 890, the regulator 2 and transformer reach the maximum tap position. Bus 852 voltage is 0.909p.u. and the grid loss is 0.71MW. If the tap of the regulator 1 is manually increased, the three-phase voltage at bus 890 changes and becomes more unbalanced. Therefore, this unbalanced heavy loading condition is selected as the base case for the rest simulation studies. The single 1.5MW DFIG (DIgSILENT provided) is connected at various bus locations to evaluate which location provides the most system-voltage improvement and the most reduction in grid loss. In order to easily analyze the difference between the average bus voltage and the system unbalanced voltage variance, an index (1.05-s) is selected. The result is shown in Figure 6.30-6.31.

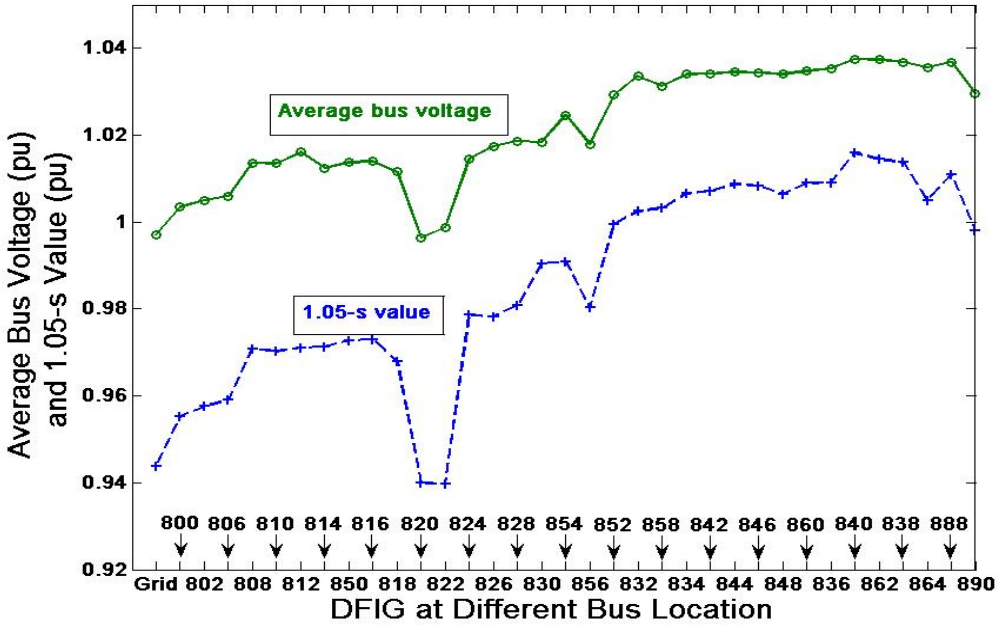

Figure 6.30. Average bus voltage and 1.05-s value when a 1.5MW DFIG placed at different locations.

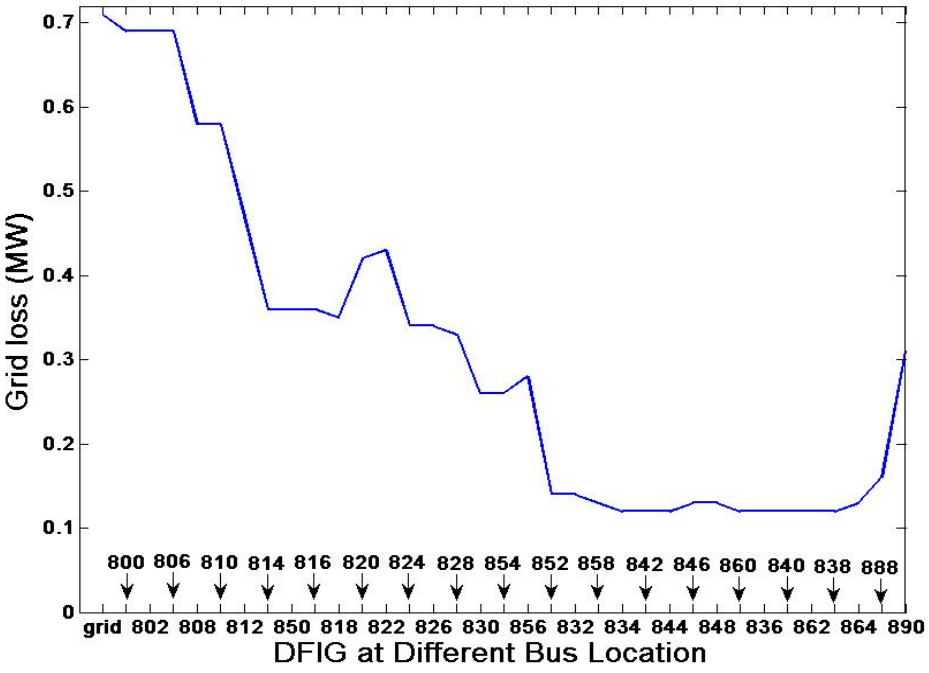

Figure 6.31. Grid loss when a 1.5MW DFIG placed at different locations.

With the DFIG's location closer to the load center (buses 840, 844, and 890), the voltage profile is improved more and the grid losses greatly reduced. The average bus

voltage and 1.05-s value basically have the same trend. However, the latter has a higher accuracy to evaluate the unbalanced system voltage improvement, especially where DFIG is connected at buses 840 and 888. The average bus voltage index could not reflect the degree of voltage unbalance. At bus 840, 1.05-s value reaches the maximum value while at buses 834, 842, 844, 860, 836, 840, 862, and 838, the grid losses are in the same minimum level. Therefore, the optimal location is determined to be bus 840.

The transformer adjusts voltage range to increase from ±0.05p.u. to ±0.1p.u. when DFIG is connected at bus 890 because it is a low-voltage bus (4.16KV), otherwise more voltage (0.13p.u.) drops in the long low-voltage line between buses 890 and 888. If more power transfers through the low-voltage line to the grid, the grid loss increases to 0.30MW. If the WT is large, it is better to install it at a high voltage transmission line and closer to the load center. However, if the load centers are far away from each other or the loads are more distributed, the optimal location should be carefully calculated by a formulating multi-objective optimization:

$$\min : p_s k_s s_i + (1 - p_s) P_{lossi}, \left(i \in WT \; at \; different \;\; bus \; cases\right) \tag{6.3}$$

Where:

s_i is the standard deviation corresponding to system unbalanced voltage variance defined in Equation 6.2.

k_s is a conversion factor in (MW/Volts) to adjust them on the same number class.

P_{lossi} is the grid power loss associated with the case s_i.

P_s is the weight associated with the case s_i; 1-P_s is the weight of P_{lossi}.

Equation 6.3 is used to find the optimal location for installing WT, simultaneously considering the system unbalanced voltage variation and the grid power loss.

6.5.3 Comparison of Steady-state and Transient Impacts between a Single Large-DFIG System and a Multiple Small-DFIG System

Two smaller DFIGs (0.75MW) are added at buses 832 and 836 to compare the steady-state impacts with a single large DFIG (1.5MW) at different buses in the system. The results are shown in Figure 6.32.

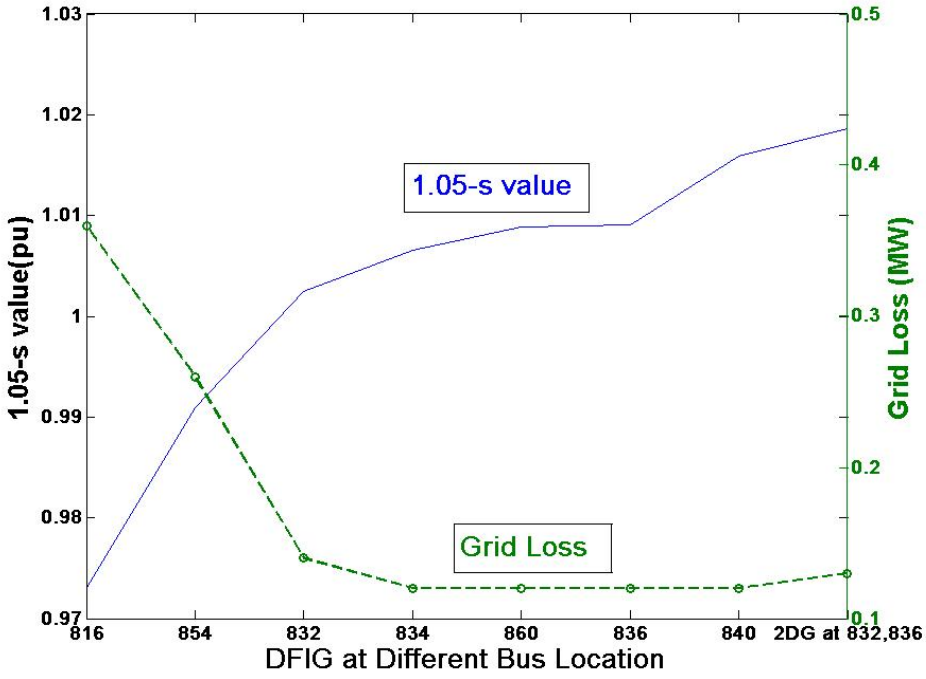

Figure 6.32. Comparison of grid loss and 1.05-s value between a single large-DFIG system and a multiple small-DFIG system.

As shown, the multiple small-DFIG system could provide higher 1.05-s value and better system voltage improvement. Its grid loss is almost the same as the optimal grid loss of the single large-DFIG system. Moreover, the optimal locations of the multiple small-DFIG system could be calculated and its grid loss would be less. Therefore, the multiple small-DFIG system is more suitable than the single large-DFIG system.

Short circuits, cutting load (including constant Z load and motors load), and DFIG cut-off or cut-in are the major disturbances in distribution systems. The load-center voltage

waveforms are determined when subjected to these disturbances. However, the size of some dynamic models is adjusted to provide a stable convergence.

Case C1: the single DFIG (0.75MW) is placed at bus 856; reactive power compensation is adjusted to 0.60MVar at bus 890 and the load at bus 890 is adjusted to 0.25 MW motor. These following disturbances occur in sequence:

At t=0.18s, a 3-phase short circuit (using fault impedance Z=15+j40Ohm to control the voltage of bus 840 at 0.5p.u. in the fault) at bus 862; At t=0.28s, clear short circuit; At t=0.35s, cut the 1MW load (at bus 840); At t=0.45s, recover the load; At t=0.65s, cut the motor; At t=0.8s, cut-in the motor; At t=1s, cut-off DFIG; At t=1.18s, cut-in DFIG.

The results are shown in Figure 6.33-6.34.

Figure 6.33. The voltages of buses 840 and 890 for case C1.

Figure 6.34. The voltages of buses 844 and 900 (connected DFIG and bus 856) for case C1.

From Figure 6.33-6.34 which are shown, the load-center voltage fluctuates about 0.1 p.u. because of the cut-off of the large load which affects almost all bus voltages. The dynamic impacts of cut-in DFIG and the motor are larger than cut-off and the motor has a significant role on the local bus voltage. Therefore, the low voltage bus 890 is the most fluctuant, and considered as a weak bus.

Case C2: Based on the condition of case C1, these following disturbances occur simultaneously: At t=0.18s, 3-phase short circuit at bus 862; At t=0.2s, cut the motor; At t=0.25s, cut-off DFIG; At t=0.38s, clear short circuit; At t=0.43s, cut-in DFIG; At t=0.5s, cut-in the motor; At t=1.4s, cut the large load; At t=1.6s, recover the load. The results are shown in Figure 6.35-6.36.

Figure 6.35. The voltages of buses 840 and 890 for case C2.

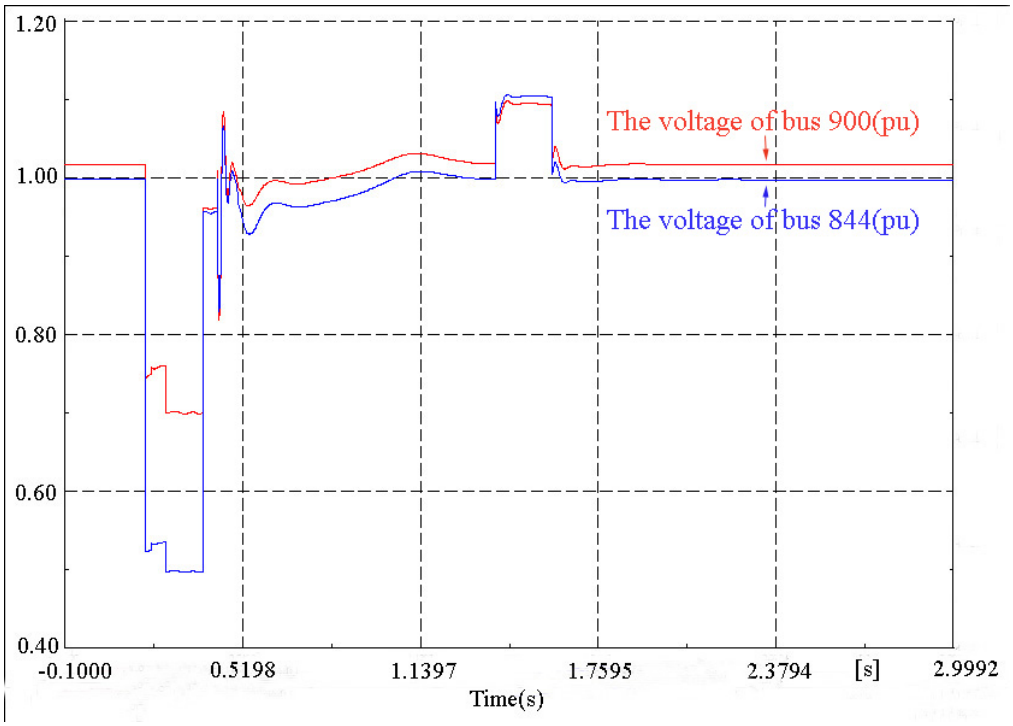

Figure 6.36. The voltages of buses 844 and 900 for case C2.

From the results shown in Figure 6.35-6.36, the voltage of bus 890 connected to the motor is more affected and it takes more time (0.5s) to return to its initial state when these disturbances simultaneously occur.

Case C3: Based on the condition of case C1, two DFIGs (0.35MW) are added at buses 856 and 840 to replace the initial DFIG; the load at 840 is adjusted to 0.7MW; the disturbances separately occur and are the same as the disturbances in case C1. The results are shown in Figure 6.37-6.38. By comparing Figure 6.37-6.38 with Figure 6.33-6.34, the multiple small-DFIG system bores a less dynamic impact and it takes less time to return to its initial state. Furthermore, the system voltage maintains in the normal range from 0.95p.u. to 1.05p.u. for longer period of time.

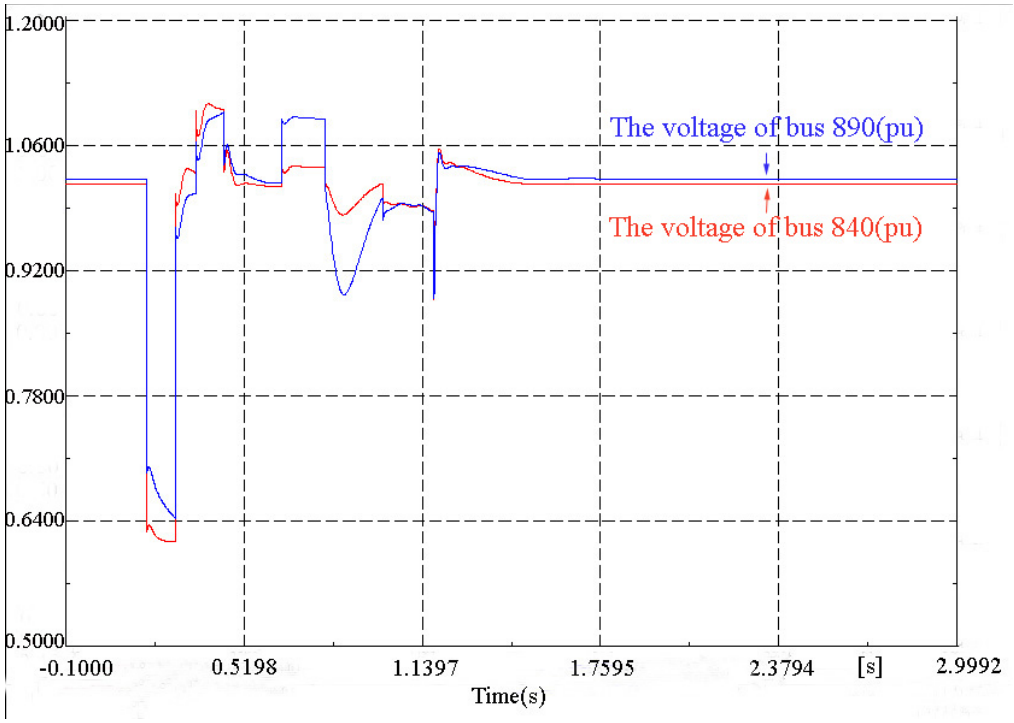

Figure 6.37. The voltages of buses 840 and 890 for case C3.

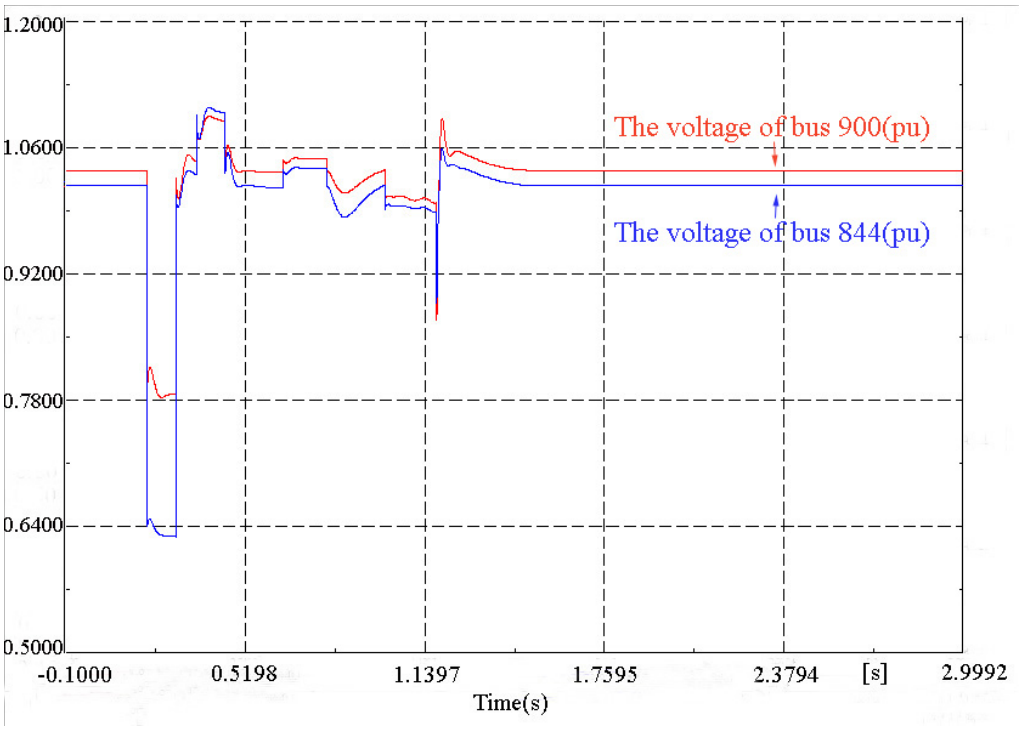

Figure 6.38. The voltages of buses 844 and 900 for case C3.

Case C4: Based on the condition of case C2, two DFIG (0.35 MW) are added at buses 856 and 840 to replace the initial DFIG and these disturbances simultaneously occur and are the same as the disturbances in case C2. The results are shown in Figure 6.39-6.40.

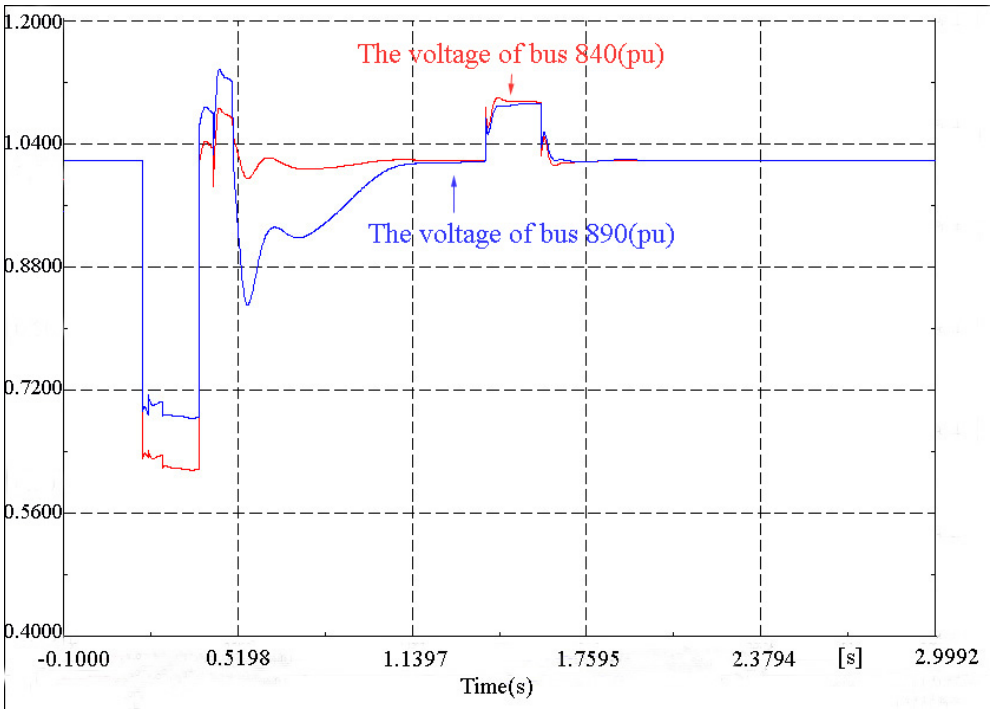

Figure 6.39. The voltages of buses 840 and 890 for case C4.

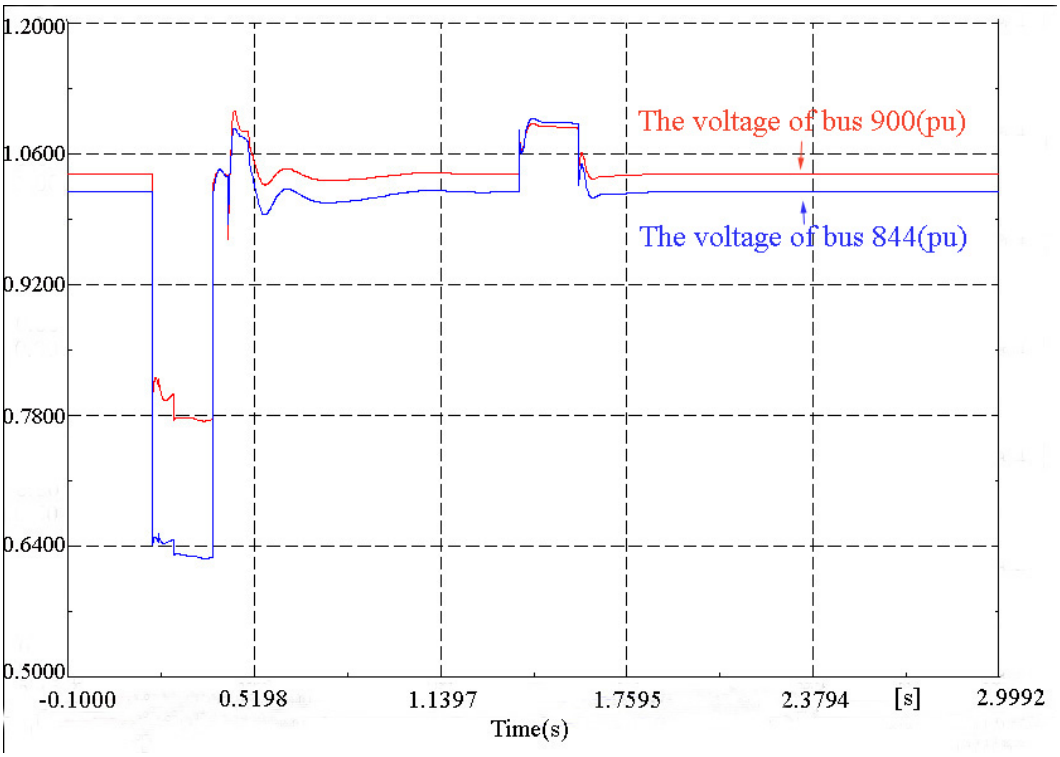

Figure 6.40. The voltages of buses 844 and 900 for case C4.

Considering the difference between Figure 6.39-6.40 with Figure 6.35-6.36, the multiple small-DFIG system has a better stability performance. The voltage fluctuation is in a smaller range and the boundary values are more suitable.

6.5.4 Summary of DFIG in Distribution System

This dissertation has investigated the effects of WT-DFIGs on voltage stability and grid loss of distributions systems under unbalanced load conditions. A new index (system unbalanced voltage variance) has been proposed to evaluate system unbalanced voltage, which is more reasonable and more accurate than that normally using system average voltage. A new multi-objective optimization function has been provided to calculate the optimal location simultaneously considering the voltage profile and grid loss. Simulations studies have been carried out in DIgSILENT software to examine the impacts of WT-DFIGs on the steady-state and dynamic behavior in the IEEE 34-bus test system under

unbalanced heavy loading conditions. The optimal location of the single large DFIG-WT in the test system has been determined. Through the comparison between the single large-DFIG system and the multiple small-DFIG system, the latter could provide higher system voltage advancement and almost the same grid loss reduction as the former. In dynamic simulation, different disturbances, short circuits, cutting load (including constant Z load and motors), cut-off and cut-in DFIG, have been applied separately or simultaneously. The load-center voltages fluctuate about 0.1p.u. in this distribution system because of cutting the large load or cut-in DFIG and they affect almost all bus voltages. The dynamic impact of cut-in DFIG is apparently more significant than cut-off DFIG. The motor has a significant role on the local bus voltage and is very sensitive to disturbances. The soft-start motor and DFIG technology should be paid more attention in distribution systems. The multiple small-DFIG system bores a less dynamic impact and needs less time to return its initial state than the single large-DFIG system. Moreover, the former voltage fluctuation is in a smaller range and the boundary values are more suitable and the system voltage maintains in the normal range from 0.95p.u. to 1.05p.u. for longer time. Therefore, the multiple small-DFIG system has a better stability performance than the single large-DFIG system.

6.6 Summary

This chapter firstly introduces the flowchart of the ANN optimal DFIG model design procedure. It mainly includes five steps: select the appropriate test system/DFIG model/ PSO parameters, specify the DFIG's PI parameters, small signal stability analysis, PSO, ANN training and controllers design. Next, attentions are focused on eigenvalues analysis and simulations of the SMIB system for three types of DFIG model. The results show

that the ANN optimal DFIG model greatly reduces low frequency oscillations and peak/trough value of T_m, P_o, I_{qr}, and v_{dc} in the transient performances of disturbances so that it has a better stability. Subsequently, eigenvalues analysis and simulations are applied in the SMWG system for three types of DFIG model. The results prove the ANN optimal model holds an obvious advantage even though the effect of improvements is not as good as the effect in SMIB. The reason is that the optimal parameters can partly weaken the influence of the weak grid, but the weak grid obviously has a stronger impact to this system than the optimal parameters. If the grid is too weak, the system will lose the stability. After that, the MMS system for 5 cases including DFIG and SG has been analyzed to discuss the different impacts of DFIG and SG. With the penetration increase from 30% to 60%, the stability and DFIG transient performance may be slightly weakened, but not obvious. Therefore, the stability of low/medium penetration systems had to be carefully analyzed case by case. If the penetration continuously increases to 90%, it is easy to find that the system has a better performance in the wind speed change disturbance than low/medium penetration systems, but it bears some worse low frequency oscillations in the fault disturbance. Finally, the issues of voltage stability improvement and grid-loss reduction of distribution systems (IEEE 34-bus test system) which include WT-DFIG under unbalanced heavy loading conditions is investigated. Simulation studies are carried out using DIgSILENT software to examine these issues during steady-state and transient operations of the system. The dynamic impact of cut-in DFIG is apparently more significant than cut-off DFIG in distribution systems. The multiple small-DFIG system bores a less dynamic impact and needs less time to return its initial state than the

single large-DFIG system. Therefore, the multiple small-DFIG system has a better stability performance.

CHAPTER 7
CONCLUSIONS AND FUTURE RESEARCH

7.1 Conclusions

In this dissertation, the approaches used for studying the impact of wind generation on grid stability and the optimizing of PI control of WTs with DFIGs via PSO were designed to improve DFIG system stability and transient performance in disturbances. A small signal stability analysis with a detailed WT-DFIG model is included, and an ANN controller has been designed, trained, and is able to directly forecast the optimal parameters according to different wind speeds, thus increasing DFIG transient performance. System studies for a single machine (DFIG) connected to the infinite bus system (SMIB), a single machine (DFIG) connected to a weak grid (SMWG), multi-machines (DFIG) connected to the grid system (MMS), and IEEE 34-bus distribution systems with DFIG have been completed.

A summary of the contributions of this dissertation follows.

1. *Discussion of the key factors which influence the stability of power systems with wind generation*

The stability of power systems with wind generation is classified and the key factors which influence the stability are discussed, including the different wind turbine generator technologies, energy storage system (ESS), reactive power compensation, wind power forecasting, system operations for the challenge of high wind penetration condition.

A. Fixed speed induction generators (FSIG), doubly fed induction generators (DFIG), and permanent magnet synchronous generators

(PMSG) are respectively the old-popular, now-popular, and future-popular wind turbine generator technologies. FSIG can improve power systems transient stability; but it is poor in comparison with DFIG. DFIG has a good ability to ride through faults, and it can work as a power reactive compensator during faults. A comparison of the different impact on the stability of DFIG and PMSG is not sufficient. Power systems transient stability is noticeably degraded at high penetration levels due to the high reactive power demand of wind generators under some disturbances. Therefore, high levels of wind power penetration not only stop improving power systems stability as compared to low penetration levels, but it can decrease power systems stability in comparison with the case without wind generation under some disturbances.

B. It has been proven via theories and experiments, that ESS can considerably improve the transient stability of a wind power plant system.

C. Reactive power compensation with wind farms has gradually proven to be an effective, easy method to improve voltage stability, power quality, and operational characteristics of wind farms. Yet, the optimal location and reactive power compensation strategy must be considered on a case-by-case basis.

D. Wind power forecasting plays an important role in enhancing the stability, efficiency, and reliability of modern power systems; and

its importance is gradually increasing. The ultimate goal is to enhance prediction accuracy and to develop models that can be used as the basis for predictive control.

E. Some system operations can be used to improve the ability to integrate the increasing amounts of wind capacity into power systems while maintaining system stability.

2. Small signal stability analysis with detailed WT-DFIG model

The model for small signal stability analysis is provided in this dissertation and includes a wind turbine with a two-mass shaft system, induction generator, detailed rotor-side/grid-side converter, and interface with the power grid. The optimization problem was formulated to maximize the objective function (the damping ratios of system eigenvalues in small signal stability analysis). The control variables are Ki and Kp of DFIG PI gains parameters. The interconnection requirements, grid code, and the impacts of crow-bar activation of wind generation are also briefly discussed, including the effects of the pre-disturbance speed of DFIG rotor, crow-bar impedance, and rotor-side converter restarting.

3. Advanced particle swarm optimization based on small signal stability analysis with DFIG

Advanced PSO is based on small signal stability analysis with a DFIG and is designed to calculate the optimal parameters of a DFIG because of PSO's attractive properties (low memory requirement, easy constructive cooperation, better and fast convergence, and robustness). The optimization should take a long time (about two hours on a PC) to solve the optimization problem. Therefore, it had to be done off-line and

couldn’t be directly used in online control. Second, these optimal parameter values only match one special operating point. At another wind speed operating point, the initial optimal parameter values may be not optimal values. So, the optimal values had to be calculated according to different wind speed operating points (from 8m/s to 14m/s) and a data set obtained with one group of optimal values matching different wind speed values.

4) Artificial neural network controller design

One of the significant contributions of this dissertation is the development of an artificial neural network controller to dynamically adjust PI gain parameters of DFIG to improve system stability and transient performances in disturbances. Using the historical data via PSO, an artificial neural network can be constructed and trained. After that, this ANN can quickly predict the optimal values according to the wind speed. The forecast result of test data showed output ≅ 0.97*Target+0.0024. The best validation performance index, Mean squared error (MSE), was 2.6669e-07. This dissertation equivalently realizes real-time optimization via training ANN to forecast optimal values and transfer much of the calculations to be done off-line.

5. System studies and simulation conclusions

System studies for several test systems were conducted using the initial DFIG model, the fix-optimal DFIG model, and the ANN optimal DFIG model. The small signal stability analysis and simulation results follow:

A. In the SMIB system, there are three main oscillation modes:

1) Low frequency oscillations near 0.05~1.1Hz (mechanical mode associated with turbine and shaft dynamics);

2) Electric-mechanical mode associated with rotor electrical (q-flux) and mechanical (speed) dynamics near 14.5Hz;

3) Electrical mode associated with stator dynamics near 62Hz. The eigenvalue frequencies of the fix-optimal DFIG model changed slightly while the eigenvalue damping ratios increased greatly, compared to the initial DFIG model. The eigenvalues of the former are farther away in the left-half phase plane. In simulation results, the ANN optimal DFIG model greatly reduced the low frequency oscillations and the peak/trough values of T_m, P_o, I_{qr}, and v_{dc} during the disturbances. The small signal stability analysis and simulation results get the same result: the ANN optimal DFIG model had better stability and transient performance.

B. In the SMWG system, the eigenvalues move closer to the right-half phase plane than SMIB. This means that the weak grid reduces the stability of the DFIG system. The eigenvalue frequencies have increased slightly, and the damping ratios have reduced some; but the weak grid has a bigger impact on the electrical mode associated with stator dynamics. If the grid is too weak (x_{TL}=0.35p.u.), the initial DFIG model will lose stability while the fix-optimal DFIG model finally goes back to the steady-state even through it bears some serious oscillations. This also shows that the optimal parameters can partly weaken the influence of the weak grid, but

the weak grid obviously has a stronger impact on this system than the optimal parameters.

C. In the MMS system, 5 cases including the initial DFIGs, the ANN optimal DFIGs, and SGs have been simulated and analyzed, considering the grid code low voltage ride through requirements and the different penetrations. With the penetration increase from 30% to 60%, the stability and DFIG transient performance may be slightly degraded, but not obviously. Therefore, the impacts of low/medium penetration systems had to be carefully analyzed case by case. If the penetration continuously increases to 90%, the system has a better performance in the wind speed change disturbance than low/medium penetration systems, but it bears some worse low frequency oscillations in the fault disturbance.

D. In the 34-bus distribution system, a new index (system unbalanced voltage variance) was proposed to evaluate the system voltage unbalanced factor. The optimal location of the DFIG was carefully calculated by a new multi-objective optimization formula, which simultaneously considers the system unbalanced voltage variation and the grid power loss. The comparison between the single large-DFIG system and the multiple small-DFIG system found that the multiple small-DFIG system could provide higher system voltage advancement and almost the same grid loss reduction as the single large-DFIG system. In dynamic simulation, different disturbances,

short circuits, cutting load (including constant Z load and motors), cut-off and cut-in DFIG, have been applied separately or simultaneously. The load-center voltages fluctuate about 0.1p.u. in this distribution system because of cut-off the large load or cut-in DFIG and they affect almost all bus voltages. The dynamic impact of cut-in DFIG is apparently more significant than cut-off DFIG. The load of motor type has a significant role on the local bus voltage and is very sensitive to disturbances. The multiple small-DFIG system bores a less dynamic impact and needs less time to return its initial state than the single large-DFIG system. Moreover, the former voltage fluctuation is in a smaller range and the boundary values are more suitable and the system voltage maintains in the normal range from 0.95p.u. to 1.05p.u. for longer time. Therefore, the multiple small-DFIG system has a better stability performance than the single large-DFIG system.

7.2 Recommendations for Future Research

1. *Improve the algorithms of PSO and ANN*

PSO may need a long time to get the optimal parameters if the algorithms are applied in a multi-machine system so that the number of variables greatly increases. Therefore, it is very important to advance and accelerate the convergence of PSO. A more complex construction of an ANN can improve the accuracy of forecasting the optimal parameters so that it is also a key point to increase the performances of the algorithms.

2. *Optimize considering reactive power of DFIG*

This dissertation neglected the capability of DFIG to adjust reactive power output. However, with the fast development of power electronics, DFIG can output more reactive power and bear a bigger impact of disturbances so that it will become a hot issue: how to improve the transient performances via optimal control of reactive power of DFIG, especially in low voltage ride-through capability and voltage stability in distribution system.

3. *Implement the application in industry*

Currently, the PI parameters are constant in an actual DFIG. This dissertation only realized the algorithms in a simulation PSCAD. How to realize it in an actual device is still a big challenge, and it will be more significant than the improvement of the algorithms.

4. *Application of wind generation control in EMS*

Currently, wind generation is not involved in the dispatch of power systems. However, with the fast increasing of wind generation penetration, wind generation should be dispatched to improve the performance of the power grid in the future so that a higher requirement for EMS will be proposed. The algorithms in this dissertation worked like a mini-EMS, collecting wind speed data in different locations, calculating the optimal parameters, and dynamically adjusting the parameters of DFIG. Next step, the application of wind generation control in EMS will become more important and popular.

5. *Integration optimization of gas turbine generators combined with intermittent sources (i.e., wind and solar generations) in system level*

The intermittency of wind and solar power generation will not be perfectly predicted for a long time. Power systems operators secure different amounts and types of operating reserves to compensate for the intermittency in order to serve load reliably and maintain the system frequency. With the rapid exploitation of shale gas in the U.S., the penetration of gas turbine generation, wind generation, and solar generation will quickly increase. This also provides a good chance to compensate for the intermittent generations because of the fast adjustment capability of gas turbine generation. How to optimize the integration and compensation of gas turbine generation combined intermittent generations is becoming a big challenge.

Appendix I: 3.6MW Synchronous Generator Data in PSCAD

3.6MW Synchronous Generator Data:

No. of Q Axis Damper Winding	2
D Axis Saturation	Disabled
Rated RMS Line to Neutral Voltage	0.48 kV
Rated RMS Line Current	2.50 kA
Base Angular Frequency	376.99 rad/s
Inertia Constant	1.361 sec
Neutral Series Resistance	10 p.u.
Neutral Series Reactance	2 p.u.
Iron Loss Resistance	30 p.u.
Armature Resistance	0.013 p.u.
Potier Reactance	0.13 p.u.
D Axis Unsaturated Reactance	2.38 p.u.
D Axis Unsaturated Transient Reactance	0.264 p.u.
D Axis Unsaturated Transient Time	2.47 sec
D Axis Unsaturated Sub-Transient Reactance	0.201 p.u.
D Axis Unsaturated Sub-Transient Time	0.018 sec
Q Axis Unsaturated Reactance	1.10 p.u.
Q Axis Unsaturated Transient Reactance	0.35 p.u.
Q Axis Unsaturated Transient Time	0.019 sec
Q Axis Unsaturated Sub-Transient Reactance	0.214 p.u.
Q Axis Unsaturated Sub-Transient Time	0.009 sec
Air Gap Factor	1.0

Appendix II: IEEE 34-bus Test System Data and DFIG Data of Digsilent

IEEE 34-bus Test System Data:

Line Segment Data

Node A	Node B	Length(ft.)	Config.
800	802	2580	300
802	806	1730	300
806	808	32230	300
808	810	5804	303
808	812	37500	300
812	814	29730	300
814	850	10	301
816	818	1710	302
816	824	10210	301
818	820	48150	302
820	822	13740	302
824	826	3030	303
824	828	840	301
828	830	20440	301
830	854	520	301
832	858	4900	301
832	888	0	XFM-1
834	860	2020	301
834	842	280	301
836	840	860	301
836	862	280	301
842	844	1350	301
844	846	3640	301
846	848	530	301
850	816	310	301
852	832	10	301
854	856	23330	303
854	852	36830	301
858	864	1620	303
858	834	5830	301
860	836	2680	301
862	838	4860	304
888	890	10560	300

Overhead Line Configurations (Config.)

Config.	Phasing	Phase	Neutral	Spacing ID
		ACSR	ACSR	
300	B A C N	1/0	1/0	500
301	B A C N	#2 6/1	#2 6/1	500
302	A N	#4 6/1	#4 6/1	510
303	B N	#4 6/1	#4 6/1	510
304	B N	#2 6/1	#2 6/1	510

Transformer Data

	kVA	kV-high	kV-low	R - %	X - %
Substation:	2500	69 - D	24.9 -Gr. W	1	8
XFM -1	500	24.9 - Gr.W	4.16 - Gr. W	1.9	4.08

Spot Loads

Node	Load Model	Ph-1 kW	Ph-1 kVAr	Ph-2 kW	Ph-2 kVAr	Ph-3 kW	Ph-4 kVAr
860	Y-PQ	20	16	20	16	20	16
840	Y-I	9	7	9	7	9	7
844	Y-Z	135	105	135	105	135	105
848	D-PQ	20	16	20	16	20	16
890	D-I	150	75	150	75	150	75
830	D-Z	10	5	10	5	25	10
Total		344	224	344	224	359	229

Shunt Capacitors

Node	Ph-A kVAr	Ph-B kVAr	Ph-C kVAr
844	100	100	100
848	150	150	150
Total	250	250	250

Regulator Data

Regulator ID:	1		
Line Segment:	814 - 850		
Location:	814		
Phases:	A - B -C		
Connection:	3-Ph,LG		
Monitoring Phase:	A-B-C		
Bandwidth:	2.0 volts		
PT Ratio:	120		
Primary CT Rating:	100		
Compensator Settings:	Ph-A	Ph-B	Ph-C
R - Setting:	2.7	2.7	2.7
X - Setting:	1.6	1.6	1.6
Volltage Level:	122	122	122
Regulator ID:	2		
Line Segment:	852 - 832		
Location:	852		
Phases:	A - B -C		
Connection:	3-Ph,LG		
Monitoring Phase:	A-B-C		
Bandwidth:	2.0 volts		
PT Ratio:	120		
Primary CT Rating:	100		
Compensator Settings:	Ph-A	Ph-B	Ph-C
R - Setting:	2.5	2.5	2.5
X - Setting:	1.5	1.5	1.5
Volltage Level:	124	124	124

Distributed Loads

Node A	Node B	Load Model	Ph-1 kW	Ph-1 kVAr	Ph-2 kW	Ph-2 kVAr	Ph-3 kW	Ph-3 kVAr
802	806	Y-PQ	0	0	30	15	25	14
808	810	Y-I	0	0	16	8	0	0
818	820	Y-Z	34	17	0	0	0	0
820	822	Y-PQ	135	70	0	0	0	0
816	824	D-I	0	0	5	2	0	0
824	826	Y-I	0	0	40	20	0	0
824	828	Y-PQ	0	0	0	0	4	2
828	830	Y-PQ	7	3	0	0	0	0
854	856	Y-PQ	0	0	4	2	0	0
832	858	D-Z	7	3	2	1	6	3
858	864	Y-PQ	2	1	0	0	0	0
858	834	D-PQ	4	2	15	8	13	7
834	860	D-Z	16	8	20	10	110	55
860	836	D-PQ	30	15	10	6	42	22
836	840	D-I	18	9	22	11	0	0
862	838	Y-PQ	0	0	28	14	0	0
842	844	Y-PQ	9	5	0	0	0	0
844	846	Y-PQ	0	0	25	12	20	11
846	848	Y-PQ	0	0	23	11	0	0
Total			262	133	240	120	220	114

Configuration 300:

--------- Z & B Matrices Before Changes ---------

Z (R +jX) in ohms per mile

1.3368 1.3343 0.2101 0.5779 0.2130 0.5015

1.3238 1.3569 0.2066 0.4591

1.3294 1.3471

B in micro Siemens per mile

5.3350 -1.5313 -0.9943

5.0979 -0.6212

4.8880

Configuration 301:

Z (R +jX) in ohms per mile

1.9300 1.4115 0.2327 0.6442 0.2359 0.5691

1.9157 1.4281 0.2288 0.5238

1.9219 1.4209

B in micro Siemens per mile

5.1207 -1.4364 -0.9402

4.9055 -0.5951

4.7154

Configuration 302:

Z (R +jX) in ohms per mile

2.7995 1.4855 0.0000 0.0000 0.0000 0.0000

0.0000 0.0000 0.0000 0.0000

0.0000 0.0000

B in micro Siemens per mile

4.2251 0.0000 0.0000

0.0000 0.0000

0.0000

Configuration 303:

Z (R +jX) in ohms per mile

0.0000 0.0000 0.0000 0.0000 0.0000 0.0000

2.7995 1.4855 0.0000 0.0000

0.0000 0.0000

B in micro Siemens per mile

0.0000 0.0000 0.0000

4.2251 0.0000

0.0000

Configuration 304:

Z (R +jX) in ohms per mile

0.0000 0.0000 0.0000 0.0000 0.0000 0.0000

1.9217 1.4212 0.0000 0.0000

0.0000 0.0000

B in micro Siemens per mile

0.0000 0.0000 0.0000

4.3637 0.0000

0.0000

DFIG Data of Digsilent:

Rated power 1.5MW, Reactive power 0.2Mvar, Slip 8%, Rated voltage 2KV.

REFERENCES:

[1] “Global wind energy outlook 2016,” Global Wind Energy Council, http://gwec.net/publications/global-wind-energy-outlook/global-wind-energy-outlook-2016

[2] “2018 U.S. Wind Industry Market Reports”, American Wind Energy Association, https://www.awea.org/resources/publications-and-reports/market-reports/2018-u-s-wind-industry-market-reports

[3] U.S. Department of Energy, "20% Wind Energy by 2030: Increasing Wind Energy's Contribution to U.S. Electricity Supply," DOE/GO-102008-2567, July 2008, http://www1.eere.energy.gov/wind/pdfs/41869.pdf.

[4] Srinivas R. Chellapilla and Badml H. Chowdhury “A dynamic model of induction generators for wind power studies.” *2003 IEEE Power Engineering Society General Meeting: Conference Proceedings*, Toronto, Ontario, Canada, Vol. 4, pp. 13-17, July 2003.

[5] L.P.Kunjumuhammed, B.C.Pal, K.K.Anaparthi, N.F.Thornhill, “Effect of wind penetration on power system stability,” IEEE Power & Energy Society General Meeting, pp.1-5, 2013.

[6] Min Hwang, Eduard Muljadi, “Dynamic Droop–Based Inertial Control of Doubly-Fed InductionGenerator,” IEEE Transactions on Sustainable Energy, Vol. 7, Issue: 3, pp. 924 – 933, 2016.

[7] Hansen A.D., Sorensen P., Janosi L., Bech J. “Wind farm modelling for power quality”, Industrial Electronics Society, 2001. IECON'01. The 27th Annual Conference of the IEEE Vol. 3, pp.1959-1964, 29 Nov 2001.

[8] Gardner P. "Flicker from wind farms", BWEA/SERC RAL Workshop on wind energy penetration into weak electricity network, Rutherford, U.K., pp. 27-37, 1993.

[9] Ladakakos P.D., Ioannides M.G., Koulouvari M.I. "Assessment of wind turbines impact on the power quality of autonomous weak grids", Harmonics and Quality of Power, 1998. Proceedings. 8th International Conference on Vol. 2, pp. 900-905, 14-16 Oct 1998.

[10] Seyoum D., Grantham C., Rahman F. "The dynamics of an isolated self-excited induction generator driven by a wind turbine", Industrial Electronics Society, IECON'2001. The 27th Annual Conference of the IEEE Vol. 2, pp. 1364-1369, 29 Nov 2001.

[11] Doyle M.T. "Reviewing the impacts of distributed generation on distribution system protection", Power Engineering Society Summer Meeting, 2002 IEEE, Vol. 1, pp. 103-105, 25-25 July 2002.

[12] Milligan, M.; Kirby, B.; Gramlich, R., “Impact of Electric Industry Structure on High Wind Penetration Potential”, http://www.nrel.gov/wind/systemsintegration/pdfs/2009/milligan_electric_structure_impact.pdf.

[13] Parsons, B.; Milligan, M.; Smith, J. C.; DeMeo, E.; Oakleaf, B.; Wolf, K.; Schuerger, M.; Zavadil, R., “Grid Impacts of Wind Power Variability: Recent Assessments from a Variety of Utilities in the United States”,

http://www.nrel.gov/wind/systemsintegration/pdfs/2006/parsons_wind_grid_impacts.pdf.

[14] Smith, J.C.; Milligan, M.R.; DeMeo, E.A.; Parsons, B., “Utility Wind Integration and Operating Impact State of the Art”, IEEE Transactions on Power Systems, Vol. 22, pp. 900-908, August 2007.

[15] Milligan, M.; Donohoo, P.; Lew, D.; Ela, E.; Kirby, B., “Operating Reserves and Wind Power Integration: An International Comparison”, http://www.nrel.gov/wind/systemsintegration/pdfs/2010/milligan_operating_reserves_comparison.pdf.

[16] “AWEA-SEIA Transmission White Paper”, http://www.awea.org/documents/issues/upload/GreenPowerSuperhighways.pdf.

[17] Gibescu, M.; Kling, W.L.; Ummels, B.C.; Pelgrum, E.; van Offeren, R.A., "Case study for the integration of 12 GW wind power in the Dutch power system by 2020", 2009 IEEE PES Joint Symposium , pp. 29-31, July 2009.

[18] Lerch, E.; Ruhle, O., "Dynamic simulation of DFIGs for wind power plants," Power Engineering Conference, 2005. IPEC 2005. pp: 92-98, 29 Nov 2005.

[19] Causebrook, A., Atkinson, D.J., Jack, A.G., "Fault Ride-Through of Large Wind Farms Using Series Dynamic Braking Resistors," Power Systems, IEEE Transactions, Vol. 22, No. 3, pp. 966-975, Aug 2007.

[20] Wei Qiao, Harley R.G, “Effect of grid-connected DFIG wind turbines on power system transient stability”, Power and Energy Society General Meeting - Conversion and Delivery of Electrical Energy in the 21st Century, pp: 1-7, 20-24 July 2008

[21] Ahmed El-Naggar, Istvàn Erlich, “Short-circuit current reduction techniques of the doubly-fed induction generator based wind turbines for fault ride through enhancement,” IET Renewable Power Generation,Vol. 11, Issue 7, pp. 1033-1040, Jun 2017.

[22] Arghya Mitra, Dheeman Chatterjee, “Active Power Control of DFIG-Based Wind Farm for Improvement of Transient Stability of Power Systems,” IEEE Transactions on power systems, Vol. 31, No. 1, pp. 82-93, Jan 2016.

[23] Ran Ou, XianYong Xiao, ZhiCe Zou, “Cooperative Control of SFCL and Reactive Power for Improving the Transient Voltage Stability of Grid-Connected Wind Farm With DFIGs,” IEEE Transactions on Applied Superconductivity, Vol. 26, No. 7, Oct 2016.

[24] Muyeen, S. M, Takahashi, R, Murata, T, Tamura, J, “Integration of an Energy Capacitor System With a Variable-Speed Wind Generator”, Power Systems, IEEE Transactions on Volume 25, Issue 1, pp. 331-340, Feb 2010.

[25] Dong-Jing Lee; Li Wang; “Small-Signal Stability Analysis of an Autonomous Hybrid Renewable Energy Power Generation/Energy Storage System Part I: Time-Domain Simulations ”,IEEE Transactions on Energy Conversion, Volume:23, Issue:1, pp. 311-320, 2008.

[26] Zhou, F., Joos, G., Ooi, B.T., "Use of large capacity SMES to improve the power quality and stability of wind farms," Power Engineering Society General Meeting, Vol. 2, pp. 2025-2030, 10 June 2004.

[27] Wei Qiao, G. K. Venayagamoorthy, and R. G. Harley, “Design of optimal PI controllers for doubly fed induction generators driven by wind turbines using

particle swarm optimization," in 2006 International Joint Conference on Neural Networks, Canada, pp. 1982-1987, Jul 2006

[28] F. Wu, X. P. Zhang, K. Godfrey, "Small Signal Stability Analysis and Optimal Control of a Wind Turbine with Doubly Fed Induction Generator," IET Generation, Transmission & Distribution , Vol. 1, Issue 5, pp. 751-760, 2007.

[29] Y. Mishra, S. Mishra, Fangxing Li, Z. Y. Dong, "Small Signal Stability Analysis of a DFIG Based Wind Power System with Tuned Damping Controller under Super/Sub-Synchronous Mode of Operation," 2009 PES General Meeting, 26-30 JULY 2009.

[30] Rosyadi, M., Muyeen, S.M., Takahashi, R., Tamura, J., "Transient stability enhancement of variable speed permanent magnet wind generator using adaptive PI-Fuzzy controller," PowerTech, 2011 IEEE Trondheim, pp. 1-6, 19-23 June 2011.

[31] Jazayeri, M., Fendereski, M., "Stabilization of gird connected wind generator during power network disturbances by STATCOM," Universities Power Engineering Conference, 2007 UPEC 42nd International, pp. 1182-1186, 4-6 Sep 2007.

[32] Faried S.O., Billinton R., Aboreshaid S., "Probabilistic Evaluation of Transient Stability of a Wind Farm", Energy Conversion, IEEE Transactions on Volume 24, Issue 3, pp. 733-739, Sep 2009.

[33] Amirthagunaraj Yogarathinam ; Nilanjan Ray Chaudhuri, "Data packet-drop-resilient wide-area damping control using DFIG-based wind farm", 2016 North American Power Symposium (NAPS), 18-20 Sep. 2016.

[34] Siwei Liu, Gengyin Li, Ming Zhou, “Power system transient stability analysis with integration of DFIGs based on center of inertia,” CSEE Journal of Power and Energy Systems, Vol. 2, Issue. 2, pp. 20-29, 2016.

[35] P. Kundur, “Power System Stability and Control”, McGraw-Hill Inc., New York, First Edition, 1994.

[36] J. J. Grainger and W. D. Stevenson, “Power System Analysis”, McGraw-Hill Inc., 1968.

[37] K. R. Padiyar, “Power System Dynamics: Stability and Control”, Anshan Limited, U.K., Second Edition, 2004.

[38] P. Kundur, J. Paserba, and S. Vitet, “Overview on definition and classification of power system stability”, CIGRE/IEEE PES International Symposium Quality and Security of Electric Power Delivery Systems, pp. 1-4, 2003.

[39] R. B. Johnson, M. J. Short, “Improved Simulation Techniques for Power System Dynamics”, IEEE Trans., Vol. PWRS-3, No. 4, pp. 1691-1698, 1988.

[40] Zhang Xing, Hao Mukai, Liu Fang, "Analysis and Control of Energy Storage Systems in Microgrid," Intelligent System Design and Engineering Application (ISDEA), 2012 Second International Conference, pp. 1375-1379, 2012.

[41] Chengyong Zhao; Lei Li; Guangkai Li, "A novel coordinated control strategy for improving the stability of frequency and voltage based on VSC-HVDC," Electric Utility Deregulation and Restructuring and Power Technologies, 2008 Third International Conference, pp. 2202-2206, 2008.

[42] Y. Xue, T. van Cutsem, and M. Ribbens-Pavella, “A simple direct method for fast transient stability assessment of large power systems”, IEEE Transactions on Power Systems, Vol. 3, pp. 400–412, 1988.

[43] J. G. Slootweg and W. L. Kling, “Impacts of distributed generation on power system transient stability”, in 2002 IEEE Power Engineering Society Summer Meeting, Chicago, Illinois, USA, Vol. 2, pp. 503–508, 21-25 July 2002.

[44] Bahramipanah, M.; Afsharnia, S.; Shahooei, Z., “A survey on the effect of different kinds of wind turbines on power system stability”, Nuclear & Renewable Energy Conference (INREC), 2010 1st International, pp.1-6, 21-24 March 2010.

[45] Muller S., Deicke M. "Doubly fed induction generator systems for wind turbines", IEEE industry application magazine, May 2002.

[46] D.THAKUR, N.MITHULANANTHAN, “Influence of Constant Speed Wind Turbine Generator on Power System Oscillation”, Electric Power Components and Systems, pp. 478–494, 2009.

[47] J. G. Slootweg, W.L. Kling, “Modeling and analyzing impacts of wind power on transient stability of power systems”, Wind Energy Vol. 25, pp. 1-6, 2001.

[48] Polinder, H.; van der Pijl, F.F.A.; de Vilder, G.-J.; Tavner, P.J.; , "Comparison of direct-drive and geared generator concepts for wind turbines," Energy Conversion, IEEE Transactions, Vol. 21, No. 3, pp. 725-733, Sep 2006.

[49] E. Spooner, P. Gordon, J. R. Bumby, and C. D. French, “Lightweight ironless-stator PM generators for direct-drive wind turbines,” Inst. Electr. Eng. Proc. Elect. Power Appl., Vol. 152, No. 1, pp. 17–26, Jan 2005.

[50] G. Bywaters, V. John, J. Lynch, P. Mattila, G. Norton, J. Stowell, M. Salata, O. Labath, A. Chertok, and D. Hablanian. “(2004) Northern Power Systems WindPACT drive train alternative design study report”, NREL, Rep. Number NREL/SR-500-35524, http://www.nrel.gov/docs/fy03osti/33196.pdf.

[51] A. Grauers and P. Kasinathan, “Force density limits in low-speed PM machines due to temperature and reactance,” IEEE Trans. Energy Convers., Vol. 19, No. 3, pp. 518–525, Sep 2004.

[52] A. Grauers, P. Kasinathan, and E. S. Hamdi, “Force density limits in low speed permanent magnet machines due saturation,” IEEE Trans. Energy Convers., Vol. 20, No. 1, pp. 37–44, Mar 2005.

[53] Muyeen, S.M.; Takahashi, R.; Murata, T.; Tamura, J.; Ali, M.H.; "Transient stability analysis of permanent magnet variable speed synchronous wind generator," Electrical Machines and Systems, 2007. ICEMS. International Conference on, pp. 288-293, 8 Oct 2007.

[54] Muyeen, S.M.; Takahashi, R.; Murata, T.; Tamura, J.; "Transient stability enhancement of variable speed wind turbine driven PMSG with rectifier-boost converter-inverter," Electrical Machines, 2008. ICEM 2008. 18th International Conference, pp.1-6, 6 Sep 2008.

[55] A. Hansen, G. Michalke, P. Sørensen, T. Lund, and F. Iov, “Co-ordinated voltage control of DFIG wind turbines in uninterrupted operation during grid faults,” Wind Energy, Vol. 10, No. 1, pp. 51–68, 2007.

[56] G. Michalke, A. D. Hansen, and T. Hartkopf, “Variable speed wind turbines—Modeling, control and impact on power systems,” in Proc. Eur. Wind Energy Conf. Exhibition, pp. 1-10, Mar 2008.

[57] Hua Geng; Dewei Xu; , "Stability Analysis and Improvements for Variable-Speed Multipole Permanent Magnet Synchronous Generator-Based Wind Energy

Conversion System," Sustainable Energy, IEEE Transactions on, Vol. 2, No. 4, pp. 459-467, Oct 2011.

[58] Feng Gao; Ning An; Ning-Hui Zhu; Feng Su; , "Comparison of operation characteristics of variable speed constant frequency wind farms into power system," Power Engineering and Automation Conference (PEAM), 2011 IEEE, Vol. 1, No. 2, pp. 170-174, 8-9 Sep 2011.

[59] Sutanto, D.; Tsang, M.W., "Power system stabilizer utilizing energy storage," Power System Technology, 2004. Power Con., Vol. 1, No. 3, pp. 957- 962, 21-24 Nov 2004.

[60] Wenjuan Du; Haifeng Wang, "A new method to study an energy storage system to damp power system oscillations," 2010 IEEE International Energy Conference and Exhibition, pp. 588-593, 18-22 Dec 2010.

[61] Hossain, M.J.; Pota, H.R.; Ugrinovskii, V.; Ramos, R.A., "Decentralized control to augment LVRT capability of wind generators with STATCOM/ESS," Power and Energy Society General Meeting, 2010, pp.1-8, 25-29 July 2010.

[62] Ha Thu Le; Santoso, S., "Increasing wind farm transient stability by dynamic reactive compensation: Synchronous-machine-based ESS versus SVC," Power and Energy Society General Meeting, 2010, pp. 1-8, 25-29 July 2010.

[63] Kusko, A., “Short-Term, Long-Term, Energy Storage Methods for Standby Electric Power Systems”, IEEE Industry Applications Conference, Vol. 4, pp: 2672-2678, 2005

[64] Ribeiro, P., Johnson, B., Crow, M., Arsoy, A. and Liu,Y.. “Energy Storage Systems for Advanced Power Applications”, Proc. IEEE, Vol. 89, No. 12, pp. 1744-1756, 2000.

[65] Cheung, K. Y. C., Cheung, S. T. H., Desilva, R. G. N., Juvonen, M. P. T., Singh, R. and Woo, J. J., “Large-Scale Energy Storage Systems”, Imperial College London, ISE2, 2003.

[66] Schoenung, S. M. and Burns, C., “Utility Energy Storage Applications Studies”, IEEE Transactions on Energy conversion, Vol. 11, No. 3, 1996.

[67] Salman, S.K.; Teo, A.L.J., "Improvement of fault clearing time of wind farm using reactive power compensation," Power Tech Proceedings, 2001, Vol. 2, No. 4, pp.6-12, 2001.

[68] Polisetty, V.K.; Jetti, S.R.; Venayagamoorthy, G.K.; Harley, R.G.; , "Intelligent Integration of a Wind Farm to an Utility Power Network with Improved Voltage Stability," Industry Applications Conference, 2006. 41st IAS Annual Meeting, Vol. 3, No. 2, pp. 1128-1133, 8-12 Oct 2006.

[69] Foster, S.; Lie Xu; Fox, B.; "Coordinated control and operation of DFIG and FSIG based Wind Farms," Power Tech, 2007 IEEE Lausanne, pp. 522-527, 1-5 Jul 2007.

[70] Pokharel, B.; Wenzhong Gao;, "Mitigation of disturbances in DFIG-based wind farm connected to weak distribution system using STATCOM," North American Power Symposium (NAPS), 2010, pp. 1-7, 26-28 Sep 2010.

[71] C. Monteiro, H. Keko, R. Bessa, V. Miranda, A. Botterud, J. Wang, G. Conzelmann, “Wind power forecasting: state-of-the-art 2009”, Decision and Information Sciences Division, Argonne National Laboratory, 2009.

[72] Lydia, M.; Kumar, S.S.;, "A comprehensive overview on wind power forecasting," IPEC, 2010 Conference Proceedings, pp. 268-273, 27-29 Oct 2010.

[73] Z. Huang, Z. S. Chalabi, “Use of time-series analysis to model and forecast wind speed”, J. of Wind Engineering and Industrial Aerodynamics, Vol. 56, pp. 311-322, 1995.

[74] T. G. Barbounis, J. B. Theocharis, “ Locally recurrent neural networks for wind speed prediction using spatial correlation”, Int. J. of Information Sciences, Vol. 177, pp. 5775-5797, 2007.

[75] V. Akhmatov, “Analysis of Dynamic Behavior of Electric Power Systems with Large Amount of Wind Power,” Ph.D. dissertation, Technical University of Denmark, Kgs. Lyngby, Denmark, Apr 2003.

[76] N. W. Miller, W. W. Price, and J. J. Sanchez Gasca, “Dynamic modeling of GE 1.5 and 3.6 wind turbine-generators,” GE-Power Systems Energy Consulting, General Electric International, Inc., Schenectady, NY, USA, 27 Oct 2003.

[77] S. K. Salman and A. L. J. Teo, “Windmill modeling consideration and factors influencing the stability of a grid-connected wind power-based embedded generator,” IEEE Trans. Power Systems, Vol. 18, No. 2, pp. 793-802, May 2003.

[78] M. V. A. Nunes, J. A. Pecas Lopes, H. H. Zurn, U. H. Bezerra, and R. G. Almeida, “Influence of the variable-speed wind generators in transient stability margin of the conventional generators integrated in electrical grids,” IEEE Trans. Energy Conversion, Vol. 19, No. 4, pp. 692-701, Dec 2004.

[79] Y. Lei, A. Mullane, G. Lightbody, and R. Yacamini, “Modeling of the wind turbine with a doubly fed induction generator for grid integration studies,” IEEE Trans. Energy Conversion, Vol. 21, No. 1, pp. 257-264, Mar 2006.

[80] J. G. Slootweg, S. W. H. de Hann, H. Polinder, and W. L. Kling, “General model for representing variable speed wind turbines in power system dynamic simulations,” IEEE Trans. Power Systems, Vol. 18, No. 1, pp.1132-1139, Feb 2003.

[81] J. B. Ekanayake, L. Holdsworth, X. G. Wu, and N. Jenkins, “Dynamic modeling of doubly fed induction generator wind turbines,” IEEE Trans. Power Systems, Vol. 18, No. 2, pp. 803-809, May 2003.

[82] Wei Qiao, "Dynamic modeling and control of doubly fed induction generators driven by wind turbines," *Power Systems Conference and Exposition, 2009. PSCE '09. IEEE/PES*, pp.1-8, 15-18 Mar 2009.

[83] D. W. Novotny and T. A. Lipo, “Vector Control and Dynamics of AC Drive,” Oxford University Press, 2000.

[84] Kundur, P., “Power System Stability and Control,” Mcgram-Hill, Inc, New York, pp. 279-306. 1994.

[85] Wei Qiao, G. K. Venayagamoorthy, and R. G. Harley, “Design of optimal PI controllers for doubly fed induction generators driven by wind turbines using particle swarm optimization,” 2006 International Joint Conference on Neural Networks, Canada, pp. 1982-1987, Jul 2006.

[86] T. Basso & R. DeBlasio, “IEEE 1547 Series of Standards: Interconnection Issues,” National Renewable Energy Laboratory, NREL/JA-560-34882, Sep 2003.

[87] IEEE Std. 1547-2003, IEEE Standard for Interconnecting Distributed Resources with Electric Power Systems, the Institute of Electrical and Electronics Engineering Inc., July 2003.

[88] Docket No. RM05-4-000 – Order No. 661, Interconnection for Wind Energy, June 2005.

[89] A. Perdana, O. Carlson, and J. Persson, “Dynamic response of grid-connected wind with doubly fed induction generator during disturbances,” Proc. Nordic Wind Power Conf., 2004.

[90] A. D. Hansen et al., “Dynamic Wind Turbine Models in Power System Simulation Tool DIgSILENT,” Denmark, Risø report Risø-R-1400(EN), 2004.

[91] V. Akhmatov, “Analysis of dynamic behaviour of electric power systems with large amount of wind power,” Ph.D. dissertation, Elect. Power Eng., Orsted-DTU, Tech. Univ. Denmark, Lyngby, 2003.

[92] Rardin, Ronald L, “Optimization in operations research.” Prentice Hall, 1997.

[93] Magnanti, Thomas L., "Twenty years of mathematical programming". Contributions to Operations Research and Economics: The twentieth anniversary of CORE, Cambridge, MA, Jan 1987.

[94] Strang, Gilbert, “Introduction to applied mathematics.” Strang's publishing company, Wellesley, MA, 1986.

[95] Donald Knuth, “The Art of Computer Programming, Sorting and Searching”, first edition, 1973.

[96] Rastrigin, L.A, "The convergence of the random search method in the extremal control of a many parameter system", Automation and Remote Control, Vol. 24, pp. 1337-1342, 1963.

[97] F. Glover, C. McMillan, "The general employee scheduling problem: an integration of MS and AI". Computers and Operations Research, 1986.

[98] Fred Glover, "Tabu Search - Part 1". ORSA Journal on Computing Vol. 1, pp. 190-206, 1989.

[99] Fred Glover, "Tabu Search - Part 2". ORSA Journal on Computing Vol. 2, pp. 4-32, 1990.

[100] Zhang, Yudong, Lenan Wu, "A Hybrid TS-PSO Optimization Algorithm". Journal of Convergence Information Technology, Vol. 6, pp: 135-142, 2011.

[101] John Holland, “Adaptation in Natural and Artificial Systems”, 1975.

[102] Goldberg, David E, “Genetic Algorithms in Search Optimization and Machine Learning”, Addison Wesley presented, 1989.

[103] Chen, Po-Hung and Hong-Chan Chang, “Large -scale economic dispatch by genetic algorithm”, IEEE Transactions on Power Systems, Vol. 10, No. 4, pp. 1919-1926, 1995.

[104] Amjady, N. and H. Nasiri-Rad, “Economic dispatch using an efficient real-coded genetic algorithm”, IET Generation, Transmission, Distribution, Vol. 3, No. 3, pp. 266-278, 2009.

[105] Fdf Hans-Paul Schwefel (1974): Numerische Optimierung von Computer-Modellen (PhD thesis). Reprinted by Birkhäuser ,1977.

[106] H.-G. Beyer and H.-P. Schwefel. Evolution Strategies: A Comprehensive Introduction. Journal Natural Computing, Vol. 1, No. 1, pp: 3-52, 2002.

[107] Coelho, L.S. and V.C. Mariani, “Improved differential evolution algorithms for handling economic dispatch optimization with generator constraints”, Energy Conversion and Management, Vol. 48, No. 6, pp. 1831-1639, 2007.

[108] Fogel, L.J., “Intelligence through Simulated Evolution: Forty Years of Evolutionary Programming”, John Wiley presented, 1999.

[109] Coelho, L.S. and V.C. Mariani, “Improved differential evolution algorithms for handling economic dispatch optimization with generator constraints”, Energy Conversion and Management, Vol. 48, No. 6, pp. 1831-1639, 2007.

[110] Jayabarathi, T., G. Sadasivam and V. Ramachandran, “Evolutionary programming based multiarea economic dispatch with tie line constraints”, Electric Machines and Power System, Vol. 28, No. 12, pp. 1165-1176, 2000.

[111] Jayabarathi, T., K. Jayaprakash, D.N. Jeyakumar, and T. Raghunathan, “Evolutionary Programming Techniques for Different Kinds of Economic Dispatch Problems”, Electric Power Systems Research, Vol. 73, No. 2, pp.169-176, Aug 2005.

[112] M. Dorigo, “Optimization, Learning and Natural Algorithms”, PhD thesis, Politecnico di Milano, Italie, 1992.

[113] Kennedy, J., and Eberhart, R.: ‘Particle swarm optimization’. Proc. IEEE Int. Conf. on Neural Network, Perth, Australia, Vol. IV, pp.1942-1948, 1995.

[114] Gaing, Zwe-Lee, “Particle Swarm Optimization to Solve the Economic Dispatch Considering the Generator Constraints”, IEEE Transactions on Power Systems, Vol. 18, No. 3, pp. 1187-1195, 2003.

[115] Abido, M.A., “Optimal design of power system stabilizers using particle swarm optimization”, IEEE Transactions on Energy Conversion, Vol. 17, No. 3, pp. 406-413, 2002.

[116] Bergh, F. van den and A.P. Engelbrecht, “A cooperative approach to particle swarm optimization”, IEEE Transactions on Evolutionary Computation, Vol. 8, No. 3, pp. 225-239, 2004.

[117] Einicke, G.A, “Smoothing, Filtering and Prediction: Estimating the Past, Present and Future”, Rijeka, Croatia, Intech presented, 2012

[118] Arbib, Michael A, “The Handbook of Brain Theory and Neural Networks”, 1995.

[119] Agre, Philip E, “Computation and Human Experience”, Cambridge University Press, 1997.

[120] Bhadeshia H. K. D. H, "Neural Networks in Materials Science", ISIJ International Vol. 39, No. 10, pp: 966-979, 1992.

[121] S. Haykin, “Neural Networks: A Comprehensive Foundation”, New Jersey: Prentice-Hall, 1999.

[122] M. G. Simoes, B. K. Bose, R. J. Spiegel, “Design and performance evaluation of a fuzzy logic based variable speed wind generation system”, IEEE Transactions on Industry Applications, Vol. 33, Issue. 4, pp.956-965, 1997.

[123] Wei Qiao, G. K. Venayagamoorthy, and R. G. Harley, “Coordinated Reactive Power Control of a Large Wind Farm and a STATCOM Using Heuristic Dynamic

Programming”, IEEE Transactions on Energy Conversion, Vol. 24 , No. 2, pp.493-503, Jun 2009.

[124] Vogl, T. P., J.K. Mangis, A.K. Rigler, W.T. Zink, and D.L. Alkon, "Accelerating the convergence of the back propagation method," Biological Cybernetics, Vol. 59, pp. 257-263, 1988.

[125] S. N. Sivanandam, Sumathi & Deepa, “Introduction to neural networks using MATLAB 6.0,” Tata McGraw-Hill Education, 2006.

[126] Aktarujjaman M., Kashem M.A., Negnevitsky M., Ledwich G. "Control Stabilisation of an Islanded System with DFIG Wind Turbine", Power and Energy Conference, pp.312-317, 2006

[127] http://ewh.ieee.org/soc/pes/dsacom/testfeeders.html

[128] http://www.digsilent.com

[129] Jones G.W., Chowdhury B.H., “Distribution system operation and planning in the presence of distributed generation technology", Transmission and Distribution Conference and Exposition, 2008. T&D. IEEE/PES, pp.1-8, Apr 2008.

[130] Y. Zhou; D. D. Nguyen; P. C. Kjær; S. Saylors, “Connecting wind power plant with weak grid - Challenges and solutions”, 2013 IEEE Power & Energy Society General Meeting